NASA Contractor Report 166619

Development of a Sensitivity Analysis Technique for Multiloop Flight Control

Alfredo Herrera Vaillard, James Paduano, and David R. Downing

Contract NCC2-293
October 1985

National Aeronautics and
Space Administration

NASA Contractor Report 166619

Development of a Sensitivity Analysis Technique for Multiloop Flight Control

Alfredo Herrera Vaillard, James Paduano, and David R. Downing
Flight Research Laboratory, University of Kansas Center for Research, Inc., Lawrence, Kansas 66045

Prepared for
Ames Research Center
Dryden Flight Research Facility
Edwards, California
Under Contract NCC2-293

1985

National Aeronautics and
Space Administration
Ames Research Center
Dryden Flight Research Facility
Edwards, California 93523

"DEVELOPMENT OF A SENSITIVITY ANALYSIS TECHNIQUE FOR MULTILOOP FLIGHT CONTROL SYSTEMS"

ABSTRACT

Traditionally, the process of developing the aerodynamic model of an aircraft has been done independently from the process of designing the aircraft control system. The result has been that, very often, additional wind-tunnel and flight tests are performed to refine the model beyond what is required for control system design. This separation between the process of refining the aerodynamic model and the design of the control system has led to inefficient use of resources.

This report presents the development and application of a sensitivity analysis technique for multiloop flight control systems. This analysis yields very useful information on the sensitivity of the relative-stability criteria of the control system, with variations or uncertainties in the system and controller elements. This technique could be used to integrate the modelling and controller design processes, through the determination of the parameters of the aircraft and controller models that have the largest effect on the relative stability of the closed-loop system.

The sensitivity analysis technique developed is based on the computation of the singular values and singular-value gradients of a feedback-control system. The method is applicable to single-input/single-output as well as multiloop continuous-control systems. The use of the singular values to obtain a relative stability criterion for sampled-data systems is also explored in this report, with promising results. A possible way to extend the sensitivity analysis method for sampled-data systems is also suggested in this report but has not been implemented.

The sensitivity analysis technique was applied to a continuous yaw/roll damper stability augmentation system of a typical business jet, and the results show that the analysis is very useful in determining the system elements which have the largest effect on the relative stability of the closed-loop system.

As a secondary product of the research reported here, the relative stability criteria based on the concept of singular values were explored. This application to a single-loop yaw damper system and a multiloop yaw/roll damper system of a business jet was demonstrated. The results showed that the stability margins obtained through the singular-value analysis are conservative when compared to the margins obtained from a Bode analysis. A way to reduce the conservativeness of the analysis is also discussed.

TABLE OF CONTENTS

TABLE OF CONTENTS, continued

LIST OF FIGURES

LIST OF FIGURES, continued

LIST OF FIGURES, continued

LIST OF FIGURES, continued

LIST OF FIGURES, continued

LIST OF TABLES

LIST OF SYMBOLS AND ACRONYMS

Symbol	Definition
a	Scalar constant
$\mathbf{a}$	Vector
A_1	Ratio of I_{XZ}/I_{XX}
A_1B	Time-domain system matrices
$\bar{A}$, $\bar{B}$	Time-domain augmented-system matrices
b	Wing span in feet
A_c, B_c	Time-domain matrices for controller dynamics
B_1	Ratio of I_{XZ}/I_{ZZ}
C	Feedback control law matrix
$\bar{C}$	Augmented feedback control law matrix
C_c, D_c	Control law matrices for controller dynamics
C_{ℓ_r}	Variation of rolling moment coefficient with yaw rate
C_{ℓ_β}	Variation of rolling moment coefficient with sideslip angle
C_{ℓ_p}	Variation of rolling moment coefficient with roll rate
$C_{\ell_{\delta_A}}$	Variation of rolling moment coefficient with aileron deflection
$C_{\ell_{\delta_R}}$	Variation of rolling moment coefficient with rudder deflection
C_{n_β}	Variation of yawing moment coefficient with sideslip angle
C_{n_p}	Variation of yawing moment coefficient with roll rate
C_{n_r}	Variation of yawing moment coefficient with yaw rate

Symbol	Definition
$C_{n_{\delta_A}}$	Variation of yawing moment coefficient with aileron deflection
$C_{n_{\delta_R}}$	Variation of yawing moment coefficient with rudder deflection
C_{y_β}	Variation of side-force coefficient with sideslip angle
C_{y_r}	Variation of side-force coefficient with yaw rate
C_{y_p}	Variation of side-force coefficient with roll rate
$C_{y_{\delta_A}}$	Variation of side-force coefficient with aileron coefficient
$C_{y_{\delta_R}}$	Variation of side-force coefficient with rudder deflection
f_1, f_2, f_3	Functions
F	Time-domain system matrix
$G_1(s)$ or $G_1(z)$	Transfer matrix given by $H(s) \cdot G(s)$. ($G_1(z)$ is for discrete systems.)
G_u	Time-domain system matrix
G(s)	Plant transfer matrix
H	Time-domain observer (or output) matrix
$\hat{H}$	Augmented matrix used in computation of singular-value gradients with respect to P
H(s)	Controller transfer matrix
I_{XZ}	Product of inertia in slug-ft^2
I_{XX}, I_{ZZ}	Moments of inertia about X and Z axes in slug-ft^2
I	Identity matrix

LIST OF SYMBOLS AND ACRONYMS, continued

Symbol	Definition
$\bar{I}$	Augmented identity matrix
j	Imaginary term $\sqrt{-1}$
K	Feedback gain or matrix of gains
K_{δ_A}	Roll-damper loop gain
K_{δ_R}	Yaw-damper loop gain
k_n	Gain change
L	Perturbation matrix (diagonal)
m	Airplane mass in slugs
p	Scalar parameter
$\hat{P}$	Matrix of parameters for which we want sensitivity information
$\bar{q}_1$	Steady-state dynamic pressure in lb/ft^2
R	Vector of command signals
R(s)	Laplace transform of command vector
r	Vector
s	Laplace variable
S	Airplane wing area in ft^2
T	Time-domain observer or output matrix
T	Sampling period in seconds
U	Control input vector
U_1	Airplane steady-state speed in ft/sec
u_i	Left normalized eigenvector
v_i	Right normalized eigenvector

Symbol	Definition
w'	Variable in the w' plane
$\mathbf{x}$	Vector
$\mathbf{X}$	State-variable vector
$\mathbf{y}$	Vector
$\mathbf{Z}$	Output-variable vector
z	Z-transform variable

Greek Symbol	
α	Parameter
β	Parameter
β	Sideslip angle in rads
λ	Eigenvalue
$\underline{\sigma}$	Minimum singular value
$\bar{\sigma}$	Maximum singular value
δ_A	Aileron deflection in rads
δ_R	Rudder deflection in rads
ϕ	Roll angle in rads
δ, θ, τ	Parameters
ω	Frequency in rads/sec
Φ	Parameter used to abbreviate $(Is - A)^{-1}$ (see Equation 4.16)
$\Lambda(T)$	State transition matrix (discrete system)
$\Gamma(T)$	Control power matrix (discrete system)
δ_{ij}	Kronecker delta

LIST OF SYMBOLS AND ACRONYMS, continued

Acronym	Definition
NASA	National Aeronautics and Space Administration
KU-FRL or FRL	Flight Research Laboratory of the University of Kansas
ICS	Information and Control Systems
SISO	Single-input/single-output
MIMO	Multiple-input/multiple output
PM	Phase margin
GM	Gain margin
SVD	Singular-value decomposition

1. INTRODUCTION

1.1 BACKGROUND

During the development of a flight control system, a series of refinements of the mathematical model of the aircraft dynamics are used, each corresponding to a different stage of the vehicle development. Often, additional wind-tunnel and flight tests are performed to refine the model beyond what is required for control system design. This separation between the process of refining the model and the design of the control system has led to inefficient use of resources.

One approach to the problem of designing a controller using a model which may not accurately represent the aircraft dymamics is to design a controller which is insensitive to model uncertainties or variations. This is the general approach known as "robust controller design." A disadvantage of using this approach is that the final controller design may be unnecessarily "robust," and this could translate into greater complexity and cost or reduced performance.

An alternative approach to the problem would be to integrate the process of model determination with the process of controller design, via a sensitivity analysis. Since the modelling process requires resources to be spent on theoretical estimates and on wind-tunnel and flight tests, a knowledge of how the controller performance changes with changes in the elements of the model would

provide a way to direct those resources to the accurate determination of only the important controller and aircraft system parameters. This selected allocation of resources would be expected to increase the efficiency of the overall system analysis and synthesis problem.

An integrated procedure, Figure 1.1, would start with the development of a preliminary model that would be based on theoretical calculations and available wind-tunnel data or flight test data. With the use of this model, a controller is designed which can be either analog or digital and can be designed using classical or optimal design procedures. Regardless of the details of the design, all of the designs will have some degree of robustness or insensitivity to variations in the model parameters. A sensitivity analysis is performed to determine the effect of model parameter variations on controller performance. This will allow an ordering of the relative importance of accurate estimates of the individual model parameters. Those model parameters that produce large changes in the closed-loop system performance for small changes in the parameter values may warrant more accurate determination if those changes in performance endanger the stability of the closed-loop system or degrade the handling qualities of the aircraft. With the aid of this sensitivity information, specific tests could be designed to determine accurately the important parameters. If, in the testing, the changes in the values of the parameters were found to be significant, the controller could be

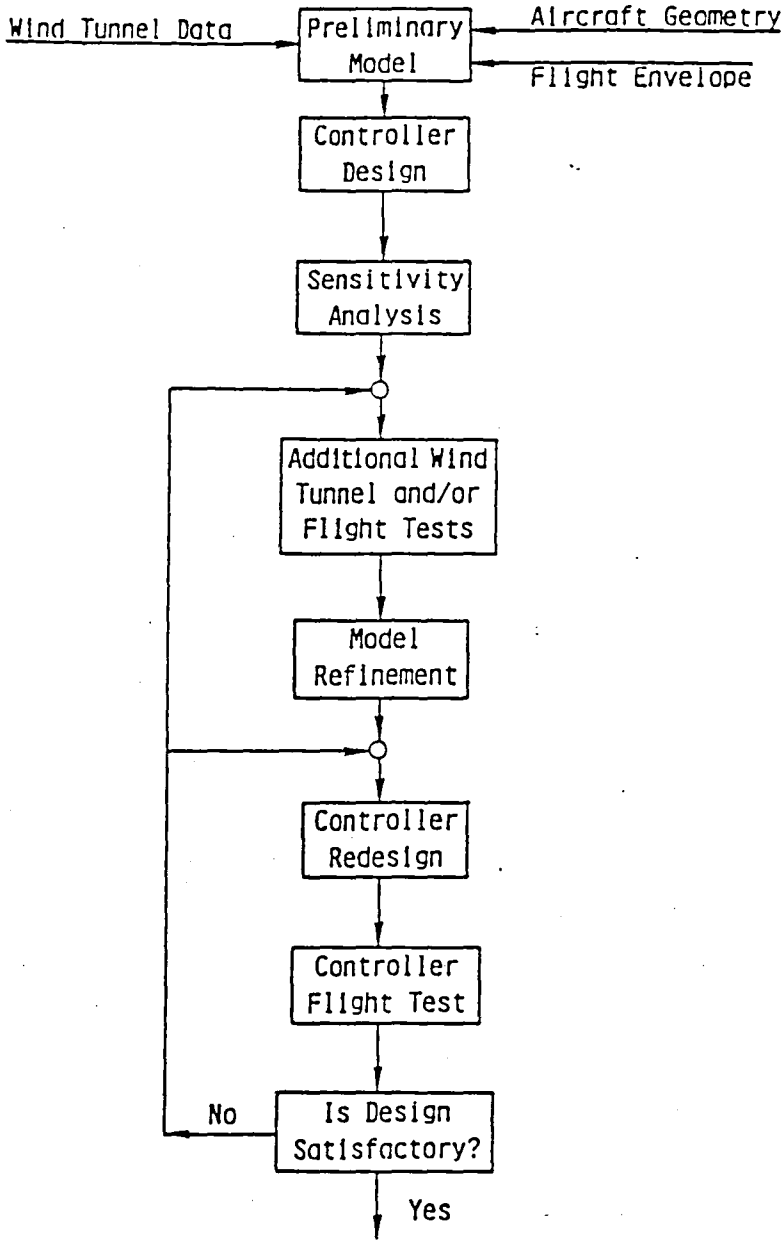

Figure 1.1: Integrated Procedure for Controller Design and Model Determination

redesigned. This procedure offers the potential for reducing the amount of wind-tunnel testing, flight testing, and data analysis required.

The present report covers the research done under NASA Cooperative Agreement NCC 2-293, at the Flight Research Laboratory of the University of Kansas, for the development of a multiloop-system sensitivity analysis method that could be used to integrate the modelling and controller design processes.

As a result of the evaluation of the state of the art of sensitivity analysis methods for multiloop systems, a method based on the singular values was selected. Also developed during this work was a method of calculating the gradients of singular values with respect to model parameters. The singular values and singular-value gradients were combined to form a sensitivity analysis technique. The use of the singular values as a multiloop-system analysis tool is demonstrated by their application to some simple third-order systems, a single-input/single-output yaw damper, and a multiloop yaw/roll damper system for a typical business jet. The use of the sensitivity analysis method developed is also demonstrated by its application to a simple, third-order system and to the multiloop yaw/roll damper system for a business jet.

1.2 REPORT OVERVIEW

The remainder of this report is divided into six chapters and four appendices. Chapter Two presents a summary of the different sensitivity analysis techniques, which are discussed in greater detail in Reference [29]. Chapter Three introduces the concept of singular values, and explores the characteristics of the singular-value analysis as compared to traditional frequency response methods. This is done through the analysis of several single-input/single-output (SISO) and multiloop (MIMO) systems. Chapter Four presents the mathematical development of the singular-value gradients and discusses the sensitivity analysis method developed. The application of the sensitivity analysis method is also explored in Chapter Four through the use of examples. Chapter Five summarizes the results obtained and presents some recommendations for future research, and Chapter Six contains the literature references. Appendix A contains a user's manual for the computer program used to calculate the singular-value gradients, Appendix B contains the aerodynamic and geometric data for the typical business jet used in the examples, and Appendix C contains a suggested approach to the development of singular-value gradients for sampled-data systems.

2. REVIEW OF SENSITIVITY ANALYSIS TECHNIQUES: ALTERNATIVE METHODS

The key element in the integration of the modelling process with the controller design processs is the sensitivity analysis of the control system. The development of the sensitivity analysis involves several fundamental questions; i.e., its applicability to a multiloop system, the type of mathematical model used (state variable form or transfer function form), and the controller performance measure (such as absolute stability, relative stability, and handling qualities).

The different techniques for sensitivity analysis were grouped as six different approaches, according to the performance measure used, their applicability to multiloop systems, and their use in discrete or continous systems. As it should be expected, not all the approaches are totally different from each other; and some of them serve as building blocks for others. These techniques have been discussed in Reference [29], and only a brief summary is presented in Table 2.1.

The classical sensitivity approach (Approach No. 1) refers to the "percentage change" sensitivity function for SISO systems; i.e., the ratio of the percentage change of system transfer function to percentage change of process transfer function or parameter. The eigenvalue sensitivity approach (No. 2) refers to the change in the eigenvalues of a system due to variations or inaccuracies in the

Table 2.1: Characterization of the Different Sensitivity Analysis Approaches

Approach	Applicable System Models	Sensitivity Measure	Comments	References
1. Classical Sensitivity	• Linear • Continuous • SISO	Ratio of % change of system TF to % change of process TF or parameter	• SISO Systems • Limited applicability to complex MIMO problems	1,2
2. Eigenvalue Sensitivity	• Linear • MIMO, SISO • Continuous	Gradient of eigenvalues with model parameters	• In the MIMO case there is no clear relation to PM and GM.	3,4,5,6
3. Performance Index Sensitivity	• Linear • MIMO, SISO • Continuous	Performance Index Variation, δI	• The relevance of the variation is measured by comparing the closed-loop system with an equivalent open-loop system. • Practical applicability is very limited: a) The designer is usually interested in the optimal values and sensitivities of the components of "I" rather than of "I" itself. b) This approach is not applicable for the case where "I" is independent of $\underline{X}(t)$. c) This approach is not applicable in cases where the end condition $\underline{X}(t_1)$ is not free.	7,8,9,10,11
4. Trajectory Sensitivity	• Linear • MIMO, SISO • Continuous	a) State Vector Gradient b) Comparison of trajectory error between closed-loop and equivalent open-loop system	• The relevance of the variation would be determined from the comparison of open-loop and closed-loop sensitivities. • No indication of what parameter variation is more important. • Requires testing of a matrix function of the return difference for positive definiteness. This was regarded (Ref. 16) as too complex to be useful as a design tool.	12,13,14,8,9
5. Gain Sensitivity	• Linear • Digital • MIMO, SISO	Variation of optimal gains with parameter variation	• Effect of sampling time T included • Possibility of coupling this approach with approach 6 could be evaluated.	15

Notes: TF = Transfer Function
SV = Singular Value
PM = Phase Margin
GM = Gain Margin

Table 2.1: Characterization of the Different Sensitivity Analysis Approaches (continued)

Approach	Applicable System Models	Sensitivity Measure	Comments	References
6. σ-Plots, σ-Gradients, and Universal Phase-Gain Margin Evaluation Diagram	• Linear • Digital, Continuous • MIMO, SISO	Gradient of SV with parameter variations + σ-Plot + PM and GM Diagram	• Relative importance of each parameter variation is determined using the SV gradients. • The relevance of the parameter variation change is determined using the σ-plot and the PM and GM diagram. • Software for σ-plots exists. • Direct relationship with PM and GM. • Results are conservative. • Current trend in control theory. • New developments appearing. • Research work being done at Langley Research Center.	16,17,18,19, 20,21,22,23, 24,25,26,27

Notes: TF = Transfer Function
SV = Singular Value
PM = Phase Margin
GM = Gain Margin

parameters of the system. The performance index sensitivity function (Approach No. 3) examines the changes in the performance index of an optimal closed-loop control system when a parameter vector deviates from its nominal value, and compares them with the changes in the performance index of the equivalent optimal open-loop control system. In general terms, the trajectory sensitivity (Approach No. 4) refers to the change in the state vector components with variation of system parameters. The two broad categories under this approach are the state-vector gradients and the comparison sensitivity. The first one allows for the explicit computation of derivatives of the root mean square value of particular state-vector components with respect to given parameters. The second one compares the state-vector trajectory error between closed-loop and equivalent open-loop control systems. The gain sensitivity approach (Approach No. 5) deals with the combined effects of sample rate and large parameter variations on the feedback gains of discrete flight control systems. Approach No. 6 utilizes the concepts of singular values and their related multiloop gain and phase margins (sigma plots) and combines them with the variation of the singular values with changes in system parameters (sigma gradients).

A goal of our research was to use a performance measure for the control system that could be easily interpreted by control system designers. The gain and phase margins criterion for SISO systems represents the type of performance measure for which the control system designer has already developed a good "feeling." This is due

to the vast experience with the design of SISO systems that has been gained through the years. Therefore, during the evaluation of the different techniques, emphasis was placed on the possible connection of the sensitivity analysis information and the relative stability of the system. For the remainder of this report, we will not be concerned with any type of performance measure other than the relative stability of the closed-loop system.

The method developed uses the singular values and singular-value gradients of the return difference matrix of a feedback control system. The use of the singular values was selected because of their direct applicability to multiloop (as well as SISO) systems, their applicability to discrete and continuous systems, the availability of efficient software to evaluate the singular values, and the direct relationship of the singular values with multiloop phase and gain margins.

Mathematical expressions for the gradients of the singular values with respect to system and controller parameters were developed; and, together with the sigma plots and the concept of multiloop relative stability margins, they were used to obtain a multiloop sensitivity analysis technique. This technique is discussed in Chapter Four, along with the development of the singular-value gradients. The fundamental concepts of singular values are introduced in Chapter Three.

3. SINGULAR-VALUE ANALYSIS

3.1 FUNDAMENTAL CONCEPTS

In this section, some fundamental concepts about singular values are introduced: their mathematical definition, their interpretation from the point of view of the control system analyst, and their relationship to multiloop gain and phase margins.

A general multiloop feedback control system is represented in Figure 3.1, where G(s) and H(s) are matrices of transfer functions called transfer matrices. The Laplace transform of the state-variable vector, $\mathbf{X}$[†], can be written as

$$\mathbf{X} = [(I + GH)^{-1}G]\mathbf{R} \tag{3.1}$$

where R is the Laplace transform of the command-input vector, and I is the identity matrix. The control-input vector, U, can be written as

$$\mathbf{U} = [(I + HG)^{-1}]\mathbf{R} \tag{3.2}$$

where, in both equations, the argument (s) has been omitted for convenience in writing. The system in Figure 3.1 can be represented by either Equation (3.1) or Equation (3.2). The matrices (I + GH) and (I + HG) are called the return difference matrices of the system for the loop broken at the plant output and input, respectively.

[†]Vectors are indicated in boldface type.

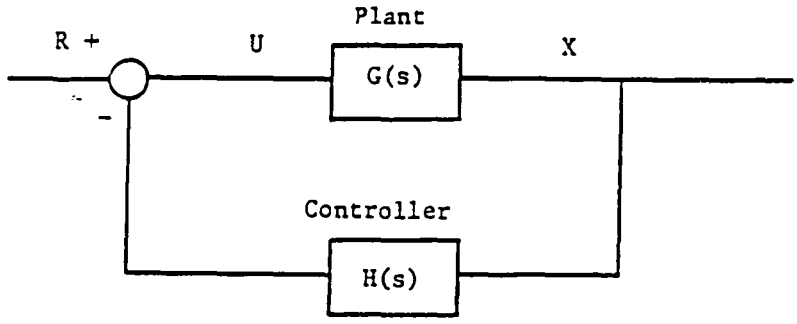

Figure 3.1: Block Diagram of a Multiloop Feedback Control System

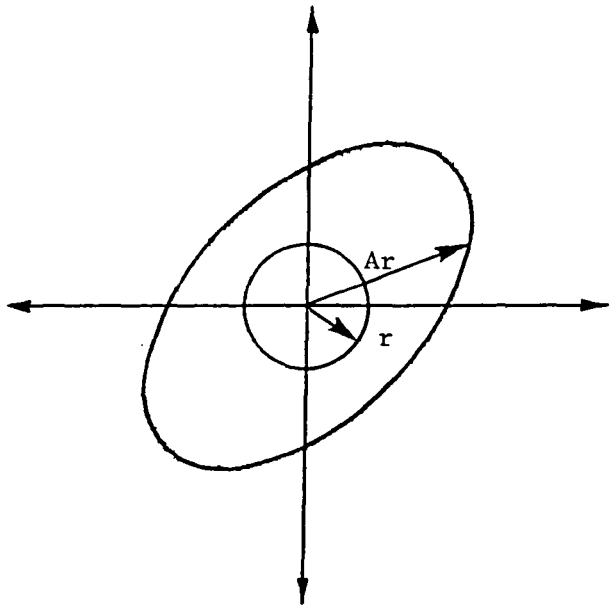

Figure 3.2: Representation of Transformation of Vector **r**, by Matrix **A**, into **u = Ar**

Defining as "absolutely stable" a system which will produce a bounded output as response to a bounded input, it can be seen that instability is related to the condition that (I + GH) or (I + HG) are singular. If (I + HG) or (I + GH) are "nearly singular," the system will be sensitive to modelling errors [22], since in such a case, a model error could make the true system unstable even though the model of the system is stable. Therefore, it is also important to consider a measure of relative stability of the system. This measure can be given by the "near singularity" of (I + HG) or (I + GH).

There are several ways to determine if a matrix A is singular. One such way is the determinant of the matrix; i.e., if

$$\det[A] = 0 \tag{3.3}$$

then matrix A is singular. However, the determinant is not a good indicator of near singularity [22]. The closeness of a matrix to singularity is related to the "size" of that matrix. Therefore, a different kind of test is needed which provides a more reliable measure of the "size" of the matrix. In the control system context, a physically meaningful measure of the "size" of a system described by a transfer matrix ought to bear some relation to the input-output gain ratio of the system [17], since such a transfer matrix transforms input signals into output signals.

Consider a matrix, A, which performs a linear transformation of a vector, r, into a vector, u (Figure 3.2). We are interested in defining the measure of the "size" of A that is related to the

effect of the transformation of **r** into **u**. To eliminate the linear effect of the size of **r** on its image, we are interested in the value of $\|\mathbf{Ar}\|/\|\mathbf{r}\|$, the factor by which the size of **r** is stretched under the transformation by A. The maximum and minimum stretching factors can be taken as definitions of the "size" of the matrix, A:

$$\|A\|_{max} = \left.\frac{\|\mathbf{Ar}\|}{\|\mathbf{r}\|}\right|_{max} = \bar{\sigma}(A) \tag{3.4}$$

$$\|A\|_{min} = \left.\frac{\|\mathbf{Ar}\|}{\|\mathbf{r}\|}\right|_{min} = \underline{\sigma}(A) \tag{3.5}$$

where $\bar{\sigma}(A)$ and $\underline{\sigma}(A)$ are the maximum and minimum singular values of A [17, 20]. The maximum and minimum singular values of a matrix, A, are given by the positive square root of the maximum and minimum eigenvalues of A^*A, respectively, where A^* is the conjugate transpose of A (the transpose of A if A is a real matrix).

For example if

$$A = \begin{matrix} 1 & 3 \\ 2 & 4 \end{matrix} \qquad \text{then } A^*A = \begin{matrix} 5 & 11 \\ 11 & 25 \end{matrix}$$

and the eigenvalues of A^*A are

$$\lambda_1 = 29.85 \; ; \; \lambda_2 = 0.15$$

and, therefore, the singular values of A are

$$\bar{\sigma} = \text{positive } \sqrt{29.85} = 5.46$$

$$\underline{\sigma} = \text{positive } \sqrt{0.15} = 0.39$$

The calculation of the singular values is generally not carried out by first computing the eigenvalues of A^*A. An efficient algorithm for the numerical computation of the singular value decomposition

(SVD) is generally used [35], which yields the singular values and their corresponding orthonormal eigenvectors.

If $\underline{\sigma}(A) = 0$, then A is singular. Therefore, the minimum singular value of A, $\underline{\sigma}(A)$, can be interpreted [16] as the distance between the matrix and the nearest singular matrix. Also note that, by definition, $\sigma(A) \geq 0$. Applying these concepts to the system of Figure 3.1, a condition for relative stability is

$$\underline{\sigma}(I + G_1) > 0 \tag{3.6}$$

where $G_1 = HG$.

In order to examine the system gain and phase margins, a square diagonal matrix, L, is introduced at the plant input, as shown in Figure 3.3(a); a convenient representation of the same system, when analyzed with the loop broken at the plant input, is shown in Figure 3.3(b). Matrix L has the special form

$$L = DIAG[k_n e^{j\phi_n}] \tag{3.7}$$

At nominal conditions, $k_n = 1$ and $\phi_n = 0$ for all n; and therefore L is the identity matrix. By selecting $k_n \neq 1$ or $\phi_n \neq 0$, it is possible to introduce a gain or phase change in loop n; this can be done for all loops simultaneously. The stability conditions are

$$\underline{\sigma}(I + G_1) > 0 \tag{3.8}$$

and

$$\underline{\sigma}(I + G_1 L) > 0 \tag{3.9}$$

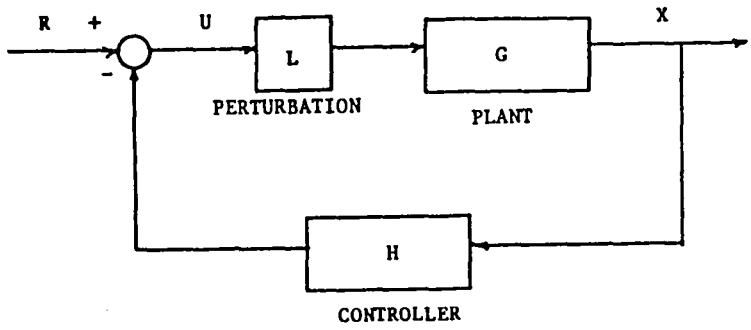

(a)

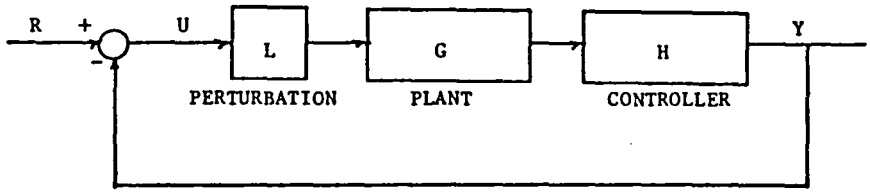

(b)

Figure 3.3: Block Diagram of Multiloop Control System with Perturbation L at the Plant Input

for the nominal and perturbed systems, respectively. It can be shown that the stability of the perturbed system is guaranteed if

$$\bar{\sigma}(L^{-1} - I) < \underline{\sigma}(I + G_1) \tag{3.10}$$

assuming L^{-1} exists [20, 22]. Lehtomaki, et al., [22] show that if inequality (3.10) holds, and

$$\underline{\sigma}(I + G_1) \geq a \tag{3.11}$$

for some constant, $a \leq 1$, then simultaneously in each loop of the feedback system of Figure 3.3 there is a guaranteed gain margin, GM, given by

$$GM = \frac{1}{1 \pm a} \tag{3.12}$$

and also a guaranteed phase margin, PM, given by

$$PM = \pm \cos^{-1}[1 - \frac{a^2}{2}] \tag{3.13}$$

where the word "simultaneously" means that the gains or the phases of all the feedback loops may be changed at the same time within the limits prescribed by Equations (3.12) and (3.13) without destabilizing the closed-loop system. It does not mean,however, that the gains and phases may be changed simultaneously. Mukhopadhyay and Newsom [20] extended this analysis to include phases and gains changing simultaneously by using the particular form of the L matrix as given by Equation (3.7); using this form, the stability condition is given by

$$\max \bar{\sigma}(L^{-1} - I) = \sqrt{(1 - \frac{1}{k_n})^2 + \frac{2}{k_n}(1 - \cos\phi_n)} \tag{3.14}$$

for all n with $k_n > 0$. Using Equation (3.14), the general case of simultaneous gain and phase changes can be examined. Equation (3.14) can also be presented as a universal diagram for gain and phase margin evaluation [20]; this diagram is shown in Figure 3.4. For example, if the smallest $\underline{\sigma}(I + G_1)$ for a system is 0.6, then the closed-loop system will tolerate simultaneous gain and phase changes of -1.5 dB to +5.3 dB, and -30 deg to +30 deg, respectively, in all input loops. In a classical sense, when either gain or phase is changed, the margins are -4.2 dB and +8 dB or ±35 deg, respectively. The same results are obtained from Equations (3.12) and (3.13).

It is important to note that condition (3.10) is a conservative condition and that it is possible to construct a matrix, L, which violates the condition yet fails to destabilize the system [20]. This means that the predicted stability margins will be smaller than the actual stability margins. This is due to the fact that some of the small perturbations that would theoretically destabilize the closed-loop system will never occur in the physical system [22]. Nevertheless, they are still detected by a small $\underline{\sigma}(I + G_1)$. A less conservative evaluation of the stability margins can be obtained by replacing the maximum and minimum singular values in Equation (3.10) with the maximum and minimum magnitudes of the eigenvalues, respectively [20, 27]. However, in that case, the stability of the system can only be guaranteed if the simultaneous gain or phase

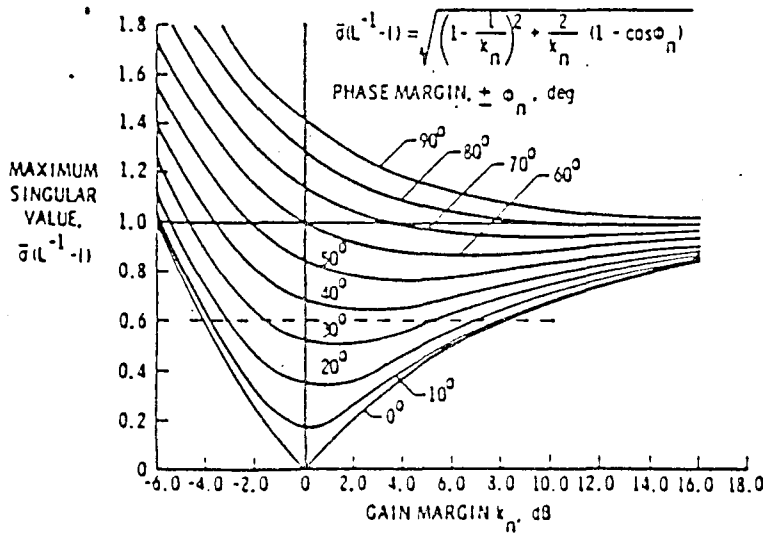

Figure 3.4: Universal Diagram for Multiloop Gain and Phase Margins Evaluation (from Reference [20])

changes in all the loops are uniform [27]; i.e., all k_n and ϕ_n are equal. A more detailed discussion of the use of these multiloop stability margins is reserved for the following chapter.

It is important to note that the return difference matrix, $(I + G_1)$, will have to be evaluated at each frequency of interest; and therefore, it is possible to construct a plot of minimum singular values as a function of frequency. Such a plot is called a sigma plot. In the next section, the characteristics of the singular-value analysis will be explored through the use of examples.

3.2 ASSESSMENT OF THE CHARACTERISTICS OF THE SINGULAR VALUE ANALYSIS

In this section, some of the basic characteristics of the singular-value analysis are explored and compared with the traditional Bode plot method. This is achieved through several examples that include simple third-order systems, a single-input/single-output (SISO) yaw damper system for a business jet, a multiloop yaw/roll damper, and a sampled-data SISO yaw damper for the business jet in Appendix B.

3.2.1 Simple Third-Order Systems

It was mentioned in Section 3.1 that the singular values are a function of frequency and that it is therefore possible to construct a plot of the minimum singular value for a range of frequencies. Such a plot is called a sigma plot (or σ-plot) and will yield a minimum at some frequency, ω.

Two simple, third-order systems are used to demonstrate the concept of the sigma plot and some of its characteristics, namely: how the sigma plot changes as system gain changes, how poles at high and low frequency affect the sigma plot, and how driving a system from stable to unstable affects the sigma plot. Also, the conservativeness of the stability margins derived from the singular value analysis is demonstrated.

A) **Case I.** The first example system is shown in Figure 3.5. The system has a real pole at -2 and a pair of complex poles at $-2 \pm 4j$. The frequency response is shown in Figure 3.6 for gains $K = 40$, 100, 120, and 140; while the sigma plots are shown in Figures 3.7 (a)-(d), at each of the different gains. The complex poles are unstable for $K = 140$. Two things are apparent. The minimum singular value usually does not occur at exactly the same frequency as the gain or phase crossover frequencies but at a slightly different frequency, and the frequency varies as the complex poles approach the imaginary axis in the s-plane. This can be explained by the fact that the sigma-plot analysis takes into account possible variations in phase and gain that are not accounted

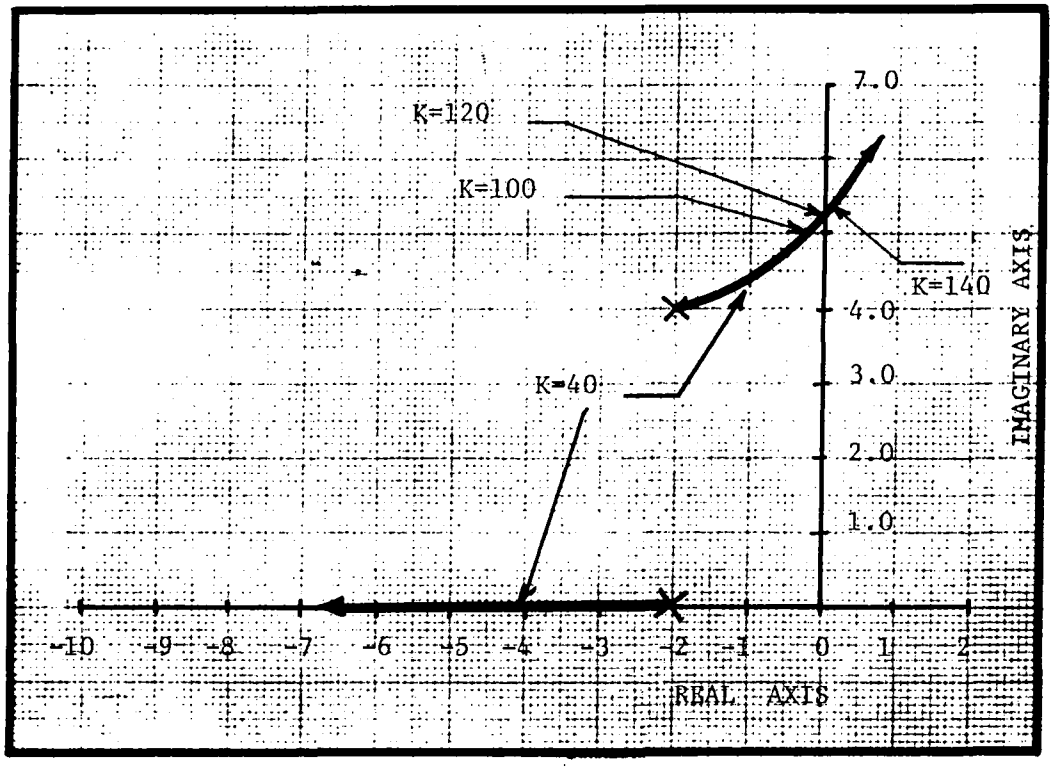

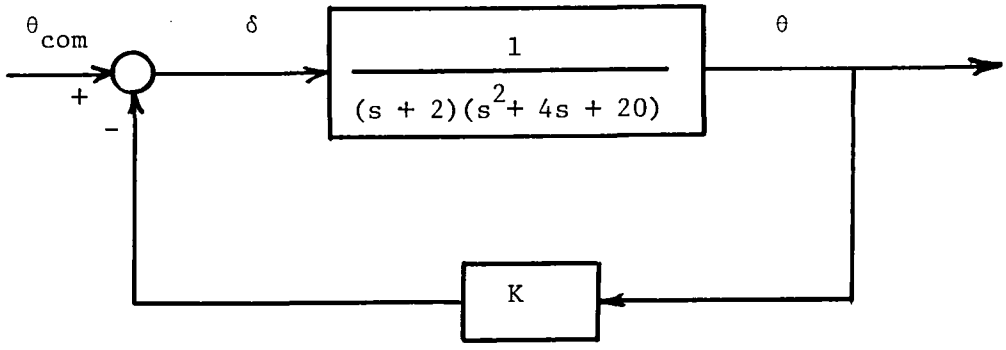

Figure 3.5: Block Diagram and Root Locus of Third-Order System in Case I

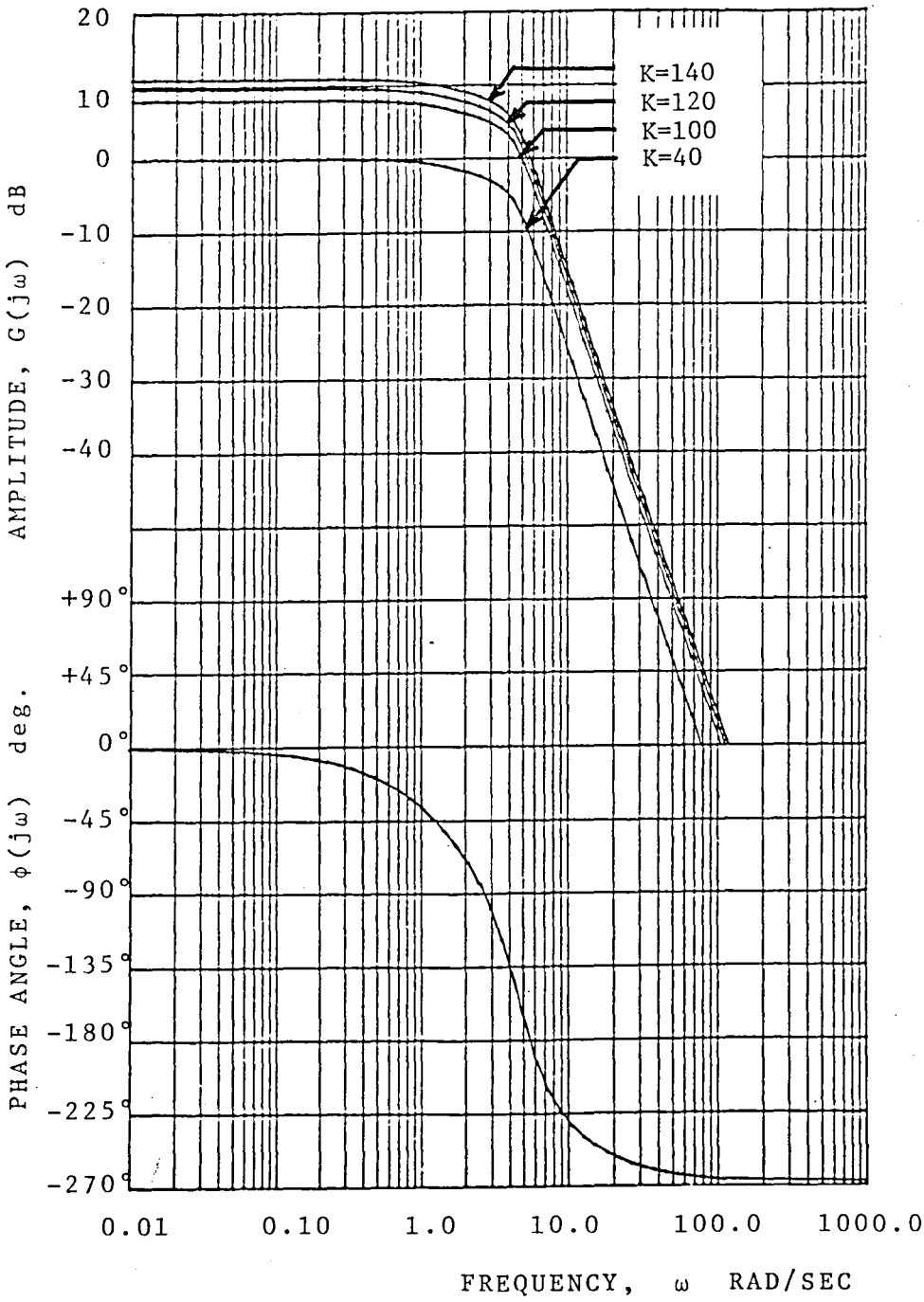

Figure 3.6: Frequency Response for the Third-Order System of Case I

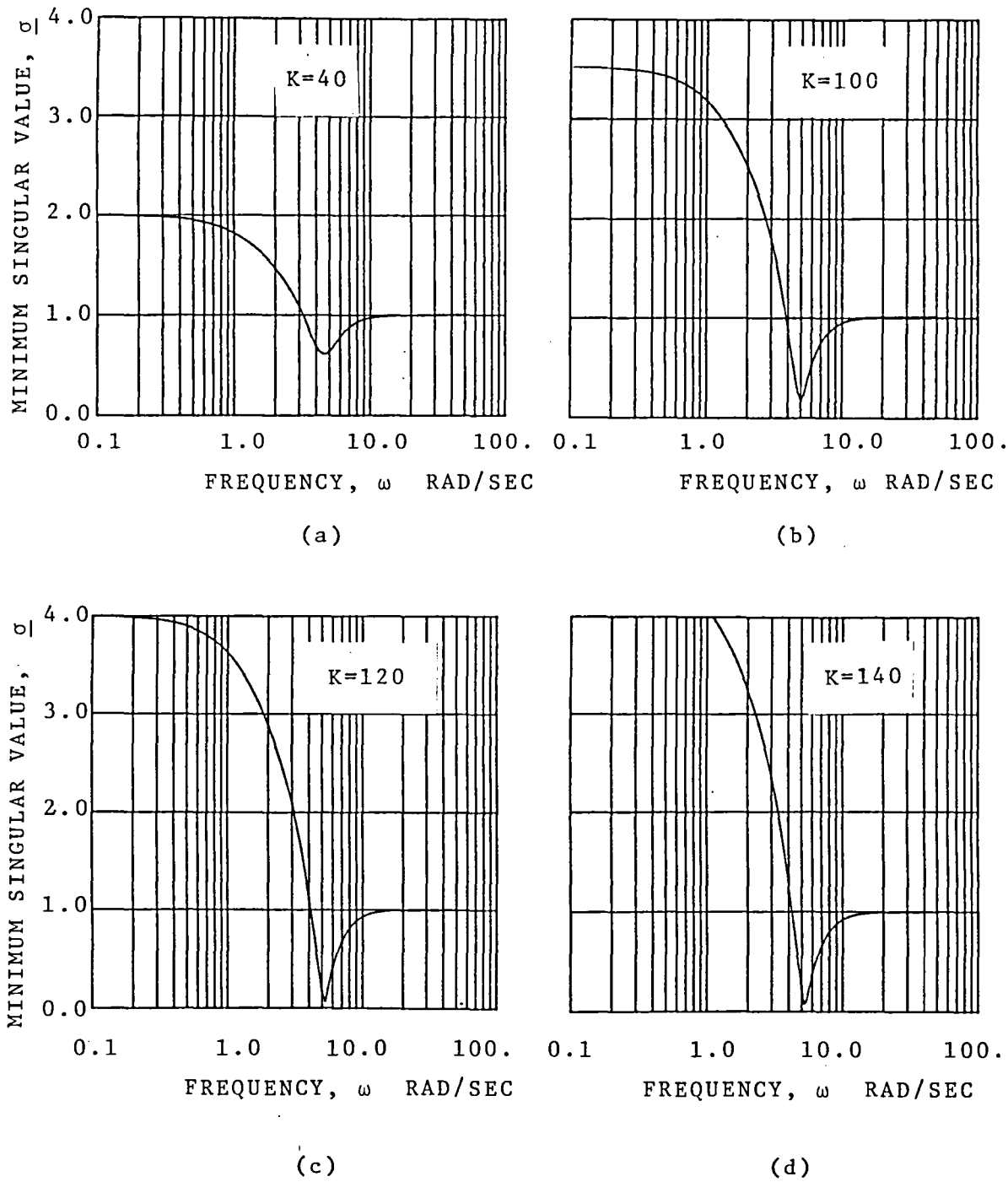

Figure 3.7: Sigma-Plots of the Third-Order System in Case I, for Several Feedback Gains

for by the Bode plot. Also, note that as the gain increases and the stability margin of the system is reduced, the minimum singular value plot at the "high-frequency" range shifts down, decreasing the value of the minimum singular value. Therefore, since the minimum singular value is a measure of the closeness to the stability boundary, the fact that the plot shifts down means that the relative stability is reduced. An important observation must be made here. Note that for K = 140, the sigma plot has "bounced" up again. This is so because the minimum singular value is a measure not of absolute stability of a system but of how far the system is from crossing the $j\omega$-axis in the s-plane; i.e., how close it is to neutral stability. Also, by definition, $\underline{\sigma}(A) \geq 0$ (Section 3.1).

In the "low-frequency" range, the sigma plot is shifted upward as K increases; this shift is related to the real pole moving to the left (away from the $j\omega$-axis) in the s-plane as K increases.

The phase and gain margins from the frequency response and the predicted phase and gain margins from the singular value analysis are shown in Table 3.1. The gain margin is defined as the smallest gain change that will destabilize the system when the phase is kept constant; the phase margin is defined as the smallest phase change that will destabilize the system when the gain is kept constant. All the phase margins (PM's) predicted by the singular values are conservative as compared to the PM from the Bode plot. The gain margins (GM's) from the sigma plots are also conservative except for gain K = 140. However, in this case, the fact that the GM from the

Table 3.1: Comparison of Stability Margins
from the Bode and Sigma-Plot Analyses,
for Case I

Feedback Gain	K = 40	K = 100	K = 120	K = 140
From Bode Analysis				
GM, dB	$-\infty$ to 10.35	$-\infty$ to 2.38	$-\infty$ to 0.804	-0.54 to ∞
PM, deg	∞	15.37°	4.46°	-7.0°
From σ-Plot Analysis				
$\underline{\sigma}$	0.6112	0.159	0.057	0.070
GM, dB	-4.15 to 8.19	-1.28 to 1.508	-0.477 to 0.505	-0.58 to 0.649
PM, deg	±35.6	±9.14°	±3.23°	±4.0°

sigma-plot analysis is larger than the GM from the Bode plot is due to lack of resolution in the computation of the singular values; i.e., if the frequency interval used for the calculation is reduced, the situation would be reversed. In any case, the GM's calculated from the sigma-plot analysis are not very conservative (i.e., they are close to the GM's from the Bode plot) for this particular example.

B) Case II. The second example is shown in Figure 3.8. This example is similar to Case I except that the real pole is unstable at +2 rather than stable at -2. The frequency response is shown in Figure 3.9 for gains K = 37, 50, 60, and 70. Note that the phase is equal to -180 deg at a frequency of zero and then again at a frequency between 3 and 4 rads/sec. This means that there are two GM's that we need to look at: one at each of the two phase-crossover frequencies. At K = 37, the real pole is unstable while the complex poles are stable; at K = 50, all the poles are stable; at K = 70, the real pole has become stable while the complex poles are now unstable.

The sigma plots are shown in Figures 3.10(a)-(d). At K = 37, the minimum singular value is provided by the "low-frequency" pole (Figure 3.10(a)), while at K = 50 the minimum singular value is provided by the "high-frequency" pole (Figure 3.10(b)). For K = 60, the "low-frequency" range of the curve continues its shift upward, while the "high-frequency" part has dipped down even more, meaning that the distance of the real pole from the $j\omega$-axis on the s-plane

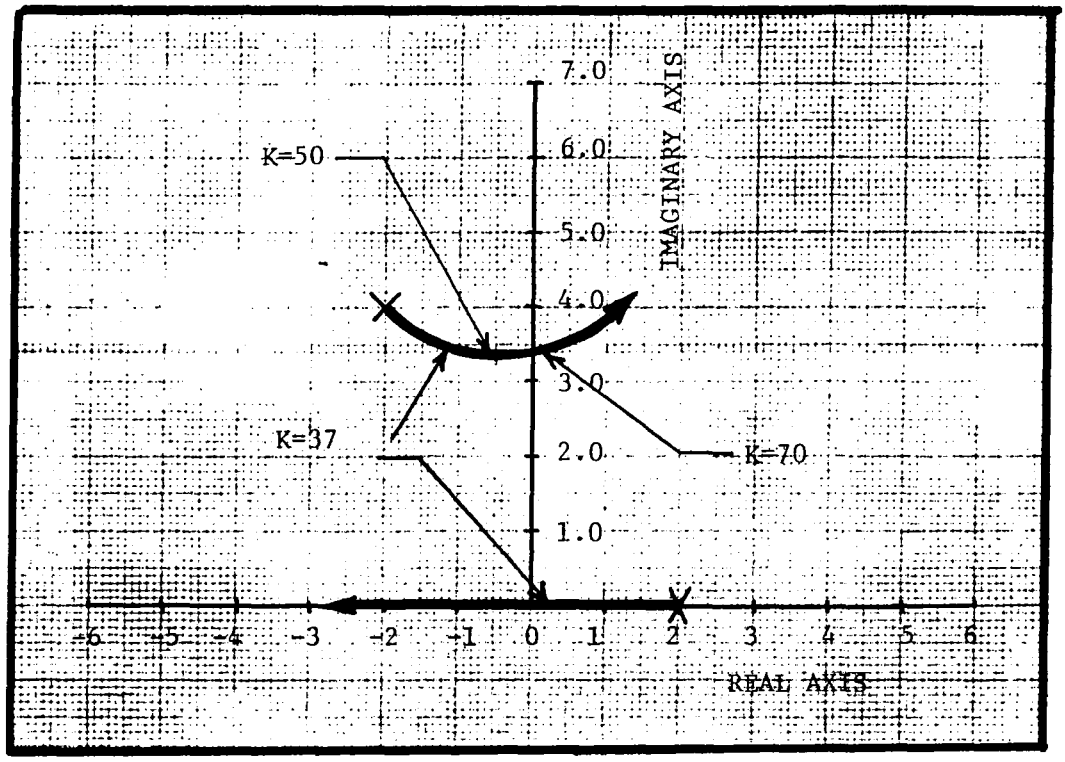

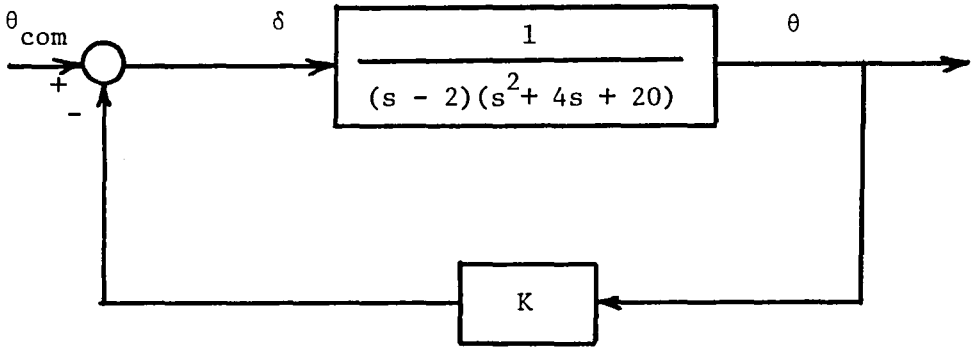

Figure 3.8: Block Diagram and Root Locus of Third-Order System in Case II

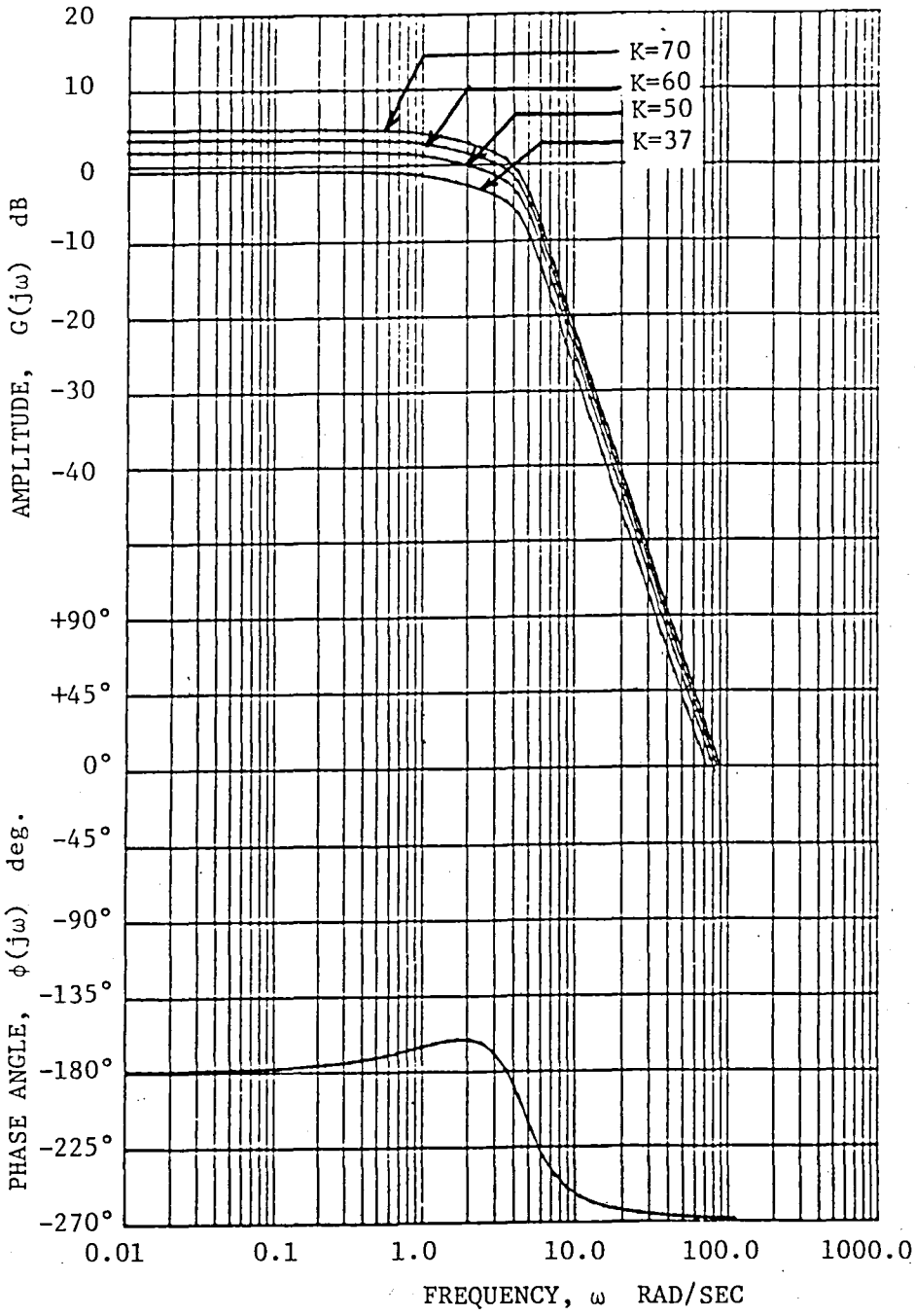

Figure 3.9: Frequency Response for the Third-Order System in Case II

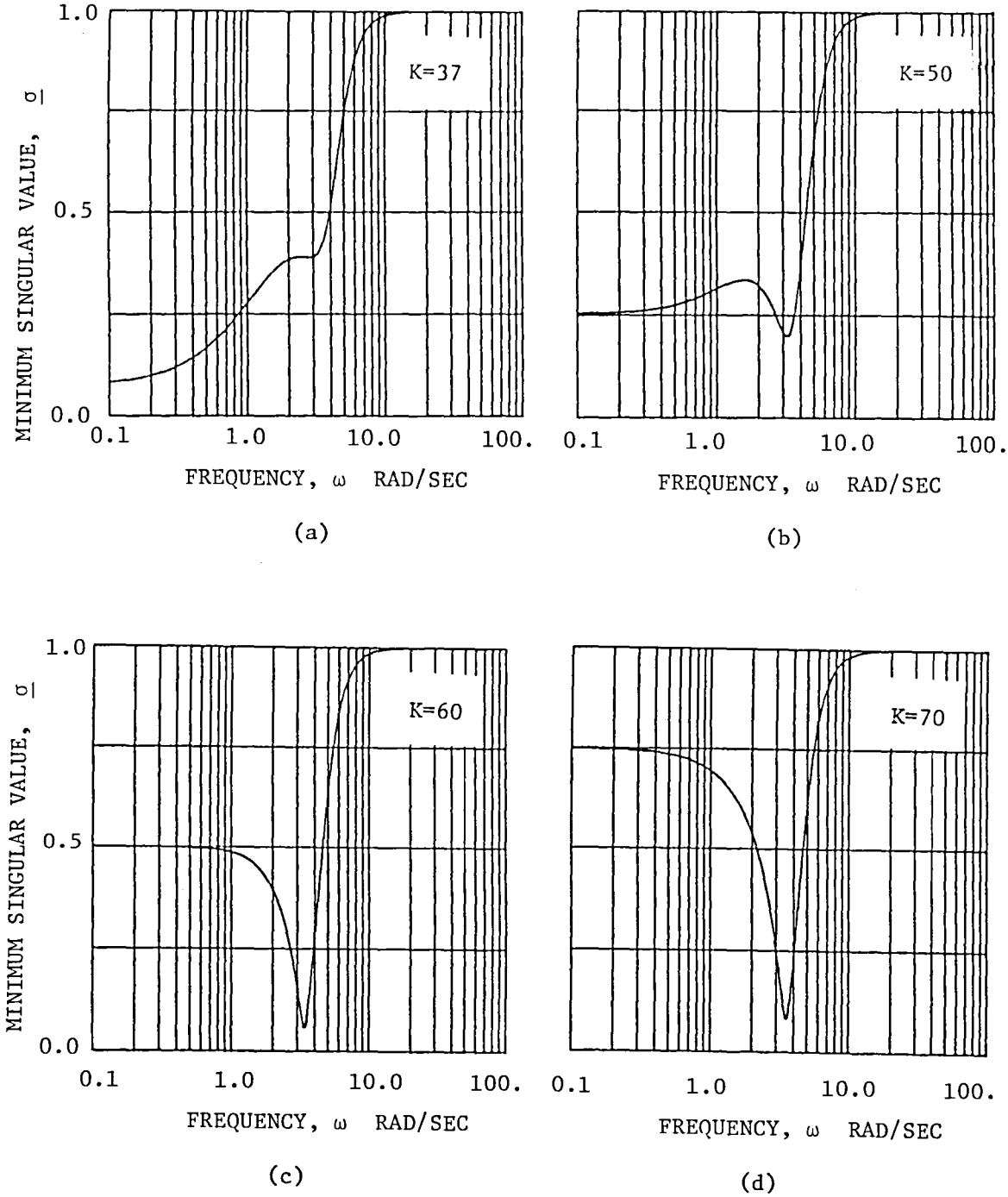

Figure 3.10: Sigma-Plots of the Third-Order System in Case II, for Several Feedback Gains

has increased while that of the complex poles has decreased. This trend continues for K = 70, where the "high-frequency" part of the curve has bounced up after reaching $\underline{\sigma} = 0$ at the crossing of the $j\omega$-axis by the complex poles.

Note that, if the analyst looks at the sigma plot for K = 70, he may erroneously conclude that the GM of the system is given by the minimum singular value at the "high-frequency" range of the curve in the direction of increasing gains. It is necessary to look at the closed-loop eigenvalues of the system to determine where the system stands from the absolute stability point of view.

The PM and GM from the Bode analysis are compared, in Table 3.2, with the stability margins from the sigma-plot analysis. The conservativeness of the sigma-plot analysis is again apparent from the comparison.

From the two examples presented, the following conclusions can be drawn:

1) The PM and GM obtained from singular values are conservative when compared to the Bode-plot stability margins.

2) In simple systems as the ones presented, the effect of the poles at different frequencies can be detected from the sigma plots.

3) It is not possible to determine if a system is stable by looking only at the sigma plots. The stability margins merely tell the designer how far the system (or a particular pole) is from the stability boundary.

Table 3.2: Comparison of Stability Margins
from the Bode and Sigma-Plot Analyses,
for Case II

Feedback Gain	K = 37	K = 50	K = 60	K = 70
From Bode Analysis				
GM, dB	$-\infty$ to 0.677	$-\infty$ to 2.16	$-\infty$ to 0.57	-0.765 to ∞
PM, deg	∞	18.25°	6.50°	-7.63°
From σ-Plot Analysis				
$\underline{\sigma}$	0.075	0.196	0.0547	0.0802
GM, dB	-0.63 to 0.67	-1.55 to 1.89	-0.463 to 0.489	-0.67 to 0.726
PM, deg	±4.29°	±11.24°	±4.59°	

4) The sigma plot information must be complemented by the determination of the closed-loop eigenvalues. If the system is SISO, the root locus is of great help.

3.2.2 Single-Input/Single-Output Yaw Damper for a Typical Business Jet

Yaw damping stability augmentation system (SAS) is employed when the dutch roll mode of an airplane is poorly damped and when an analysis of the stability derivatives shows that increasing C_{n_r} is the most effective way to improve dutch-roll damping [31]. This is the case with many business and general aviation airplanes, particularly on final approach.

To prevent the yaw damper from interfering with the pilot in turn entries and in steady turns, a washout circuit is usually added [31]. The washout filter assures that the rate-gyro output is effective as a feedback signal only during transient motions, by filtering out low-frequency signals and allowing the passage of only high frequency signals.

The yaw damper system presented in this section was obtained from Reference [31]. The airplane aerodynamic and inertial characteristics, and the flight condition data needed for the yaw damper design, are those of the business jet contained in Appendix B of this report. The handling qualities requirements for a typical business jet on dutch-roll damping, and time to double amplitude for

the spiral mode, are shown in Table 3.3. The open-loop airframe characteristics are also shown in Table 3.3, along with the open-loop eigenvalues. Note that the airframe dutch-roll damping is very low; also, although the spiral mode is slightly unstable, this mode is of no concern, due to the large time to double amplitude.

The root locus and block diagram for the yaw damper are shown in Figure 3.11. A gain of K = 1.3 is selected to maximize the dutch-roll damping. The system has a positive feedback, due to the negative gain in the r/δ_R transfer function; and therefore the ± 0 deg criterion applies when determining the GM from the frequency response plot shown in Figure 3.12. The system is unstable in the spiral mode; but without looking at the root locus or closed-loop eigenvalues, it is not possible to determine this from the Bode plot. The GM and PM for the dutch-roll mode are

GM = $-\infty$ to 10.6 dB

PM = -97° and 50.4°.

The sigma plot for this system is shown in Figure 3.13, which gives GM and PM of

GM = -4.3 to 9.03 dB

PM = ±38°

for $\underline{\sigma} = 0.6466$. The GM obtained from the sigma plot analysis is very conservative in the negative direction (decreasing gain) and less conservative in the positive (increasing gain) direction. The PM appears to be very conservative in both directions. Note that for low frequencies ($\omega < 0.02$ rad/sec) the sigma plot approaches $\underline{\sigma} = 1$ asymptotically. This means that for the low-frequency pole

Table 3.3: Handling Quality Requirements and Open-Loop Airframe Characteristics for a Typical Business Jet

Flight Condition: Final Approach; Cat. C, Class II, Level 1

	Minimum Time to Double Amplitude, T_{2_S}	Minimum Dutch Roll Damping, ζ_D	Minimum $\zeta_D \omega_{n_D}$	Minimum ω_D	Maximum Roll Time Constant T_R
Handling Quality Requirement	20 secs	0.08	0.15 rad/sec	0.4 rad/sec	1.4 sec
Open-Loop Characteristics	185.2 secs	0.00239	0.00263 rad/sec	1.10 rad/sec	1.20 sec

Open-Loop Eigenvalues

Dutch-roll poles: $-0.00263 \pm 1.101j$
Roll pole: -0.83178
Spiral pole: $+0.003743$

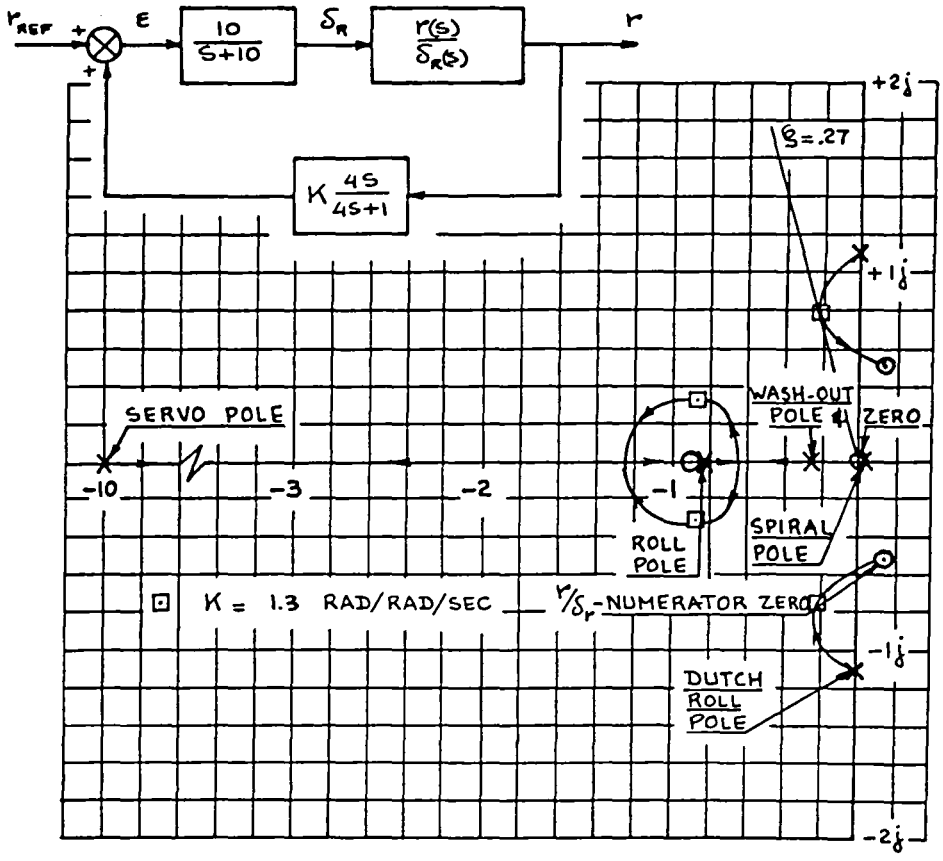

Yaw-Rate-To-Rudder Transfer Function:

$$\frac{r}{\delta_R}(s) = -0.708 \frac{(s + 0.912)[(s - .136)^2 + (.521)^2]}{(s + 0.832)(s - .004)[(s + .0031)^2 + (1.10)^2]}$$

Figure 3.11: Yaw Damper Root Locus for a Business Jet (taken from Reference [31])

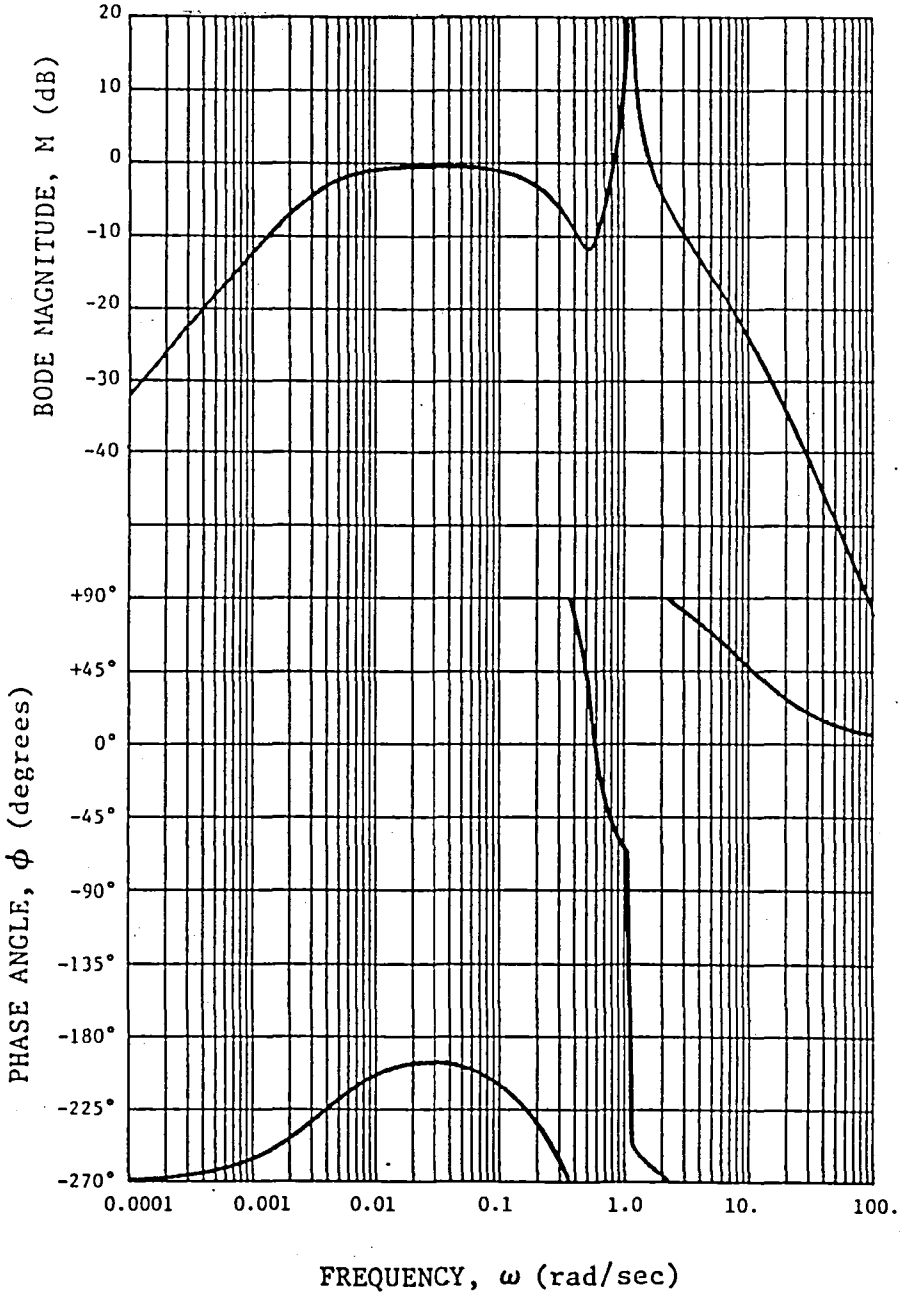

Figure 3.12: Frequency Response for a Yaw Damper with Washout Filter $(4s/(4s + 1))$ for a Typical Business Jet, K = 1.3

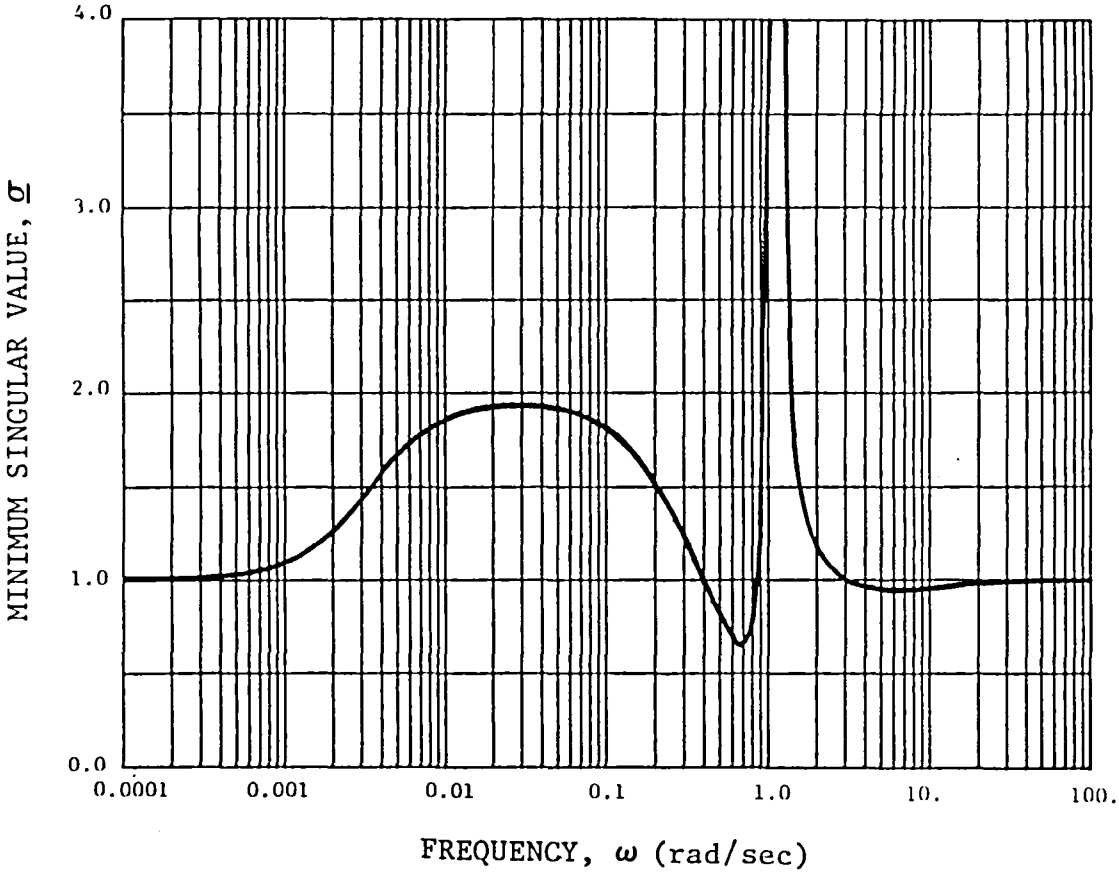

Figure 3.13: Singular-Value Plot for Yaw Damper with Washout Filter $(4s/(4s + 1))$ for a Typical Business Jet, K = 1.3

the GM is about -6 dB and ∞ in the decreasing and increasing gain directions, respectively, as determined from Figure 3.4.

A second yaw-damper design was tested in which the washout filter was replaced by a lead-lag filter to allow the spiral root to move into the stable region of the s-plane. In this manner, it was possible to compare an unstable system with a stable one. The lead-lag filter used was $(4s + 0.04)/(4s + 1)$; the Bode plot for gain $K = 1.3$ is shown in Figure 3.14. Observe that, in this case, the low-frequency part of the curve crosses over the 0 dB line, indicating that the spiral root has crossed to the left-hand side of the s-plane for the particular gain chosen ($K = 1.3$).

At a high frequency (dutch-role poles) there is not much difference between the design with the lead-lag filter and the one with the washout filter. The GM and PM for the dutch-roll mode are

GM = $-\infty$ to 10.2 dB

PM = 46.8° to -99°.

For the spiral mode, the margins are

GM = -8.4 dB to ∞

PM = 212.

The sigma plot (Figure 3.15) yields a $\underline{\sigma} = 0.6523$ for the high-frequency poles, which corresponds to

GM = -4.36 to 9.18 dB

PM = ±38.07°

and a "relative minimum" $\underline{\sigma}_R = 1.587$ at low frequency ($\omega \approx 0.0$ rad/sec), which gives

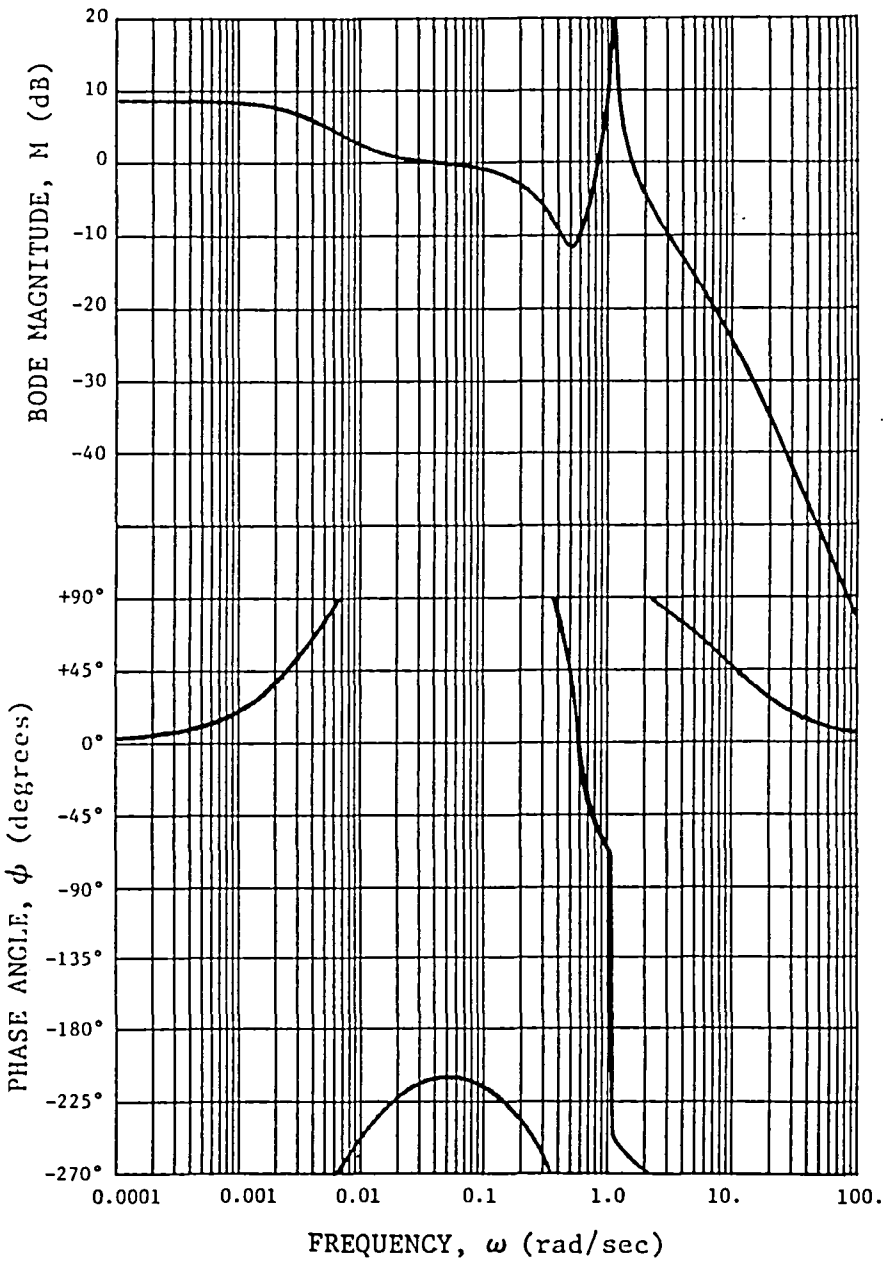

Figure 3.14: Frequency Response for a Yaw Damper with Lead-Lag Filter (4s + 0.04)/(4s + 1) for a Typical Business Jet, K = 1.3

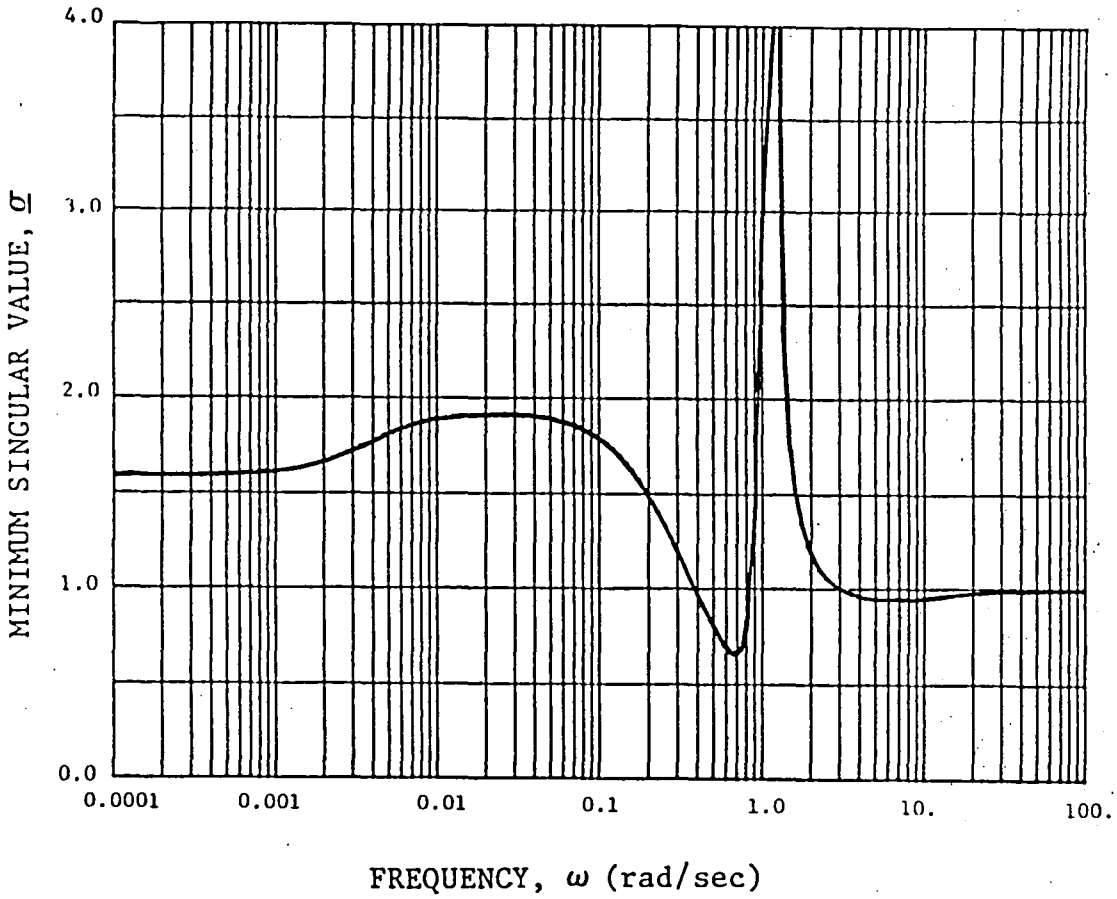

Figure 3.15: Singular-Value Plot for a Yaw-Damper with Lead-Lag Filter $(4s + 0.04)/(4s + 1)$ for a Typical Business Jet, $K = 1.3$

GM = -8.25 dB to ∞

PM = $\pm 105°$.

In both cases the stability margins obtained from the sigma plot analysis are conservative with respect to the Bode plot analysis. Note that the low-frequency part of the sigma plot has shifted upward in relation to the plot in Figure 3.13; it is evident that the sigma plot alone is not enough to understand what is happening with the system.

To demonstrate the effects of the spiral root more clearly, the gain was changed from K = 1.3 to K = 0.65 for the yaw-damper design with lead-lag filter. The gain change reduced the GM for the low-frequency range of the curve, as shown in the Bode plot of Figure 3.16. The same effect is detected in the sigma plot (Figure 3.17) by a downward movement of the low-frequency range of the curve. In this case, the minimum $\underline{\sigma}$ has become the one at low frequency with $\underline{\sigma} = 0.2932$, while the former minimum has become a "relative-minimum" with $\underline{\sigma}_R = 0.794$. Therefore, at K = 0.65, the spiral pole is closer to instability than the dutch-roll poles.

In the following section, the yaw-damper design is augmented with a roll damper to improve the dutch-roll damping beyond what was achieved with the yaw-damper system. This arrangement also provides the opportunity to analyze a multiloop control system.

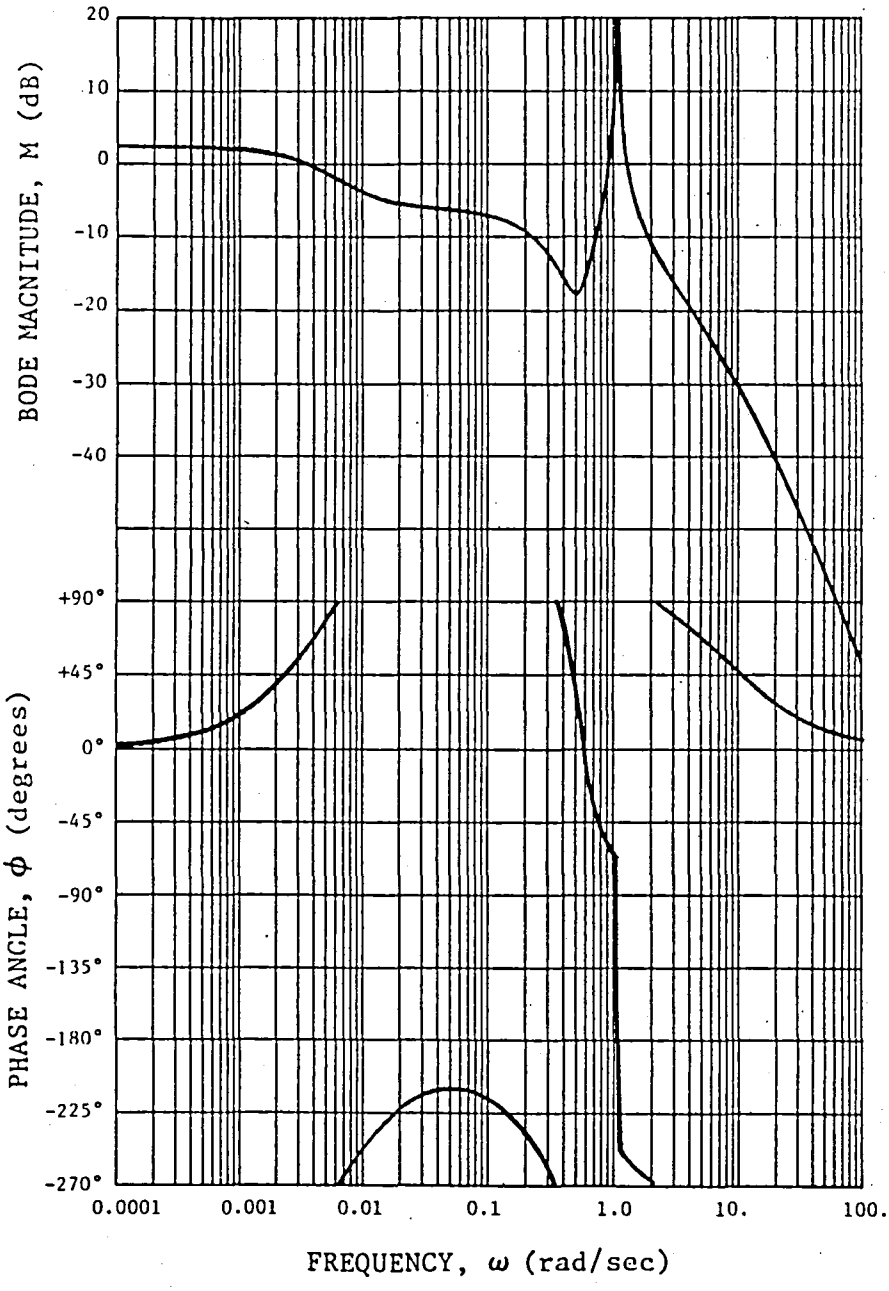

Figure 3.16: Frequency Response for a Yaw Damper with Lead-Lag Filter (4s + 0.04)/(4s + 1) for a Typical Business Jet, K = 0.65

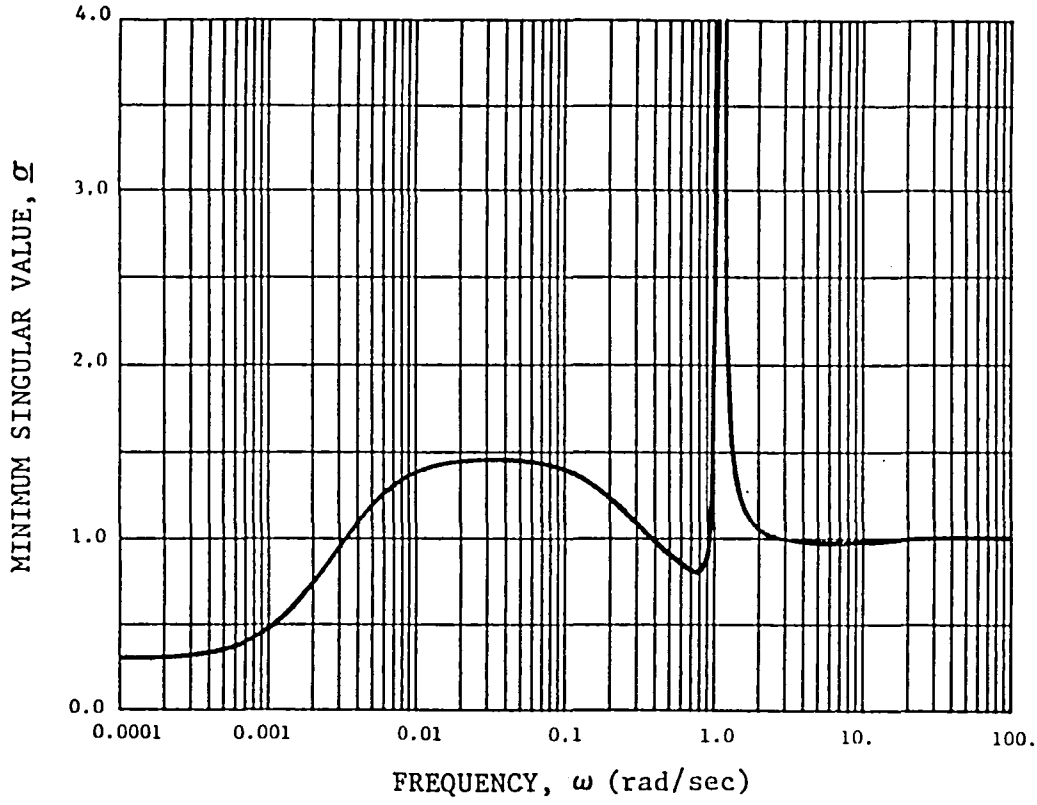

Figure 3.17: Singular-Value Plot for a Yaw-Damper with Lead-Lag Filter (4s + 0.04)/(4s + 1) for a Typical Business Jet, K = 0.65

3.2.3 A Multiloop Yaw/Roll Damper System for a Typical Business Jet

The yaw/roll-damper system for the business jet in Appendix B is shown in Figure 3.18. A plot showing how the locus for the dutch-roll poles changes for several values of roll-damper-loop gain, K_{δ_A}, is contained in Figure 3.19. A gain of $K_{\delta_R} = 1.0$ for the yaw-damper loop, and a gain of $K_{\delta_A} = 0.2$ for the roll-damper loop were chosen for the multiloop design.

Traditionally, the multiloop design would be analyzed using a frequency response method (example: Bode plot) following a one-loop-at-a-time approach. This situation is depicted schematically in Figure 3.20. The GM and PM of each loop are each obtained independently, by "closing" the other loop with its respective design values and reducing it as part of the dynamics of the loop being analyzed. In this manner, the stability margins of either loop can be estimated when that particular loop is subjected to uncertainties, and assuming that the parameters of the other loop are kept constant. The problem with this approach is that the analysis will not give any information on the stability margins of the whole system when subjected to simultaneous gain or phase uncertainties in both loops. It can be expected that the stability margins for each loop are dependent, to some degree, on the actual parameters of the other loop. This is a case in which the use of the sigma-plot analysis is useful in determining the multiloop stability margins.

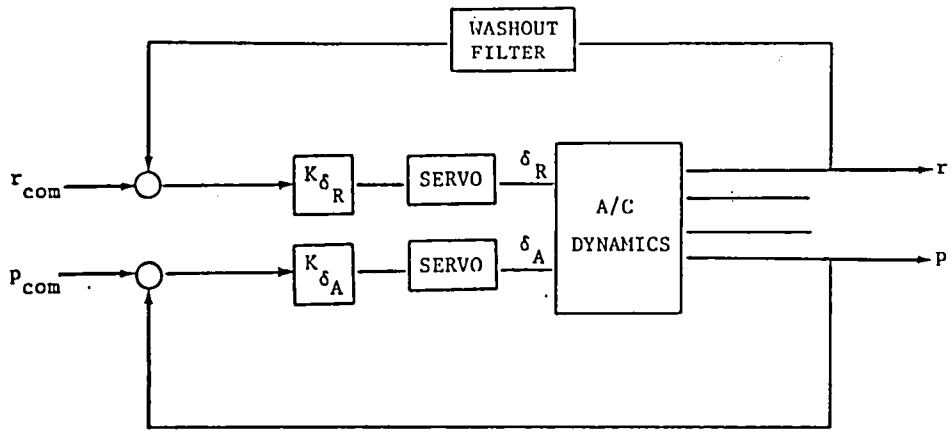

Figure 3.18: Block Diagram for Yaw/Roll Damper System for a Typical Business Jet

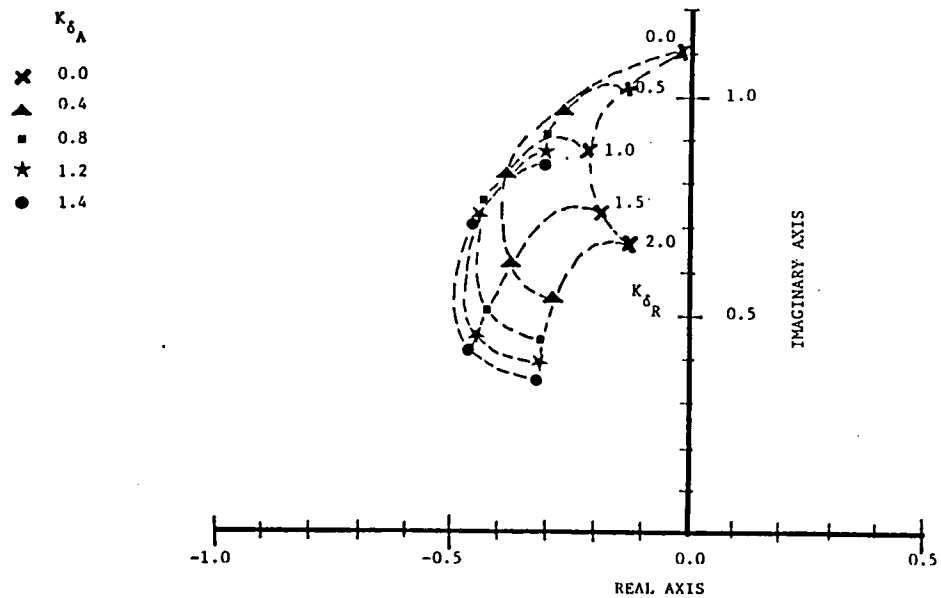

Figure 3.19: Change of the Locus of Dutch-Roll Poles with Roll-Damper-Loop Gain, K_{δ_A}.

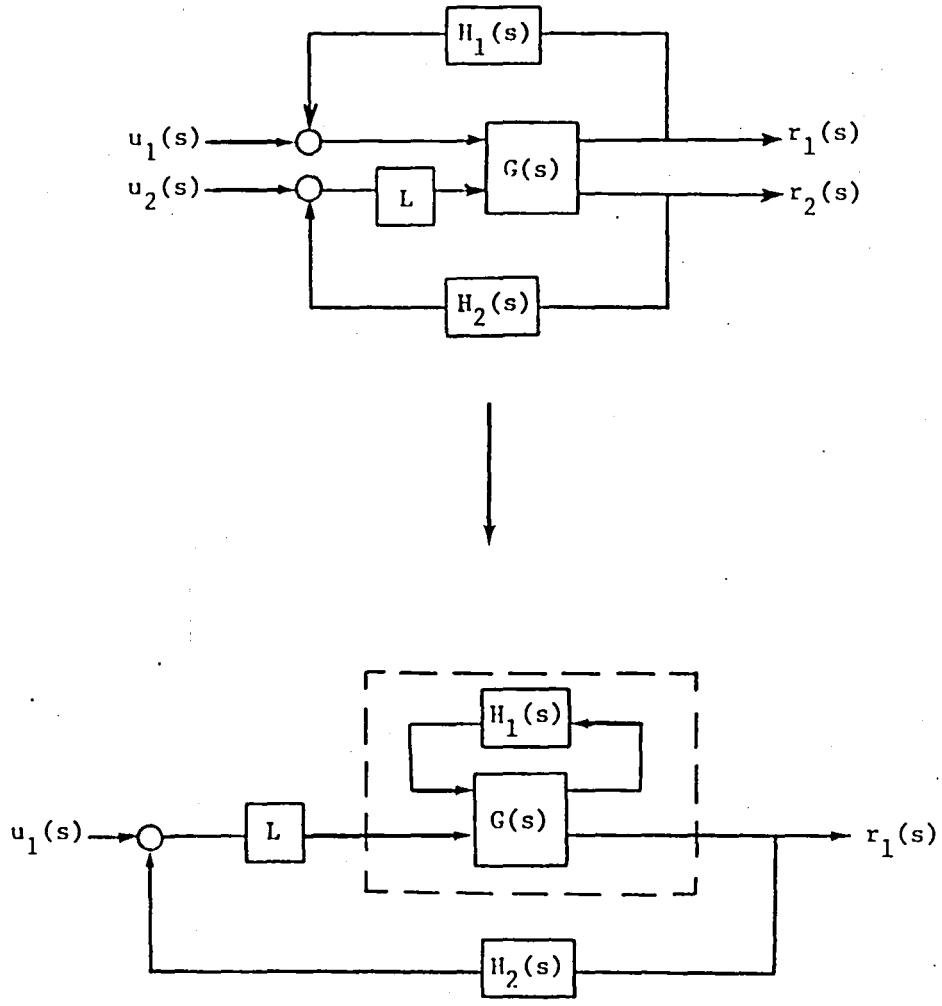

Figure 3.20: Reduction of a Multiloop Control System to a Single-Loop System to Carry Out the One-Loop-at-a-Time Frequency Response Analysis

In order to explore how the sigma-plot analysis compares to the traditional one-loop-at-a-time Bode analysis, the following analyses were made:

1) Frequency response of the yaw-damper loop with the roll-damper loop "closed" at the design gain value $K_{\delta_A} = 0.2$.

2) Sigma-plot analysis for case (1) above. Note that this is not the multiloop analysis but a one-loop-at-a-time sigma-plot analysis used to explore how the Bode and sigma-plot analyses compare.

3) Frequency response of the roll-damper loop with the yaw-damper loop closed at the design gain value $K_{\delta_R} = 1.0$.

4) Sigma-plot anlaysis for case (3) above.

5) Multiloop sigma-plot analysis.

6) Eigenvalue-plot analysis.

In the eigenvalue-plot analysis, the minimum magnitude of the eigenvalues of the return difference matrix, $(I + G_1)$, is plotted along with the minimum singular values for a range of frequencies. By substituting the minimum and maximum magnitudes of the eigenvalues for the minimum and maximum singular values respectively in Equation (3.10), less conservative PM and GM can be obtained [27].

The frequency response analysis for the yaw-damper loop in Figure 3.21 ($\pm 0°$ criterion) gives

GM = $-\infty$ to 21 dB at ω = 0.49 rad/sec

PM = $+90°$ at ω = 0.87 rad/sec

$-108.4°$ at ω = 1.42 rad/sec.

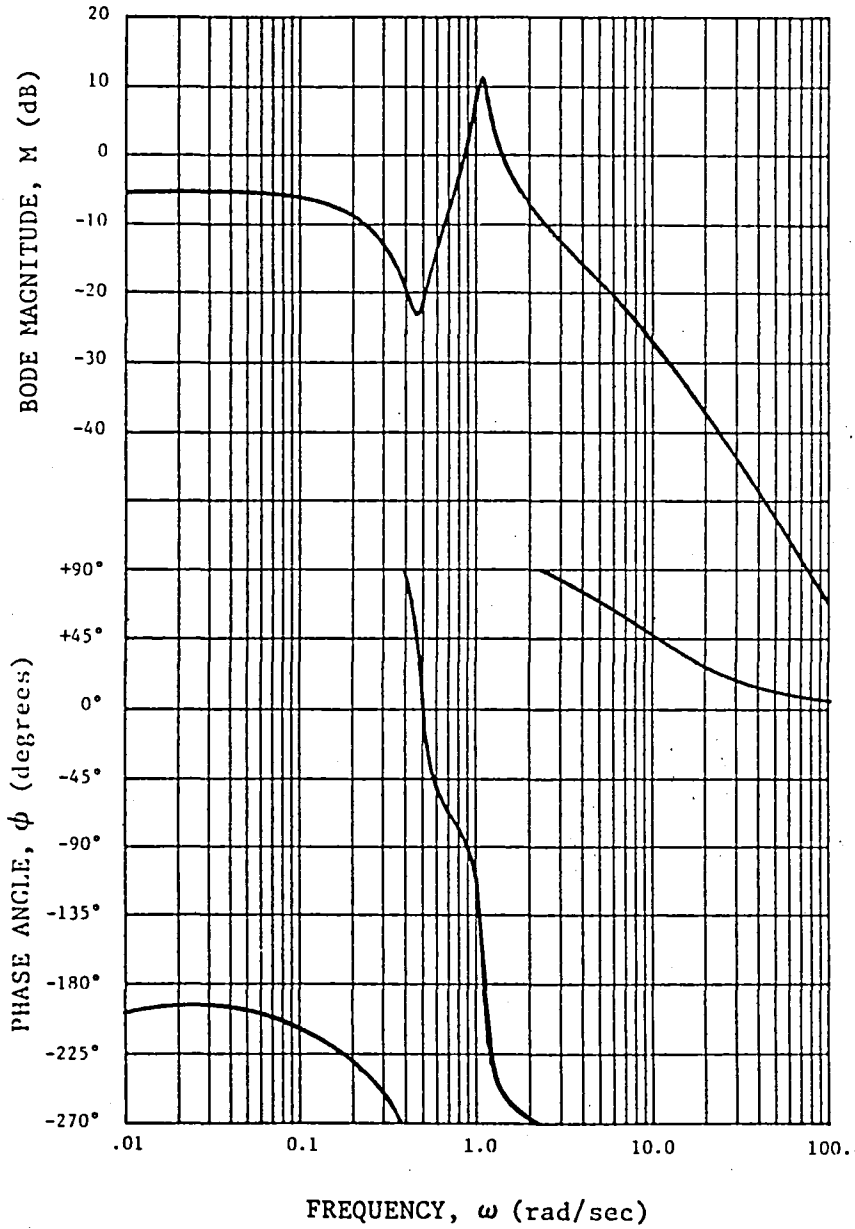

Figure 3.21: Frequency Response of the Yaw-Damper Loop of a Yaw/Roll Damper Multiloop System for $K_{\delta_R} = 1.0$. (This "single-loop" analysis includes the roll-damper loop, closed at $K_{\delta_A} = 0.2$, in the dynamics of the yaw-damper loop.)

The corresponding sigma plot in Figure 3.22 shows

$\underline{\sigma}$ = 0.8862 at ω = 0.547 rad/sec

GM = -5.51 to 18.87 dB

PM = ±52.6°.

The stability margins from the sigma-plot analysis are conservative compared to the frequency response analysis: the GM is very conservative in the direction of decreasing gains, and the PM is very conservative in both directions. Note that the frequency for minimum $\underline{\sigma}$ does not match any of the crossover frequencies but lies at a slightly different frequency; this is usually the case [20, 34] and can be explained by the fact that the singular-value analysis accounts for simultaneous changes in phase and gain. If we look at the frequency response plot, at the frequency for minimum $\underline{\sigma}$ (ω = 0.547) the worst direction of simultaneous gain and phase change is found to be about 18 dB and 38° [20, 34]. If now we look at the phase crossover frequency (ω = 0.49 rad/sec) on the sigma plot, we find that the predicted GM is 21 dB, matching the GM from the Bode analysis [20].

Similarly for the roll-damper loop, the frequency reponse in Figure 3.23 (±180° criterion) shows

GM = $\pm\infty$

PM = $\pm\infty$

while the sigma-plot analysis in Figure 3.24 shows

$\underline{\sigma}$ = 0.97237

GM = -5.89 to 31.17 dB

PM = ±58°.

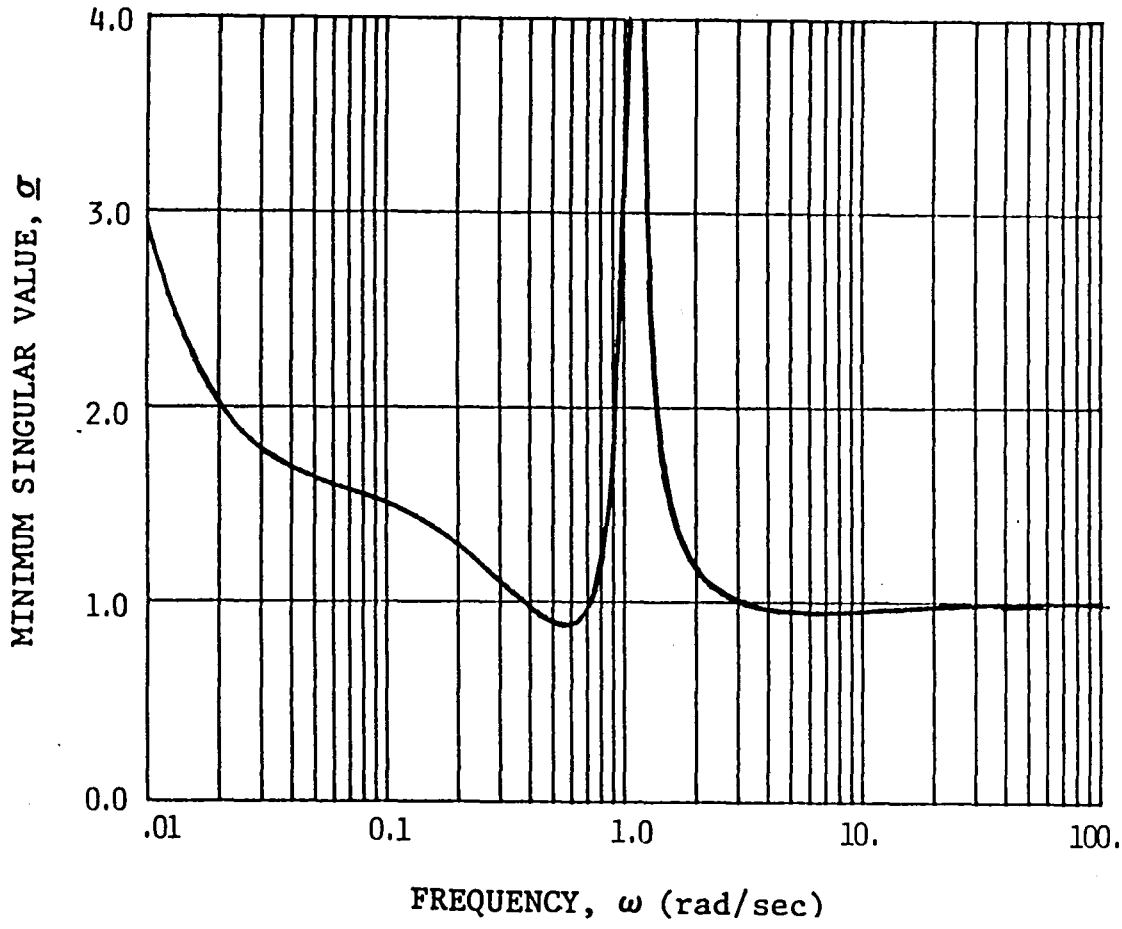

Figure 3.22: Singular-Value Plot for Yaw-Damper Loop of a Yaw/Roll Damper Multiloop System, for $K_{\delta_R} = 1.0$ and Roll-Damper Loop Gain, $K_{\delta_A} = 0.2$

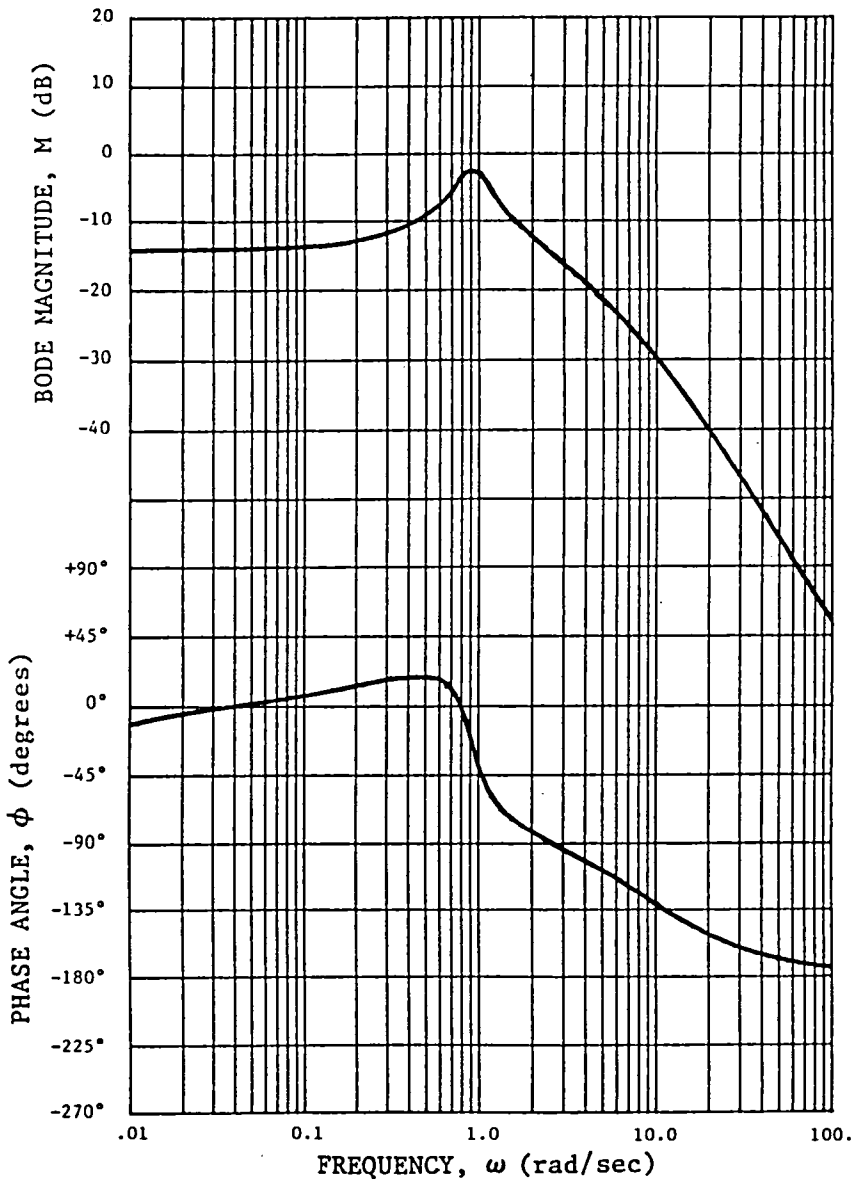

Figure 3.23: Frequency Response for Roll-Damper Loop of a Yaw/Roll Damper Multiloop System, for K_{δ_R} = 1.0 and Roll-Damper Loop Gain, K_{δ_A} = 0.2

Similar conclusions can be drawn for this analysis as for the yaw-damper loop analysis, and they will not be repeated here.

The next analysis of interest is given by the multiloop singular value plot. Figure 3.25 shows the sigma plot (lower curve) and the eigenvalue plot. Two things are apparent from the multiloop sigma plot: the minimum $\underline{\sigma}$ is much smaller than either of the two previous single-loop minimum $\underline{\sigma}$ of Figures 3.22 and 3.24. This means that, according to the multiloop analysis, the stability margins are smaller than the ones obtained through the one-loop-at-a-time approach. The multiloop margins obtained are

$$GM = -3.53 \text{ to } 6.05 \text{ dB}$$

$$PM = \pm 29.1°$$

for $\underline{\sigma} = 0.502$ at $\omega = 0.76$ rad/sec.

The important characteristic of these multiloop margins is that they represent the limits within which the gains or the phases of the two feedback loops may be changed simultaneously and independently without destabilizing the closed-loop system. In other words, K_{δ_R} can be changed by +5 dB while K_{δ_A} is changed by -3 dB, and the system would still be stable. Furthermore, if we were interested to know the permissible range for gain variations considering that the phases may simultaneously change within ±20°, Figure 3.4 could be used to obtain a GM = -2.2 to 4.8 dB.

The upper curve in Figure 3.25 is a frequency plot of the minimum magnitude of the eigenvalues of $(I + G_1)$, which represents an upper boundary of the $\underline{\sigma}(I + G_1)$ plot [20, 21]. The

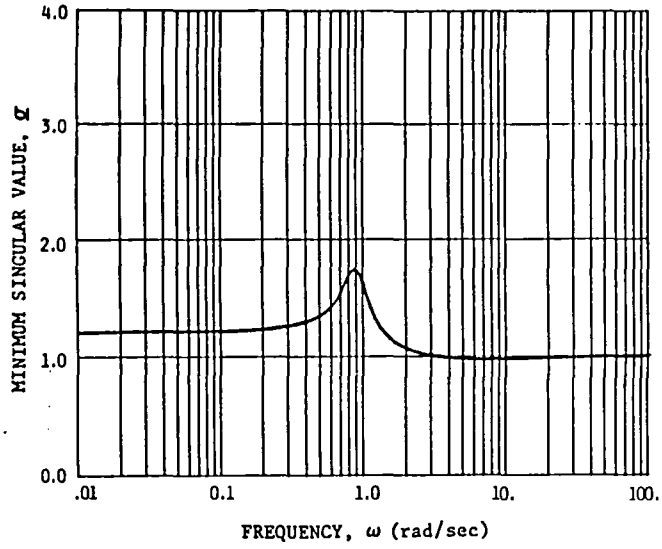

Figure 3.24: Singular-Value Plot for Roll-Damper Loop of a Yaw/Roll Damper Multiloop System, for K_{δ_A} = 0.2 and Yaw-Damper Loop, K_{δ_R} = 1.0

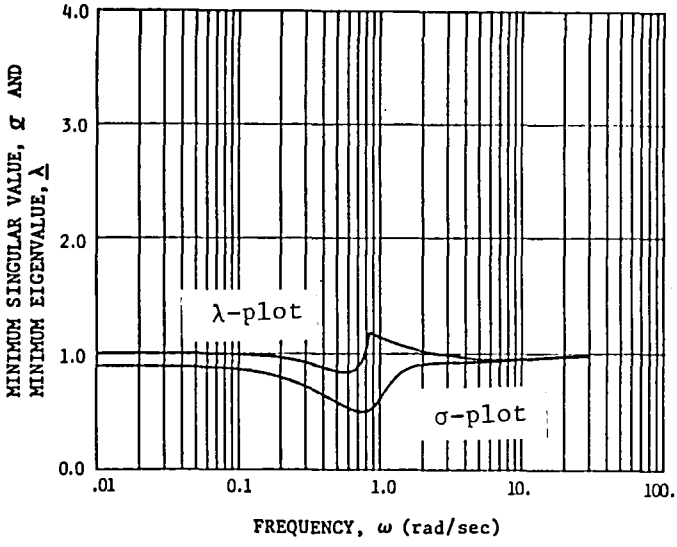

Figure 3.25: Multiloop Singular-Value and Eigenvalue Plot for Yaw/Roll Damper System with Yaw-Damper Loop Gain, K_{δ_R} = 1.0, and Roll-Damper Loop K_{δ_A} = 0.2

$\min|\lambda_i(I + G_1)|$ represents the radial distance of the eigenvalue closest to the origin and is a measure of the closeness of $(I + G_1)$ to singularity in a limited sense; i.e., for uniform perturbations of gain or phase in each of the loops.

By uniform perturbations, it should be understood that if the perturbation matrix, L, is given as in Equation (3.7)

$$L = \begin{bmatrix} k_1 e^{j\phi_1} & & & \\ & k_2 e^{j\phi_2} & & \\ & & \ddots & \\ & & & k_n e^{j\phi_n} \end{bmatrix} \qquad (3.7)$$

and if the gain change in one loop is k_j, then the gain changes in the remaining loops must also be given by $k_i = k_j$, for i = 1,n. The same restriction applies to the simultaneous variations in phase in each loop [27]. Yeh, et al. [27], claim that this is the least conservative computation that is possible when a norm-bounded robust stability criterion is used.

Mukhopadhyay and Newsom [20] propose the use of the eigenvalue plot to obtain a set of "relaxed-stability" margins, where the gain or phase in each loop can be allowed to change in any manner within the prescribed limits. The only shortcoming of these limits is that the stability of the closed-loop system is not always guaranteed, unless the phase or gain variations are uniform in the sense described by Yeh, et al. [27].

Independently of how the limits obtained from the eigenvalue plot are interpreted (uniform or nonuniform), they are given by

GM = -5.29 to 15.88 db

PM = ±49.6°

for $\min|\lambda_i|$ = 0.839 at ω = 0.566 rad/sec.

Observe that these margins are considerably less conservative than the ones obtained from the multiloop sigma plot, although still conservative compared to the Bode analysis.

The plot in Figure 3.26 contains the actual stability boundary for the dutch-roll mode of the airplane, for combinations of gains in the yaw- and roll-damper loops, and assuming no variations in phase. For a simple example like the one presented here, this stability boundary can be calculated very easily by an iterative procedure. For a more complex problem, the calculation of the actual stability boundary is very cumbersome; however, this example allows us to show a very interesting and important situation.

The design point is given by K_{δ_R} = 1.0 and K_{δ_A} = 0.2. The stability boundary given by the ABCD block contains the combinatins of K_{δ_R} and K_{δ_A} which, according to the Bode analysis, will not destabilize the system (point D is not shown in the figure; it lies at $K_{\delta_A} = \infty$ and $K_{\delta_R} \cong 0.5$. This situation is also present in the other boundary blocks to avoid overcrowding the figure.) Note that, for the large amount of possible combinations of K_{δ_R} and K_{δ_A} that lie to the right of the curve, the dutch-roll mode will be unstable. This situation is not detected by doing a one-loop-at-a-time Bode analysis.

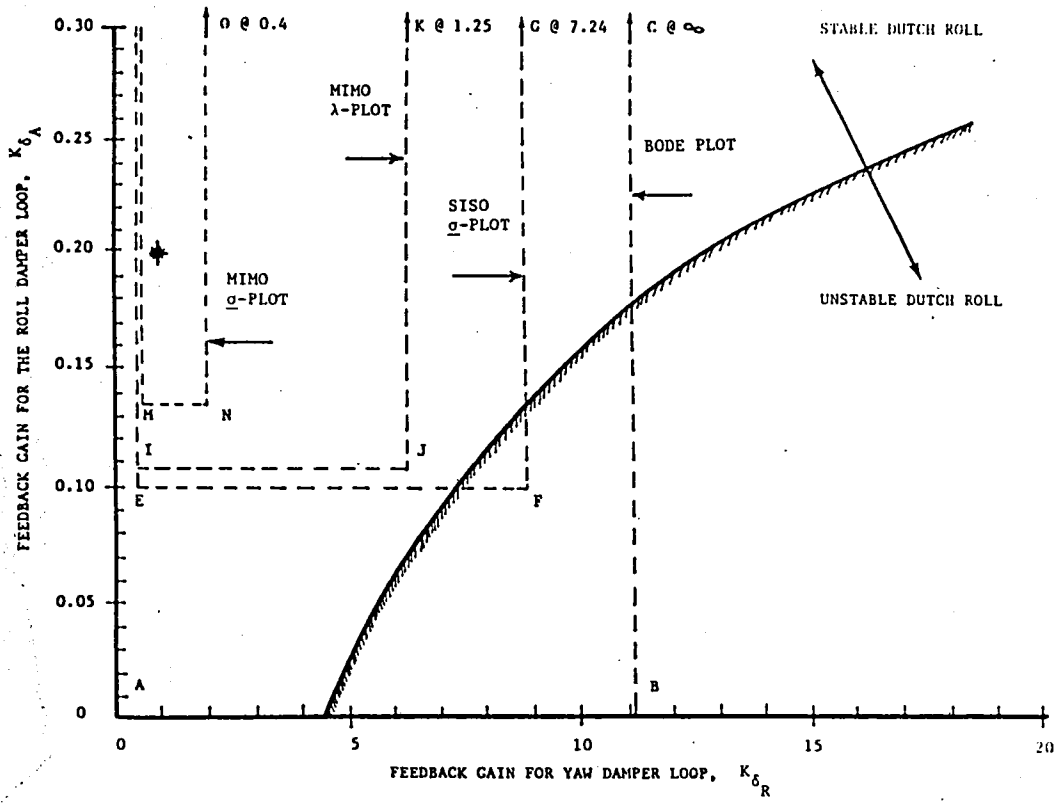

Figure 3.26: Comparison of Predicted and Actual Stability Boundaries for the Dutch-Roll Poles of a Business Jet. (Block MNOP represents the boundary predicted by the multiloop singular-value analysis.)

Boundary EFGH (point H is not shown) is given by the "SISO" singular-value analysis. The amount of unstable combinations of K_{δ_R} and K_{δ_A} that have not been predicted has been reduced considerably due to the conservativeness of the margins; however, since it does not account for simultaneous variations of gains in both loops, stability is not always guaranteed.

Boundary IJKL (point L is not shown) is given by the "relaxed-stability" margins obtained using the eigenvalue plot instead of the sigma plot. Although stability is generally not guaranteed unless K_{δ_R} and K_{δ_A} change by the same factor, for our present example there are no possible unstable combinations of K_{δ_R} and K_{δ_A}. Therefore, in this case, the relaxed-stability margins seem to provide the least conservative approach to the determination of the multiloop stability margins. However, it is very important to remember that we have assumed that there is no change in the phase of each loop. If we considered simultaneous phase and gain changes, the limits would be reduced.

The most conservative of the limits are given by the multiloop sigma-plot analysis and are represented by block MNOP (point P is not shown). Although very conservative, these limits guarantee that the closed loop system will be stable when the gains are varied, in any manner, within the limits. In this case it has also been assumed that there is no change in phase; otherwise, the limits would be reduced further.

3.2.4 A Sampled-Data Yaw-Damper System for a Typical Business Jet

This section explores briefly the application of the singular-value concepts to a sampled-data yaw-damper SAS. The system is represented in the block diagram of Figure 3.27. The transfer function, $r(s)/\delta_R(s)$, is the same as for the continuous system given in Figure 3.11.

The fundamental concepts of the singular value analysis presented in Section 3.1 are also applicable to sampled data systems; i.e., the stability condition is given by

$$\underline{\sigma}(I + G_1(z)) > 0 \tag{3.15}$$

where $G_1(z)$ is evaluated at

$$z = e^{j\omega T} \tag{3.16}$$

where z is the z-transform variable, and T is the sampling period [25]. However, the concepts of simultaneous phase and gain margins (Equations 3.12 and 3.13) were derived for continuous systems and there is no information in the literature relative to their applicability to sampled-data and discrete systems.

In the following analysis, no attempt was made to prove (or disprove) theoretically the applicability of Equations (3.12) and (3.13) to sampled-data systems. Instead, the concept of stability margins was explored by predicting the phase and gain margins, of a sampled-data yaw-damper SAS, using singular values and then comparing them with the phase and gain margins obtained from a frequency response in the w'-plane.

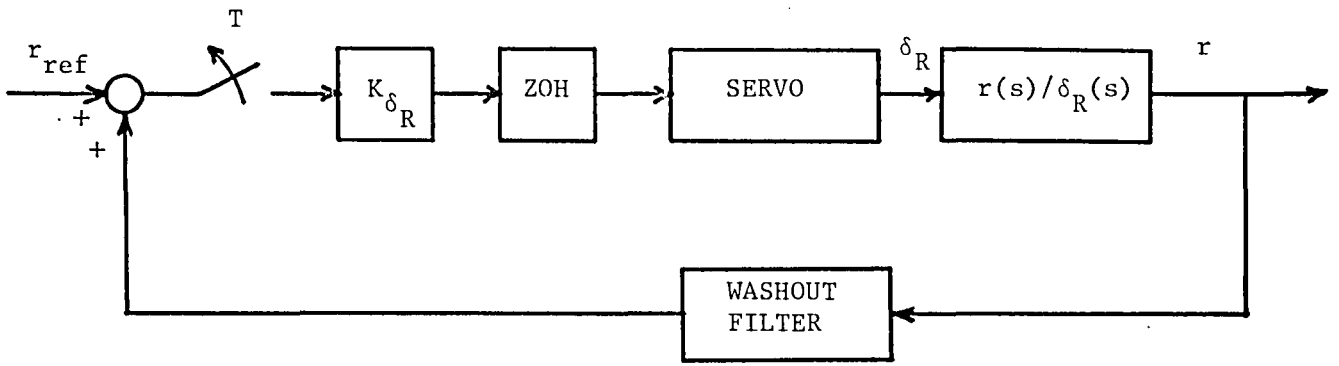

Figure 3.27: Block Diagram of the Sampled-Data Yaw-Damper SAS for a Typical Business Jet. (ZOH = zero-order hold.)

The transformation from the z-plane to the w'-plane is made by using [38]

$$w' = \frac{2}{T}\frac{z - 1}{z + 1} \tag{3.17}$$

This transformation is used to regain the resolution lost as z takes on values around the unit circle. Also the use of the w'-plane allows us to regain the simplicity of the Bode frequency response technique which is not present in the z-domain due to the nonrational nature of the discrete transfer functions, where the frequency appears in the form $z = e^{j\omega T}$.

The w'-transform of Equation (3.17) can also be expressed as

$$w' = \frac{2}{T}\frac{e^{sT} - 1}{e^{sT} + 1} = \frac{2}{T} \tan h \frac{sT}{2} \tag{3.18}$$

and, for the frequency response ($s = j\omega$) we have

$$w' = j\nu = j \frac{2}{T} \tan \frac{\omega T}{2} \tag{3.19}$$

and we see that while z goes around the unit circle, the w'-plane frequency, ν, stays real and goes from 0 to ∞.

The frequency response for the sampled-data yaw-damper SAS is shown in Figure 3.28 for a design gain of $K_{\delta_R} = 0.39$ and a sampling period of T = 0.3 seconds. The corresponding singular value plot is shown in Figure 3.29.

Note that the Bode plot is calculated in the w'-plane, and therefore the frequency in the horizontal axis of Figure 3.28 is the w'-plane frequency, ν. Although the singular value analysis is done using the s-plane frequency, ω, the horizontal axis in Figure 3.29

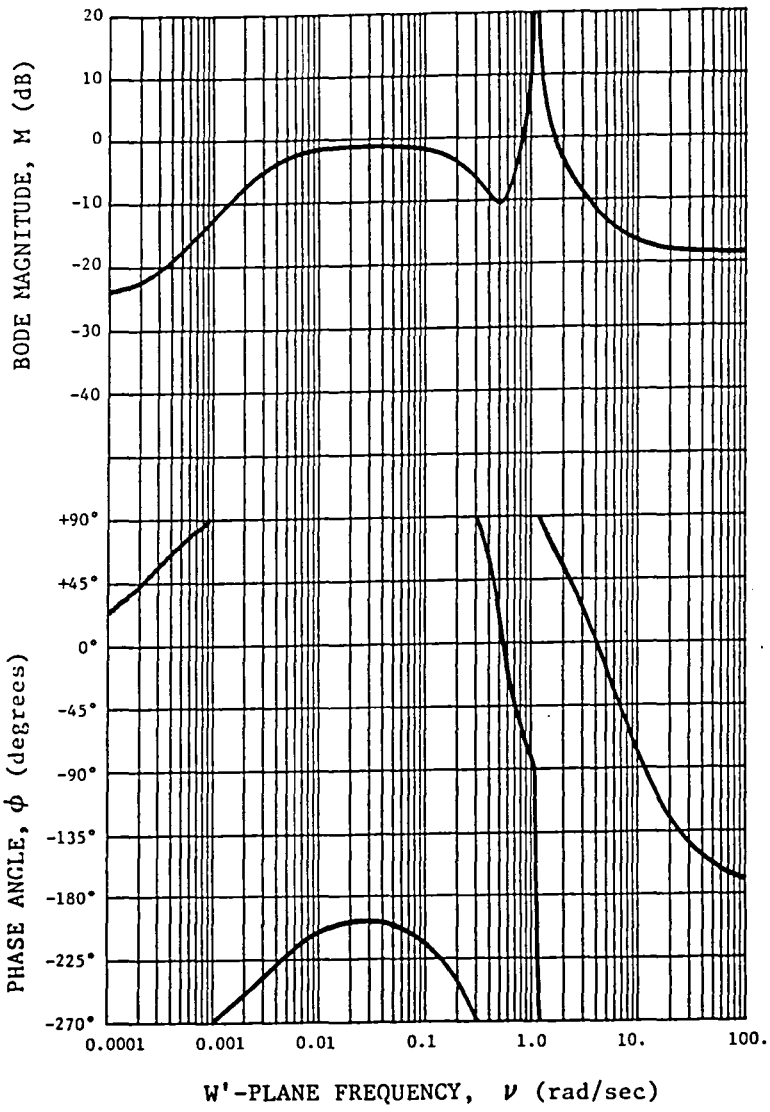

Figure 3.28: Frequency Response for Sampled-Data Yaw-Damper SAS with K_{δ_R} = 0.39 and T = 0.3 Seconds

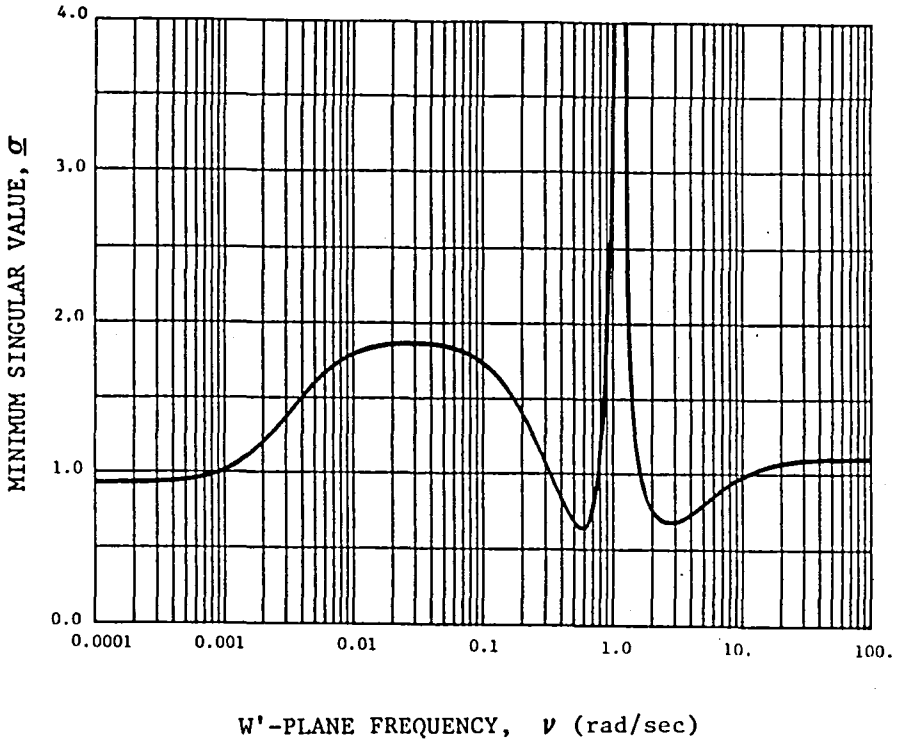

Figure 3.29: Singular-Value Plot for Sampled-Data Yaw-Damper SAS with $K_{\delta_R} = 0.39$ and T = 0.3 Seconds

also shows the w'-plane frequency, ν. This transformation was done using Equation (3.19) with the objective of having the Bode and sigma plots expressed as functions of the same frequency.

The stability margins from the frequency response computation are given by ($\pm 0°$ criterion)

$$GM = \begin{cases} -\infty \text{ to } 9.53 \text{ dB } @\ \nu = 0.5575 \text{ rad/sec} \\ \qquad\qquad (\text{or } \omega = 0.5562 \text{ rad/sec}) \\ -\infty \text{ to } 11.52 \text{ dB } @\ \nu = 4.107 \text{ rad/sec} \\ \qquad\qquad (\text{or } \omega = 3.68 \text{ rad/sec}) \end{cases}$$

$$PM = \begin{cases} 62.72^{\circ} @\ \nu = 0.8319 \text{ rad/sec} \\ \qquad (\text{or } \omega = 0.8277 \text{ rad/sec}) \\ -68.4^{\circ} @\ \nu = 1.6164 \text{ rad/sec} \\ \qquad (\text{or } \omega = 1.586 \text{ rad/sec}) \end{cases}$$

The predicted stability margins from the sigma plot (Figure 3.29) are

$$GM = -4.35 \text{ to } 9.12 \text{ dB}$$

$$PM = \pm 37.9°$$

for $\underline{\sigma} = 0.65007$ @ $\omega = 0.6015$ rad/sec ($\nu = 0.6032$ rad/sec)

As it occurrs in the continuous-system example (Section 3.2.2), the GM predicted from the singular value computation is very conservative in the direction of decreasing gains and only slightly conservative in the direction of increasing gains. The PM predicted is just as conservative as predicted for the continuous system in Section 3.2.2. In general, the relative stability of this sampled-data design is very similar to the relative stability of the continuous-system design of Section 3.2.2.

An important check on the correspondence between the stability margins from the Bode analysis in the w'-plane, and the stability margins predicted from the singular value analysis, is given by the fact that [20], for a SISO system, the stability margins predicted by the minimum singular values at the crossover frequencies (phase-and-gain-crossover frequencies) must match the stability margins from the Bode analysis. This correspondence is shown below to exist for the sampled-data yaw-damper SAS analyzed here:

Phase-Crossover Frequency, ν (rad/sec)	GM from Bode Plot (dB)	Predicted GM from Sigma Plot (dB)
0.5575	$-\infty$ to 9.53	-4.46 to 9.65
4.107	$-\infty$ to 11.52	-4.78 to 11.54

The match of GM in the increasing-gain direction is achieved within the accuracy permitted by the analysis. Note that no match exists for the GM in the decreasing-gain direction. This is also true for continuous systems, and we do not have an explanation for this occurrence at the present time. In the case of the PM's, the analysis shows

Gain-Crossover Frequency, ν (rad/sec)	PM from Bode Plot (degrees)	Predicted PM from Sigma Plot (degrees)
0.9319	62.72	±63.05
1.6164	-68.4	±68.4

Again, the match exists at least in one direction (decreasing or increasing phase).

From the results presented above, we feel that there is correspondence between the stability margins obtained from the w'-plane frequency response and those predicted from the sigma plot, for sampled-data systems. However, we suggest that further research should be carried out to prove the validity of Equations (3.12) and (3.13) when used in analyzing sampled-data systems. Also the conditions for such validity should be investigated.

Some important conclusions about the use of the multiloop singular-value analysis are as follows:

1) The use of the one-loop-at-a-time frequency response methods to analyze multiloop control systems does not allow the analyst always to detect instabilities which arise when simultaneous changes in gain or phase in each loop are considered.

2) The stability margins obtained from the singular-value analysis are very conservative in some directions compared to the limits obtained through the Bode-plot analysis; this applies to multiloop and SISO systems.

3) The use of the limits obtained from both the sigma- and eigenvalue-plot analysis seems to provide the best alternative, today, to the use of the SISO Bode plot in the analysis of multiloop control systems. The sigma plot provides a lower boundary while the eigenvalue provides the upper boundary to the relative stability of the multiloop systems. If these two plots are close together, the conservativeness of the analysis is small.

4) The use of the singular values in a way similar to the one-loop-at-a-time frequency response, in the analysis of multiloop systems, also provides some insight for potential problems that could arise with simultaneous changes in phase and gain in each loop.

5) The use of singular-value analysis to obtain stability margins of sampled-data systems seems feasible; however, more research is recommended in this area.

In this chapter we have presented the fundamental concepts of singular values and several SISO and MIMO control system examples to explore the use of the singular-value analysis and how it compares with the traditional Bode method. In the following chapter we present the derivation of the singular-value gradients and discuss the use of the sensitivity analysis technique developed. A simple third-order example is used to show how to interpret the informaton provided by the sensitivity analysis, and the multiloop yaw/roll damper system for the business jet is used to demonstrate how the method can be used in determining the important model parameters.

4. MULTILOOP SENSITIVITY ANALYSIS METHOD

In this chapter, expressions for the singular-value gradients are developed, and their use in a sensitivity analysis technique is discussed. The application of this sensitivity analysis technique is demonstrated with a simple third-order example and the multiloop yaw/roll damper system of the business jet in Appendix B.

4.1 MATHEMATICAL DEVELOPMENT OF THE SINGULAR-VALUE GRADIENTS

In order to determine the effect that changes in the system and controller parameters have on the relative stability of a closed-loop system, the derivatives of the singular values with respect to those parameters must be evaluated. Newsom and Mukhopadhyay [24] determined the gradients of the singular value $\underline{\sigma}(I + G_1)$, with respect to controller parameters, and used them to perform a numerical optimization to search for the controller design variables that increase the minimum singular value of the system return difference matrix.

For the present application what is desired is a measure of the effect on system relative stability caused by variations in the system and controller models. Therefore, the gradients of the singular value with respect to elements in the system and controller matrices are required.

Consider the state-space representation of the control system of Figure 3.1 to be given by

Plant:

$$\dot{\mathbf{X}} = \mathbf{AX} + \mathbf{BU} \tag{4.1}$$

$$\mathbf{Z} = \mathbf{TX} \tag{4.2}$$

Control Law:

$$\mathbf{U} = -\mathbf{KZ} + \mathbf{R} \tag{4.3}$$

Equation (4.1) represents a plant of order Ns having No output measurements, **Z**, modeled by Equation (4.2) and Nc control inputs, **U**. Equation (4.3) represents the feedback control law driven by the sensor output, **Z**, and reference input signal, **R**. In terms of transfer matrices (taking Laplace transforms), the control law is given by

$$\mathbf{U}(s) = -K[T(Is - A)^{-1}B]\mathbf{U}(s) + \mathbf{R}(s) \tag{4.4}$$

Therefore, the control input can be written as

$$\mathbf{U}(s) = \big(I + H(s)G(s)\big)^{-1}\mathbf{R}(s) \tag{4.5}$$

where $K = H(s)$ and $G(s) = [T(Is - A)^{-1}B]$.

Equations (4.1) to (4.3) can be written in an augmented form as

$$\dot{\mathbf{X}} = \bar{A}\mathbf{X} + \bar{B}\mathbf{U} \tag{4.6}$$

$$\mathbf{U} = -\bar{C}\mathbf{X} + \mathbf{R} \tag{4.7}$$

where $\bar{A} = A$, $\bar{B} = B$, and $\bar{C} = KT$. Then the Laplace transform of the control input can be expressed as follows (the argument "(s)" has been omitted):

$$\mathbf{U} = [I + \bar{C}(Is - \bar{A})^{-1}\bar{B}]^{-1}\mathbf{R} \tag{4.8}$$

and, therefore, the return difference matrtix, $(I + G_1)$, can also be represented as

$$(I + G_1) = \left(I + \bar{C}(Is - \bar{A})^{-1}\bar{B}\right) \tag{4.9}$$

In the case in which the control law includes controller dynamics, a similar derivation would be involved in the computation of $\bar{A}$, $\bar{B}$, and $\bar{C}$ matrices augmented with the controller dynamics.

The singular values of $(I + G_1)$ are σ_i, and the corresponding right and left normalized eigenvectors are $\mathbf{v_i}$ and $\mathbf{u_i}$, respectively [20, 24]. Hence by definition

$$(I + G_1)\mathbf{v_i} = \mathbf{u_i}\sigma_i \tag{4.10}$$

$$(I + G_1)^* \mathbf{u_i} = \mathbf{v_i}\sigma_i \tag{4.11}$$

for i = 1, 2, ... Nc, where A^* means the conjugate transpose of A.

The normalized eigenvectors satisfy the following orthogonal properties:

$$\mathbf{u_i}^* \mathbf{u_j} = \delta_{ij} \text{ and } \mathbf{v_i}^* \mathbf{v_j} = \delta_{ij} \tag{4.12}$$

where δ_{ij} is the Kroneker delta which is unity when i = j and zero when $i \neq j$.

Let p be a parameter for which sensitivity information is needed. Differentiating Equations (4.10) and (4.11) with respect to p and then premultiplying the result by $\mathbf{u_i}^*$ and $\mathbf{v_i}^*$, respectively (where $\mathbf{a}^*$ is the conjugate transpose of **a**), and adding them together, one obtains

$$u_i^* \frac{\partial(I + G_1)}{\partial p} v_i + v_i^* \frac{\partial(I + G_1)^*}{\partial p} u_i + (u_i^*(I + G_1) - v_i^* \sigma_i) \frac{\partial v_i}{\partial p} +$$

$$+ (v_i^*(I + G_1)^* - u_i^* \sigma_i) \frac{\partial u_i}{\partial p} = \frac{\partial \sigma_i}{\partial p} (u_i^* u_i + v_i^* v_i) \qquad (4.13)$$

Using Equations (4.10) to (4.12) in (4.13), one obtains

$$\frac{\partial \sigma_i}{\partial p} = \frac{1}{2} \left(u_i^* \frac{\partial(I + G_1)}{\partial p} v_i + v_i^* \frac{\partial(I + G_1)^*}{\partial p} u_i\right) \qquad (4.14)$$

where the first and second terms in the right-hand side of the equation are complex conjugates. Therefore, Equation (4.14) can be written as

$$\frac{\partial \sigma_i}{\partial p} = \text{Real part of } \left[u_i^* \frac{\partial(I + G_1)}{\partial p} v_i\right]$$

$$= \text{Re}\left[u_i^* \frac{\partial(I + G_1)}{\partial p} v_i\right] \qquad (4.15)$$

Using Equation (4.9) and letting

$$\Phi = (Is - \bar{A})^{-1} \qquad (4.16)$$

Then, Equation (4.15) can be written as

$$\frac{\partial \sigma_i (I + G_1)}{\partial p} = \text{Re} \cdot \text{tr}\left[\frac{\partial(I + \bar{C}\Phi\bar{B})}{\partial p} v_i u_i^*\right] \qquad (4.17)$$

where tr[W] means the trace of W and is equal to the sum of the elements in the principal diagonal of W. Equation (4.17) can be expanded as

$$\frac{\partial \sigma_i}{\partial p} = \text{Re} \cdot \text{tr}\left[\left\{\frac{\partial \bar{C}}{\partial p} \Phi\bar{B} + \bar{C}\Phi \frac{\partial \bar{B}}{\partial p} + \bar{C}\Phi \frac{\partial \bar{A}}{\partial p} \Phi\bar{B}\right\} v_i u_i^*\right] \qquad (4.18)$$

It is now possible to obtain three expressions for $\partial\sigma_i/\partial p$, one each for the following cases:

1) The parameter p is an element of $\bar{A}$; i.e., $\hat{P} = \bar{A}$

2) The parameter p is an element of $\bar{B}$; i.e., $\hat{P} = \bar{B}$

3 The parameter p is an element of $\bar{C}$; i.e., $\hat{P} = \bar{C}$.

Then, we obtain

$$\frac{\partial \sigma_i}{\partial p_{\bar{A}}} = Re \cdot tr[\bar{C}\Phi \frac{\partial \bar{A}}{\partial p_{\bar{A}}} \Phi \bar{B} \mathbf{v}_i \mathbf{u}_i^*] \tag{4.19}$$

$$\frac{\partial \sigma_i}{\partial p_{\bar{B}}} = Re \cdot tr[\bar{C}\Phi \frac{\partial \bar{B}}{\partial p_{\bar{B}}} \mathbf{v}_i \mathbf{u}_i^*] \tag{4.20}$$

$$\frac{\partial \sigma_i}{\partial p_{\bar{C}}} = Re \cdot tr[\frac{\partial \bar{C}}{\partial p_{\bar{C}}} \Phi \bar{B} \mathbf{v}_i \mathbf{u}_i^*] \tag{4.21}$$

By recalling the following matrix operation [30],

$$\frac{\partial}{\partial A} [tr\{BAC\}] = B^T C^T \tag{4.22}$$

and the matrix trace property [24],

$$Re \cdot tr(A) = Re \cdot tr(A^*) \tag{4.23}$$

it is possible to extend Equations (4.19) through (4.21) to all the elements $p_{\bar{A}}$, $p_{\bar{B}}$, and $p_{\bar{C}}$ of the $\bar{A}$, $\bar{B}$, and $\bar{C}$ matrices, respectively. Therefore, for $\bar{A}$,

$$\frac{\partial \sigma_i}{\partial \bar{A}} = \frac{\partial}{\partial \bar{A}} [Re \cdot tr\{\bar{C}\Phi\bar{A}\Phi\bar{B}(\mathbf{v}_i \mathbf{u}_i^*)\}]$$

$$= Re[(\bar{C}\Phi)^*(\Phi\bar{B}\mathbf{v}_i \mathbf{u}_i^*)^*] \tag{4.24}$$

or, using the transpose of $\bar{A}$ in order to avoid transposing the matrices within brackets,

$$\frac{\partial \sigma_i}{\partial \bar{A}^T} = \mathrm{Re}[\Phi \bar{B} \mathbf{v}_i \mathbf{u}_i^* \bar{C} \Phi] \tag{4.25}$$

Similarly, for $\bar{B}$,

$$\frac{\partial \sigma_i}{\partial \bar{B}} = \mathrm{Re}[(\bar{C}\Phi)^* (\mathbf{v}_i \mathbf{u}_i^*)^*] \tag{4.26}$$

or using the transpose,

$$\frac{\partial \sigma_i}{\partial \bar{B}^T} = \mathrm{Re}[\mathbf{v}_i \mathbf{u}_i^* \bar{C} \Phi] \tag{4.27}$$

and for matrix $\bar{C}$,

$$\frac{\partial \sigma_i}{\partial \bar{C}} = \mathrm{Re}[I^T (\Phi \bar{B} \mathbf{v}_i \mathbf{u}_i^*)^*] \tag{4.28}$$

or using the transpose of $\bar{C}$,

$$\frac{\partial \sigma_i}{\partial \bar{C}^T} = \mathrm{Re}[\Phi \bar{B} \mathbf{v}_i \mathbf{u}_i^*] \tag{4.29}$$

Expressions (4.25), (4.27), and (4.29) can be used to evaluate the singular-value gradients with respect to elements of the system and controller matrices. Note that the gradients, like the singular values, are also a function of frequency; and therefore a singular-value-gradients plot (or sigma-gradients plot) can be obtained for a range of frequencies. Also, note that the information necessary to obtain the gradients is evaluated in the calculation of the singular-values plot (or sigma plot), since Φ has to be evaluated at each frequency, and $\mathbf{v}_i$ and $\mathbf{u}_i$ are a product of the singular value decomposition routine used in the calculation of the singular values. Therefore, little additional computational effort is needed

to calculate the sigma gradients for each singular value in a range of frequencies, beyond what is required to evaluate the singular values.

In the following section, the information from the sigma plot and sigma-gradients plot is combined into a sensitivity analysis method for multiloop control systems.

4.2 SENSITIVITY ANALYSIS METHOD FOR MULTILOOP SYSTEMS

There are three important aspects of a sensitivity analysis of a control system that need to be considered so that the information provided by the analysis is useful. The first is a measure of how sensitive the particular control system is to changes in the elements of the system model and controller. The second is some information (or engineering judgement) on the magnitude of the expected changes in the different system and controller parameters, according to the degree of refinement of the models. The third point that needs to be considered is the effect of those changes on the relative stability of the closed-loop system. In this manner, a control system may be very sensitive to inaccuracies in a certain parameter, p_i; but if the model is considered to be very accurate at the time of the analysis, the effect of the expected inaccuracy on the relative stability of the system may be negligible. On the other hand, if the sensitivity of the system to changes in p_i is not very high but the expected change in p_i is large, the closed-loop system may be driven unstable. A reduction in the stability margins

may be very important for a certain closed-loop system; but if the nominal system was very stable, the reduction may not be very relevant. These examples illustrate that a sensitivity analysis needs to include enough information to determine what parameter changes are most important. The method presented here does not attempt to obtain a "one-number" answer but, rather, to combine several tools to help the designer (or analyst) determine which parameters are most important for his (her) particular problem.

The sensitivity analysis method follows the steps illustrated in Figure 4.1. First, the sigma plot of the nominal control system is calculated, along with the closed-loop system eigenvalues. The sigma plot will tell the designer what is the minimum singular value, and therefore the phase and gain margins of the nominal system can be evaluated using the universal diagram (Figure 3.4) or Equations (3.12) and (3.13). If the nominal system is stable, the phase and gain margins will only determine "how far" the system is from the stability boundary. If the system is unstable, the phase and gain margins will again determine "how far" the system is from the stability boundary; however, they will not give information on the absolute stability of the system. (The same kind of information is obtained from a Bode Plot in the SISO case.) Thus, the need for evaluating the eigenvalues of the closed-loop system to determine absolute stability. It must be stressed that the closed-loop eigenvalues must not be confused with the eigenvalues of the return difference matrix, which were mentioned in Section 3.2 as an

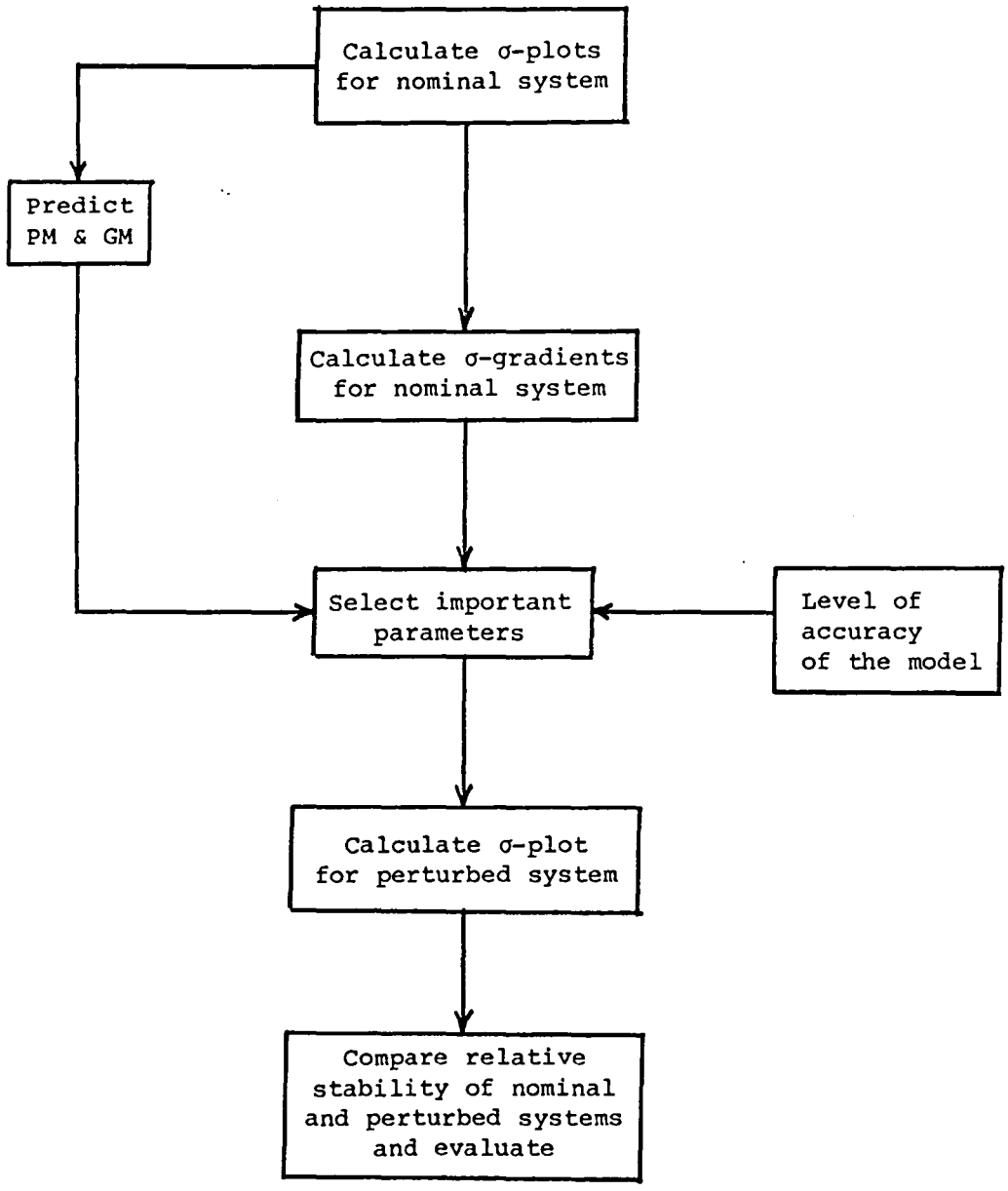

Figure 4.1: Multiloop Sensitivity Analysis Technique

additional measure for judging relative stability. The second step in the sensitivity analysis is to evaluate the singular-value gradients (sigma-gradients plots) for the nominal closed-loop system. This information will tell the designer which parameter variations (or inaccuracies) are the most important from the relative stability point of view. With the aid of information about the expected variations of those parameters, the third step is to select the parameters of interest. This also includes a look at the values of the sigma gradients at the different frequencies and how they compare with the minimum singular value at that frequency. The next step is to evaluate the sigma plot for the closed-loop system perturbed by the variations on the selected parameters. Comparing the nominal-system and perturbed-system sigma plots, the designer can judge the overall effect of those variations on the relative stability of the system, and check if the correct parameters were selected.

An illustration of the use of the sensitivity analysis is included in Section 4.3, using a simple third-order system and a yaw/roll damper system for a typical business jet.

4.3 APPLICATION OF THE SENSITIVITY ANALYSYS TECHNIQUE

In this section, the sensitivity analysis technique is applied to two different feedback control systems. The first example is a SISO third-order system; the objective is to show how the technique

can be used and the information interpreted. The second example is the multiloop yaw/roll damper design presented in Section 3.23; the objective in this case is to show how the sensitivity analysis information can be used to select the model parameters that have the greatest effect on the relative stability of the system. As we have discussed before, this information can be very useful in the selection and design of flight and wind-tunnel tests, when the objective is the optimization of the allocation of such resources as budget, flying time, wind-tunnel time, and instrumentation.

4.3.1 Sensitivity Analysis of a Simple Third-Order System

The single-input/single-output system we are dealing with in this section is shown in Figure 4.2. We will carry out a sensitivity analysis for two cases. Case I explores the sensitivity of the system to an error in the location of the zero; i.e., when the plant transfer function is given by

$$G(s) = \frac{s + \alpha}{(s + 2)(s^2 + 4s + 20)} \tag{4.30}$$

and in Case II we look at the sensitivity of the system to an error in the location of the second-order poles; i.e., when the plant transfer function is given by

$$G(s) = \frac{s}{(s + 2)[(s + \beta)^2 + 4^2]} \tag{4.31}$$

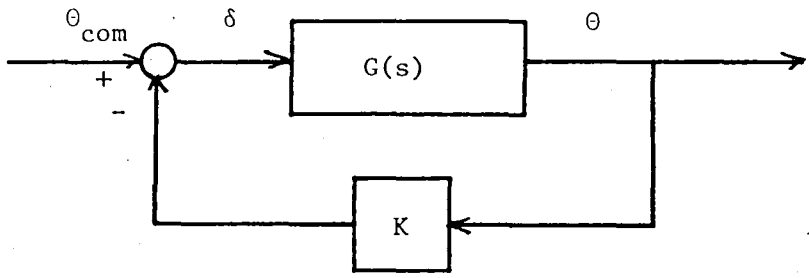

Figure 4.2: Block Diagram of SISO Feedback Control System

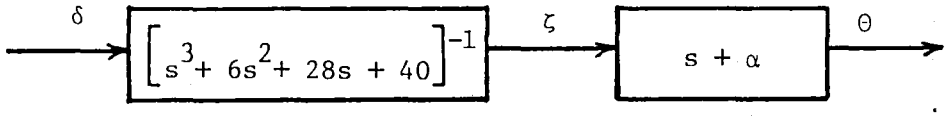

Figure 4.3: Representation of the Plant Given by $\frac{\Theta}{\delta}(s) = \frac{s + \alpha}{s^3 + 6s^2 + 28s + 40}$ Used to Find the State-Space Form

A) **Case I.** The state-space representation of the system is given by

$$\begin{bmatrix} \dot{x}_1 \\ \dot{x}_2 \\ \dot{x}_3 \end{bmatrix} = \begin{bmatrix} 0 & 1 & 0 \\ 0 & 0 & 1 \\ -40 & -28 & -6 \end{bmatrix} \begin{bmatrix} x_1 \\ x_2 \\ x_3 \end{bmatrix} + \begin{bmatrix} 0 \\ 0 \\ 1 \end{bmatrix} \delta \tag{4.32}$$

and

$$z = [\alpha \quad 1 \quad 0] \begin{bmatrix} x_1 \\ x_2 \\ x_3 \end{bmatrix} \tag{4.33}$$

for the plant, where $x_1 = \zeta$, where ζ is a variable used as a mathematical artifact in the representation of the plant (see Figure 4.3), and $z = \Theta$; and

$$\delta = -Kz \tag{4.34}$$

for the feedback-control law, when $\Theta_{com} = 0$. Equations (4.32) to (4.34) are equivalent to Equations (4.1) to (4.3). The system can then be reduced to the form given by Equations (4.6) and (4.7), by using Equation (4.32) and

$$\delta = -[\, K\alpha \quad K \quad 0\,] \begin{bmatrix} x_1 \\ x_2 \\ x_3 \end{bmatrix} = -\bar{C} \begin{bmatrix} x_1 \\ x_2 \\ x_3 \end{bmatrix} \tag{4.35}$$

In this case, we are interested in $\partial\underline{\sigma}/\partial\alpha$; i.e., the sensitivity of the relative stability of the system to changes in α; and it is obtained through Equation (4.29).

The feedback gain, K, chosen for the nominal design ($\alpha = 0$) is $K = 200$; the corresponding closed-loop eigenvalues are

pole	real part	imaginary part
1	-0.17623	0.0
2	-2.91188	14.78
3	-2.91188	-14.78

The singular value plot for the nominal system is shown in Figure 4.4, with the minimum $\underline{\sigma}$ occurring at $\omega = 15.81$ rad/sec. The stability margins are

$$GM = -2.89 \text{ to } 4.36 \text{ dB}$$

$$PM = \pm 22.7^\circ$$

for $\underline{\sigma} = 0.3948$.

Since Equation (4.29) calculates the singular-value gradients with respect to elements in the $\bar{C}$ matrix, Figure 4.5 shows $\partial\underline{\sigma}/\partial(K\alpha)$, which is the gradient with respect to element $\bar{C}(1,1)$; and Figure 4.6 presents the singular-value gradient with respect to α, $\partial\underline{\sigma}/\partial\alpha$, which was obtained by using

$$\frac{\partial\underline{\sigma}}{\partial\alpha} = K \frac{\partial\underline{\sigma}}{\partial(K\alpha)} \tag{4.36}$$

The singular-value gradient plots show that the system is very sensitive with respect to α (i.e., the gradient is large) at frequencies below $\omega = 1.0$ rad/sec, with a maximum sensitivity at $\omega = 0$. The importance of this sensitivity will also depend on the magnitude of the perturbation (i.e., the value of α) and on the value of $\underline{\sigma}$ at those frequencies.

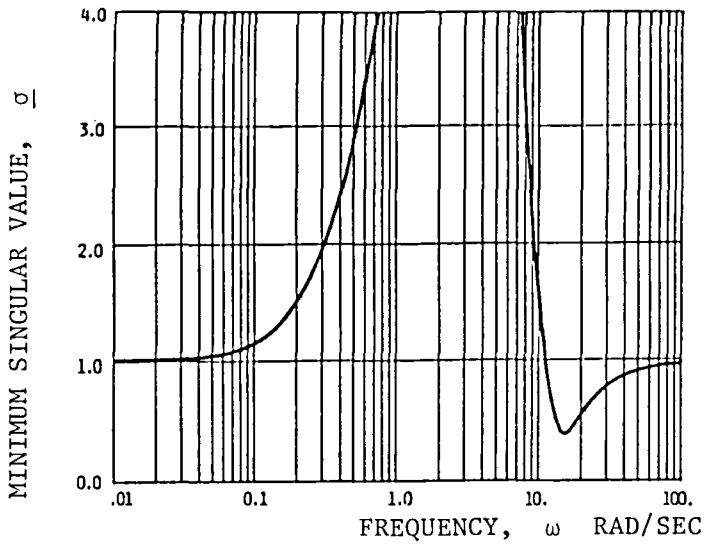

Figure 4.4: Sigma Plot of the Nominal System ($\alpha = 0$, $\beta = 2$)

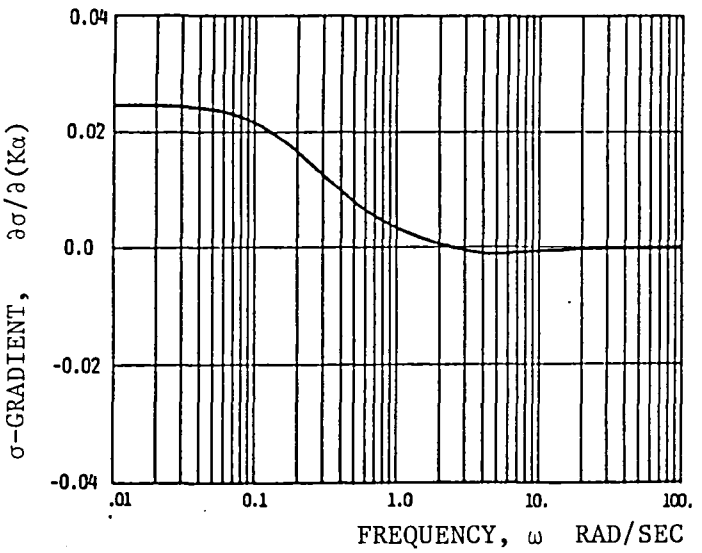

Figure 4.5: Gradient of the Minimum Singular Value with Respect to Kα, i.e. $\partial\sigma/\partial(K\alpha)$, as a Function of Frequency

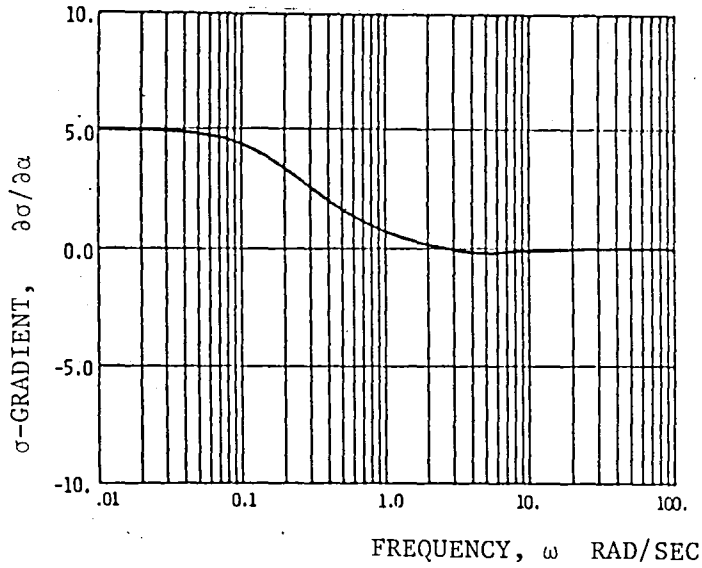

Figure 4.6: Frequency Plot of the Gradient of $\underline{\sigma}$ with α

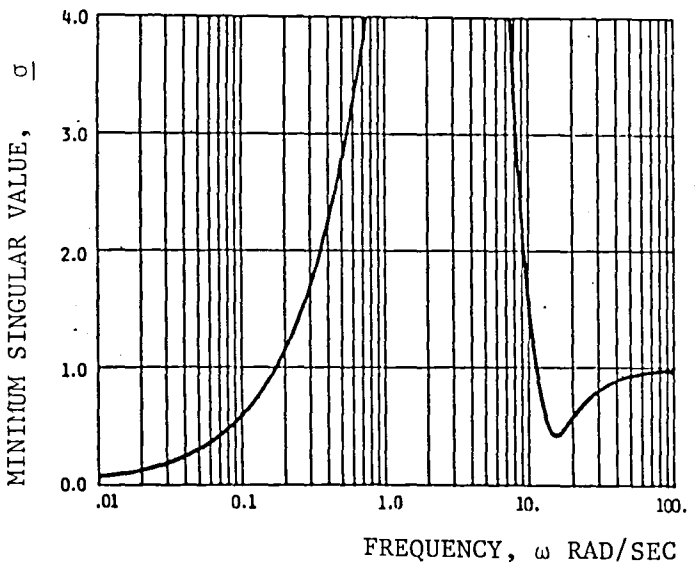

Figure 4.7: Sigma Plot of the Perturbed System (α = -0.2) Showing the $\underline{\sigma}$ at a Frequency of $\omega \approx 0$ rad/sec

If we let $\alpha = -0.2$, which means that the zero is on the right hand side of the s-plane, the estimated change in $\underline{\sigma}$, at $\omega = 0$ rad/sec, is $\Delta\underline{\sigma} \approx -1.0$; this means that the stability margins at very low frequencies will be considerably reduced. This is shown in the sigma plot of Figure 4.7, where the minimum $\underline{\sigma}$ now appears at $\omega = 0$ rad/sec. Also, the closed-loop eigenvalues of the perturbed system are

pole	real part	imaginary part
1	0.0	0.0
2	-3.0	14.79
3	-3.0	-14.79

which confirms the results of the sensitivity analysis.

B) **Case II.** The state-space representation of the system is given by

$$\begin{bmatrix} \dot{x}_1 \\ \dot{x}_2 \\ \dot{x}_3 \end{bmatrix} = \begin{bmatrix} 0 & 1 & 0 \\ 0 & 0 & 1 \\ f_1(\beta) & f_2(\beta) & f_3(\beta) \end{bmatrix} \begin{bmatrix} x_1 \\ x_2 \\ x_3 \end{bmatrix} + \begin{bmatrix} 0 \\ 0 \\ 1 \end{bmatrix} \delta \qquad (4.37)$$

and

$$z = \begin{bmatrix} 0 & 1 & 0 \end{bmatrix} \begin{bmatrix} x_1 \\ x_2 \\ x_3 \end{bmatrix} \qquad (4.38)$$

for the plant, where $x_1 = \zeta$, ζ is defined in Figure 4.3, and $z = \Theta$; and

$$\delta = -[\ 0 \quad K \quad 0\ ] \begin{bmatrix} x_1 \\ x_2 \\ x_3 \end{bmatrix} \tag{4.39}$$

In this case, we are interested in $\partial\underline{\sigma}/\partial f_1$, $\partial\underline{\sigma}/\partial f_2$, $\partial\underline{\sigma}/\partial f_3$, and $\partial\underline{\sigma}/\partial\beta$. Since $f_1(\beta)$, $f_2(\beta)$, and $f_3(\beta)$ are elements of the $\bar{A}$ matrix, Equation (4.25) must be used.

The closed-loop eigenvalues and the sigma-plot for the nominal system ($K = 200$, $\alpha = 0$, $\beta = 2$) are the same as in Case I. The singular-value gradients are plotted in Figure 4.8. Note that these gradients are important only in the frequency range between 1.0 and 20.0 rad/sec, with $\partial\underline{\sigma}/\partial f_3$ being the most important.

In order to obtain the sensitivity with respect to β, the contribution of each of the elements, $\partial\underline{\sigma}/\partial f_1$, $\partial\underline{\sigma}/\partial f_2$, and $\partial\underline{\sigma}/\partial f_3$ has to be accounted for. This is done by using the chain rule to obtain

$$\frac{\partial\underline{\sigma}}{\partial\beta} = \frac{\partial f_1}{\partial\beta}\frac{\partial\underline{\sigma}}{\partial f_1} + \frac{\partial f_2}{\partial\beta}\frac{\partial\underline{\sigma}}{\partial f_2} + \frac{\partial f_3}{\partial\beta}\frac{\partial\underline{\sigma}}{\partial f_3} \tag{4.40}$$

where $\partial f_1/\partial\beta$, $\partial f_2/\partial\beta$, and $\partial f_3/\partial\beta$ are determined from

$$f_1(\beta) = -2(\beta^2 + 16) \quad \text{and} \quad \frac{\partial f_1}{\partial\beta} = -4\beta \tag{4.41}$$

$$f_2(\beta) = -(\beta^2 + 4\beta + 16) \quad \text{and} \quad \frac{\partial f_2}{\partial\beta} = -2(\beta + 2) \tag{4.42}$$

$$f_3(\beta) = -2(\beta + 1) \quad \text{and} \quad \frac{\partial f_3}{\partial\beta} = -2 \tag{4.43}$$

which, when evaluated at nominal conditions ($\beta = 2$), give

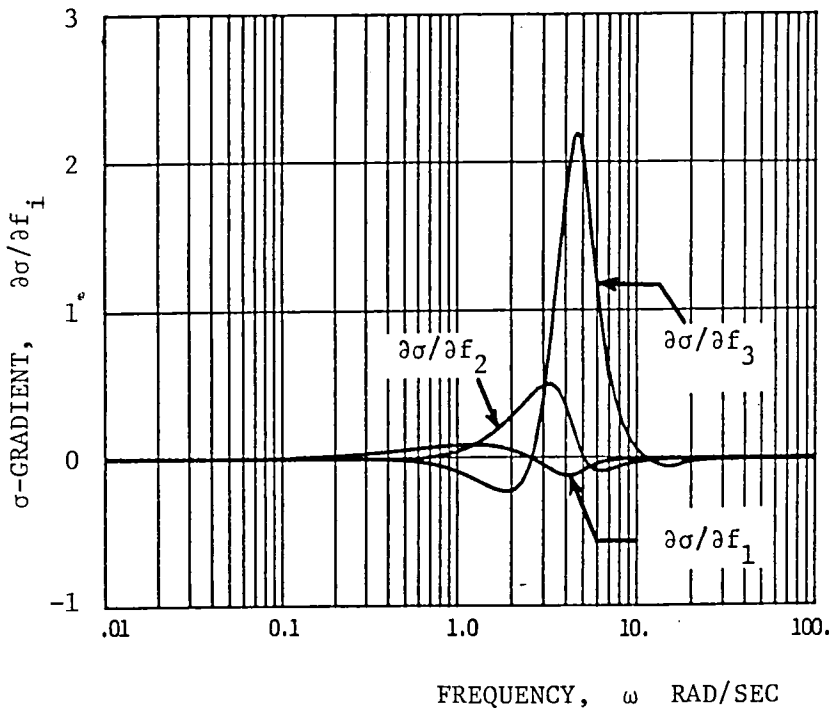

Figure 4.8: The singular-value gradients with respect to f_1, f_2, and f_3 are important only between 1.0 and 20 rad/sec.

$$\frac{\partial \underline{\sigma}}{\partial \beta} = -8 \frac{\partial \underline{\sigma}}{\partial f_1} - 8 \frac{\partial \underline{\sigma}}{\partial f_2} - 2 \frac{\partial \underline{\sigma}}{\partial f_3} \tag{4.44}$$

The plot for the gradient with respect to β is shown in Figure 4.9. At low frequency the gradient approaches zero; and it reaches a maximum in the negative direction at $\omega = 3.84$ rad/sec, with $\partial \underline{\sigma}/\partial \beta = -5.7$. However, the sigma plot in Figure 4.4 shows that, at that frequency, the $\underline{\sigma} = 11.7$; and, therefore, the effect of any expected changes in β will not be very important. Figure 4.9 also shows a maximum gradient in the positive direction occurring at $\omega = 13.2$ rad/sec. This gradient has a value of $\partial \underline{\sigma}/\partial \beta = 0.139$, while the corresponding $\underline{\sigma}$ is $\underline{\sigma} = 0.53$. In this case, the minimum singular value is relatively small; however, the gradient is also very small and therefore not very important.

To check the validity of our conclusions, the value of β is assumed to be off by -10% (i.e., $\beta = 1.8$), the singular-value plot of the "perturbed" system is given in Figure 4.10. No significant change from the nominal plot (Figure 4.4) is observed. The stability margins have changed slightly to

GM = -2.75 to 4.05 dB

PM = ±21.5°

for $\underline{\sigma} = 0.373$.

The results obtained above can be interpreted in the following manner: If the model of the plant is determined such that the parameter α might be expected to vary from $\alpha = 0$ to $\alpha = -0.2$, the closed-loop system may contain instabilities. Also, if the accuracy

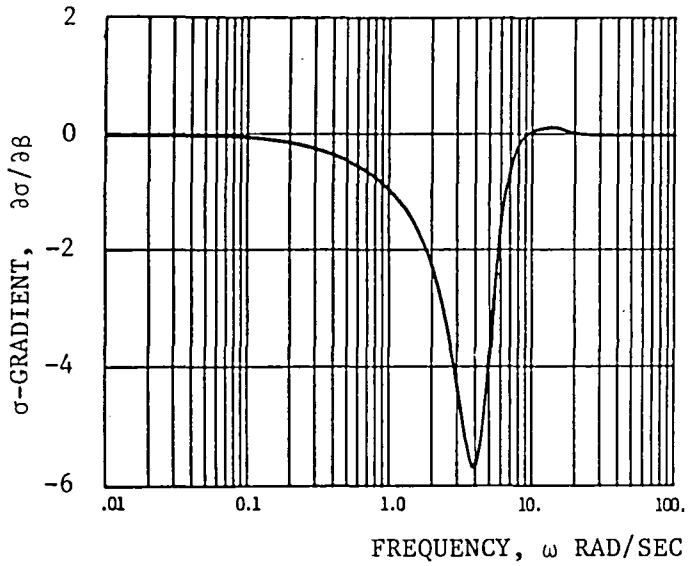

Figure 4.9: Singular-Value Gradient Plot that Shows the Sensitivity of the Relative Stability of the System with β

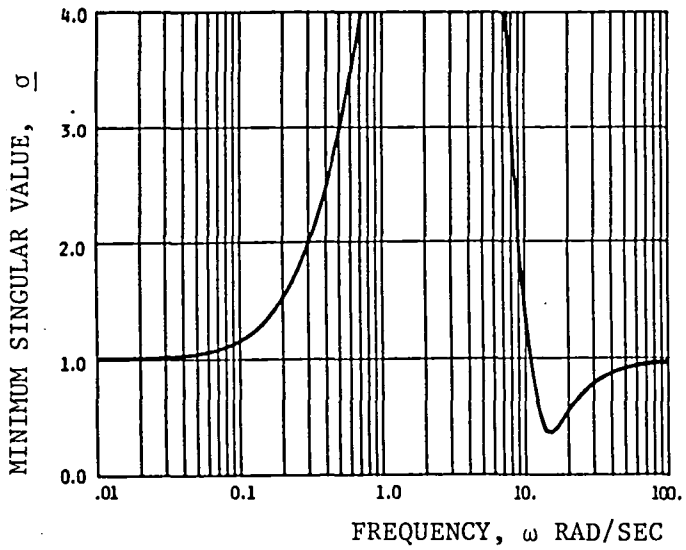

Figure 4.10: Sigma Plot of the Perturbed System (α = 0, β = 1.8), that Shows no Apparent Change of Relative Stability with the Nominal System

on β is of about $\pm 10\%$ of the nominal value, no instabilities should result from such an inaccuracy.

4.3.2 Sensitivity Analysis of the Multiloop Yaw/Roll-Damper System of a Typical Business Jet

The system analyzed in this section was discussed in Section 3.2.3, where the controller design was given for a yaw-damper-loop gain of $K_{\delta_R} = 1.0$ and a roll-damper-loop gain of $K_{\delta_A} = 0.2$.

The main objective here is to show how the sensitivity analysis can be used to determine the parameters that have a large effect on the relative stability of MIMO closed-loop systems.

The lateral-directional, small-perturbation equations of motion for the business jet are shown in Table B.1. These equations were used to obtain the state-space representation of the system, where the servo dynamics and the washout filter have been included. The construction of the state-space form is presented in Table 4.1, where the $\bar{A}$, $\bar{B}$, and $\bar{C}$ matrices of Equations (4.6) and (4.7) are shown.

The analysis was limited to the singular-value gradients with respect to elements of the $\bar{A}$ matrix. Since many of the zero elements in the $\bar{A}$ matrix are the result of kinematic relations, they will not change with modelling errors (example: a(5,1) is one such element which is a result of the construction of the state-space representation of the system); it was therefore chosen not to obtain

Table 4.1: Construction of the State-Space Representation of the Roll/Yaw Damper SAS for Which Sensitivity Information Was Obtained

$$\begin{bmatrix} \dot{\beta} \\ \dot{p} \\ \dot{r} \\ \dot{\phi} \\ \dot{\delta}_R \\ \dot{\zeta} \\ \dot{\delta}_A \end{bmatrix} = \begin{bmatrix} -0.111 & 0 & -0.995 & 0.1594 & 0.0209 & 0 & 0 \\ -2.133 & -0.534 & 0.416 & 0 & 0.3207 & 0 & 2.441 \\ 1.0168 & -0.0515 & -0.1875 & 0 & -0.7051 & 0 & -0.3416 \\ 0 & 1 & 0 & 0 & 0 & 0 & 0 \\ 0 & 0 & 0 & 0 & -10 & 0 & 0 \\ 0 & 0 & 1 & 0 & 0 & -0.25 & 0 \\ 0 & 0 & 0 & 0 & 0 & 0 & -10 \end{bmatrix} \begin{bmatrix} \beta \\ p \\ r \\ \phi \\ \delta_R \\ \zeta \\ \delta_A \end{bmatrix} + \begin{bmatrix} 0 & 0 \\ 0 & 0 \\ 0 & 0 \\ 0 & 0 \\ 10 & 0 \\ 0 & 0 \\ 0 & 10 \end{bmatrix} \begin{bmatrix} \delta_{R_C} \\ \delta_{A_C} \end{bmatrix}$$

which is equivalent to

$$\dot{X} = \bar{A}X + \bar{B}U \qquad \text{Equation (4.6)}$$

Table 4.1: (Continued)

$$\begin{bmatrix} p \\ r_2 \end{bmatrix} = \begin{bmatrix} 0 & 1 & 0 & 0 & 0 & 0 & 0 \\ 0 & 0 & 1 & 0 & 0 & -0.25 & 0 \end{bmatrix} \begin{bmatrix} \beta \\ p \\ r \\ \phi \\ \delta_R \\ \zeta \\ \delta_A \end{bmatrix}$$

which is equivalent to

$$Z = TX \qquad \text{Equation (4.2)}$$

and

$$\begin{bmatrix} \delta_{R_c} \\ \delta_{A_c} \end{bmatrix} = - \begin{bmatrix} 0 & 0 & -K_{\delta_R} & 0 & 0 & 0.25K_{\delta_R} & 0 \\ 0 & K_{\delta_A} & 0 & 0 & 0 & 0 & 0 \end{bmatrix} \begin{bmatrix} \beta \\ p \\ r \\ \phi \\ \delta_R \\ \zeta \\ \delta_A \end{bmatrix}$$

which is equivalent to

$$U = -\bar{C}X \qquad \text{Equation (4.7)}$$

for R = 0

$K_{\delta_R} = 1.0$

$K_{\delta_A} = 0.2$

Table 4.1: (Continued)

With the following representations:

I) 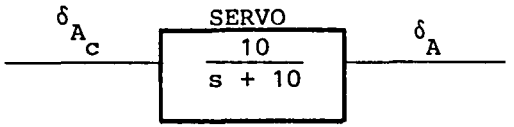

$$\dot{\delta}_A = -10\delta_A + 10\delta_{A_C}$$

II) 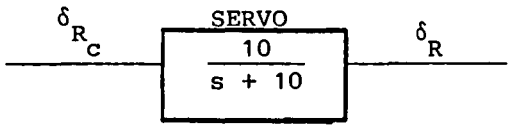

$$\dot{\delta}_R = -10\delta_R + 10\delta_{R_C}$$

III) 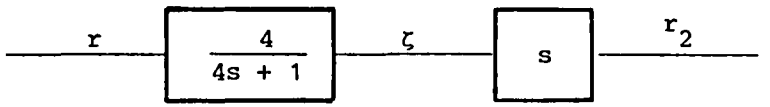

$$\dot{\zeta} = -0.25\zeta + r$$

$$r_2 = \dot{\zeta}$$

WASHOUT FILTER

their gradients. From the remaining elements in matrix $\bar{A}$, only fourteen appeared to be important. All of these elements are functions of stability or control power derivatives; their gradients are shown in Figures 4.11 to 4.14.

In the selection of the important parameters, several factors must be considered: the value of the sigma gradients, the magnitude of the particular element, the magnitude of the minimum singular value, and the value of the expected inaccuracies or changes in each of the elements being considered.

To account for the magnitude of the elements and thus facilitate the selection, the gradient of each element was multiplied by the magnitude of the element. These are the normalized gradients shown in Figures 4.11 to 4.14, and they can be interpreted as the expected change in the singular value with a percentage change in the element.

Table 4.2 summarizes the information used in the final selection of the important elements. Column 6 gives the approximate percentage change in the element, p, required to obtain a 10% increase in the minimum singular value, $\underline{\sigma}$; and column 5 contains the normalized gradients. The difference between columns 5 and 6 is that column 6 takes the magnitude of the minimum singular value into account. This is achieved by using the following approximation:

$$\left.\frac{\Delta p}{p}\right|_{10\%\underline{\sigma}} = \left.\frac{\partial \underline{\sigma}}{\partial p/p}\right|_{max} \times \frac{1}{0.10\underline{\sigma}} \qquad (4.45)$$

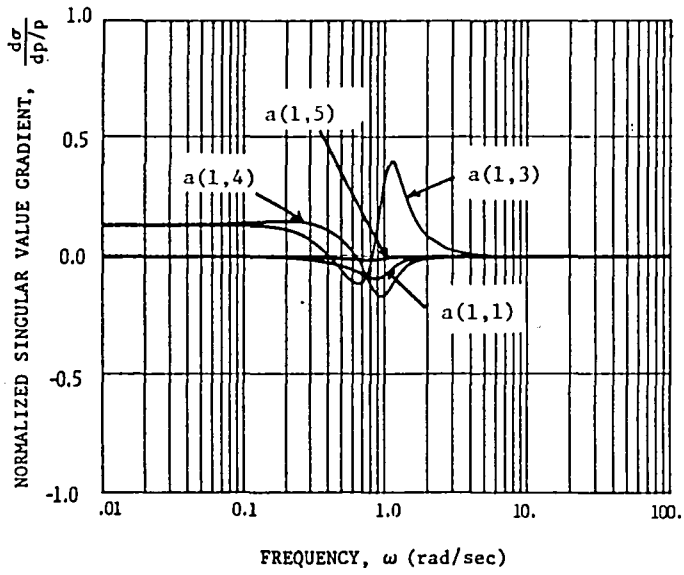

Figure 4.11: Singular-Value Gradients with Respect to Elements a(1,1), a(1,3), a(1,4), and a(1,5) of Matrix $\bar{A}$ of the Yaw/Roll Damper SAS

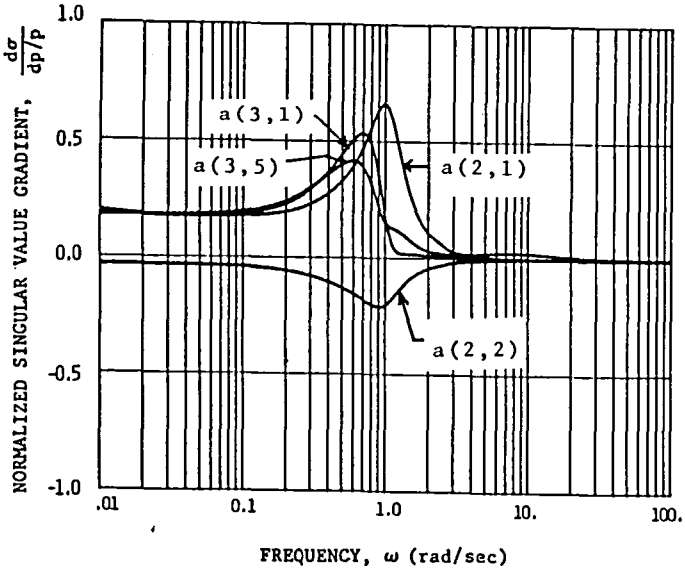

Figure 4.12: Singular-Value Gradients with Respect to Elements a(2,1) a(2,2), a(3,1), and a(3,5) of Matrix $\bar{A}$ of the Yaw/Roll Damper SAS

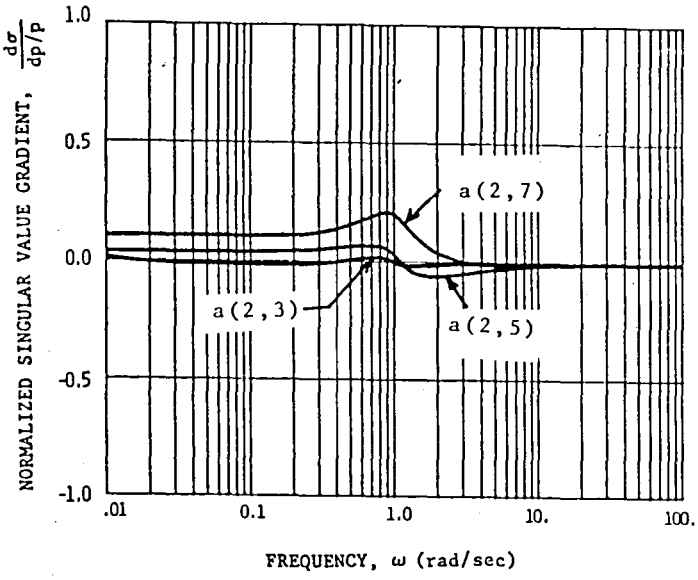

Figure 4.13: Singular-Value Gradients with Respect to Elements a(2,3), a(2,5), and a(2,7) of Matrix $\bar{A}$ of the Yaw/Roll Damper SAS

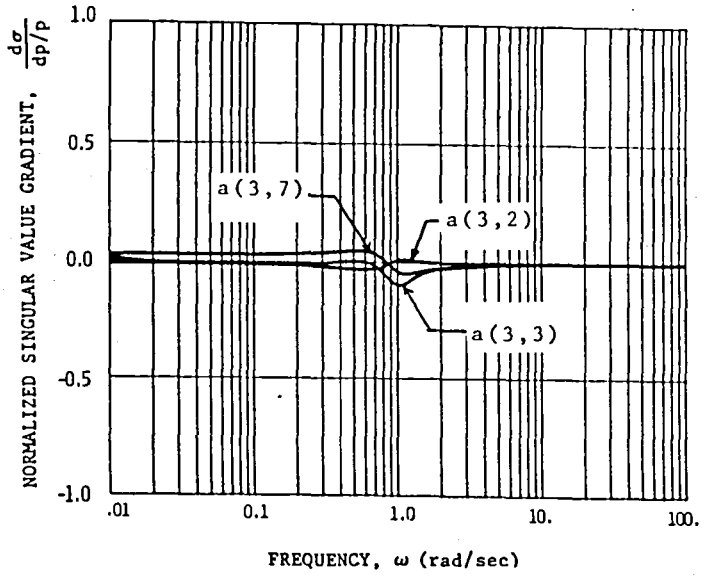

Figure 4.14: Singular-Value Gradients with Respect to Elements a(3,2), a(3,3), and a(3,7) of Matrix $\bar{A}$ of the Yaw/Roll Damper SAS

Table 4.2: Summary of the Sensitivity Analysis Information Used in the Selection of the Important Elements for the Yaw/Roll Damper SAS

	(1) Element of $\bar{A}$	(2) Frequency (rad/sec)	(3) Approximated $\underline{\sigma}$	(4) $\partial\underline{\sigma}/\partial p\big\|_{max}$	(5) $\partial\underline{\sigma}/(\partial p/p)\big\|_{max}$	(6) Approximated $\Delta p/p\big\|_{10\%\underline{\sigma}}$
1)	a(1,1)	0.86	0.52	-0.82	-0.091	-57%
2)	a(1,3)	1.12	0.70	0.41	0.41	17%
3)	a(1,4)	0.95	0.57	-1.10	-0.17	-34%
4)	a(1,5)	0.72	0.50	-0.064	-0.014	-370%
5)	a(2,1)	0.95	0.57	0.31	0.67	9%
6)	a(2,2)	0.89	0.53	-0.39	-0.21	-25%
7)	a(2,3)	0.73	0.503	0.05	0.021	240%
8)	a(2,5)	0.65	0.523	0.022	0.070	75%
9)	a(2,7)	0.86	0.52	0.043	0.21	25%
10)	a(3,1)	0.67	0.52	0.53	0.54	10%
11)	a(3,2)	0.56	0.55	-0.57	-0.030	-190%
12)	a(3,3)	1.00	0.60	-0.51	-0.095	-65%
13)	a(3,5)	0.56	0.55	0.059	0.42	13%
14)	a(3,7)	0.49	0.59	0.074	0.050	120%

The largest gradients are given by elements a(1,3) a(2,1), a(2,2), a(2,7), a(3,1), a(3,5). Although element a(1,3) has a large gradient, it is discarded because it is given by the following equation:

$$a(1,3) = \frac{Y_r}{U_1} - 1 \qquad (4.46)$$

Since $U_1 >> Y_r$, a large change in Y_r will have almost no effect on the value of the element; therefore, a very accurate determination of Y_r is not warranted. This points out the importance of having a good understanding of the model being considered, when interpreting the information provided by the gradients.

As a final check, five of the important elements (a(2,1), a(2,7), a(2,2), a(3,1), and a(3,5) were allowed to change by 15% in their worst direction (i.e., so as to decrease $\underline{\sigma}$), and the sigma plot of the perturbed closed-loop system was calculated. This plot is shown in Figure 4.15. The minimum singular value is now given by $\underline{\sigma} = 0.256$ with the following stability margins:

GM = -1.98 to 2.57 dB

PM = ±14.7°

Comparing the perturbed-system sigma plot ($\underline{\sigma} = 0.256$) with the nominal-system sigma plot of Figure 3.25 ($\underline{\sigma} = 0.502$), a reduction of 49% in the minimum singular value is observed. This reduction translates into reduced stability margins. The nominal system GM was -3.53 to 6.05 dB compared to -1.98 to 2.57 dB for the perturbed system. Similarly, the nominal system had a PM of ±20.1° while the perturbed-system PM is ±14.7°.

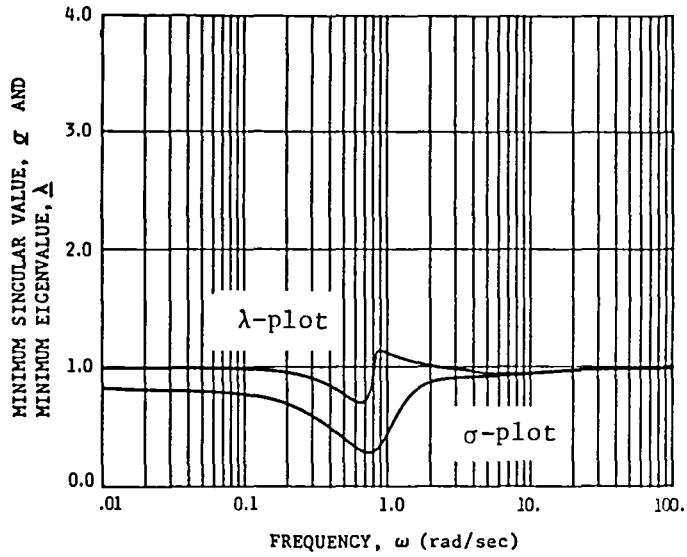

Figure 4.15: Sigma Plot for System with Elements a(2,1), a(2,2), a(2,7), a(3,1), and a(3,5) Perturbed by 15% in Their Worst Direction (σ = 0.256)

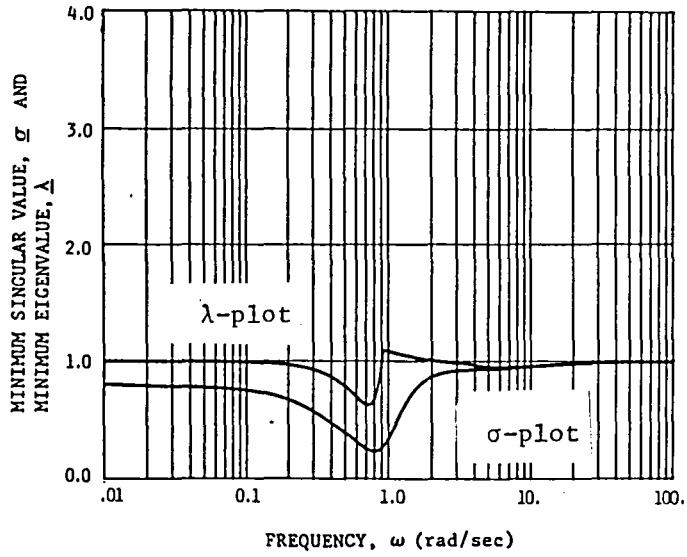

Figure 4.16: Sigma Plot for System with all $\bar{A}$ Matrix Elements Initially Selected Perturbed by 15% in Their Worst Direction ($\underline{\sigma}$ = 0.2292)

As a way of comparison, all fourteen elements that were initially selected were allowed to change by 15% (in their worst directions), and the corresponding sigma plot was calculated. This plot is shown in Figure 4.16. The minimum singular value is $\underline{\sigma} = 0.2292$ with the following stability margins:

GM = -1.79 to 2.26 dB

PM = ±13.16°

The minimum singular value has been reduced by 54% from the nominal system singular value, with 49% of the change due to the five variables selected as the most important and only 5% due to the remaining variables.

A more qualitative way of looking at the same effect is given in the time histories of Figure 4.17 (a) and (b), where the difference in performance between the nominal and perturbed systems is noticeable; but the difference in perturbing fourteen elements, or only the five most important ones, is negligible.

These results confirm the usefulness of the sensitivity analysis technique in the selection of the parameters that have the largest effect in the relative stability of the system. As has been mentioned before, the information obtained from the sensitivity analysis can be used to assign priorities for accurate determination of the parameters of the model. For instance, Table 4.3 shows the five elements selected in the previous example, along with their respective formulas. The stability and control power derivatives that affect those elements are also shown in the table. Using this information, a wind-tunnel test (or flight test) could be designed

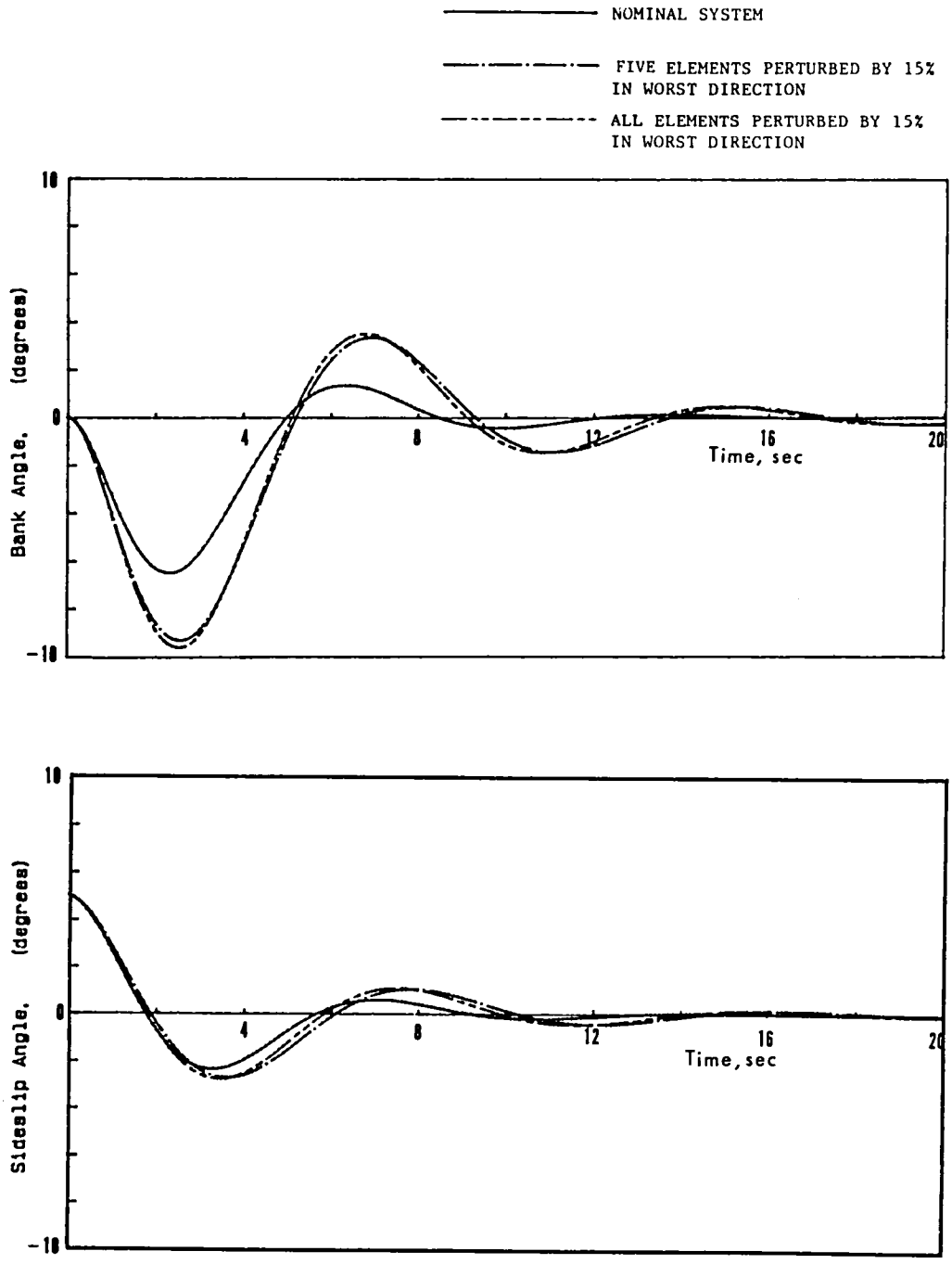

Figure 4.17: Time Histories of (a) Bank Angle and (b) Sideslip Angle, Showing the Effect of Perturbing the Elements in the $\bar{A}$ Matrix of the Yaw/Roll Damper SAS by 15% in Their Worst Direction

Table 4.3: Summary of the Five Elements of the $\bar{A}$ Matrix with Largest Effect on the Relative Stability of the Yaw/Roll Damper SAS

Element	Corresponding Formula	Stability or Control Power Derivatives
a(2,1)	$\frac{A_1 N_\beta + L_\beta}{1 - A_1 B_1}$	C_{n_β}, C_{ℓ_β}
a(2,2)	$\frac{A_1 N_p + L_p}{1 - A_1 B_1}$	C_{n_p}, C_{ℓ_p}
a(3,1)	$\frac{B_1 L_\beta + N_p}{1 - A_1 B_1}$	C_{ℓ_β}, C_{n_β}
a(3,5)	$\frac{B_1 L_{\delta_R} + N_{\delta_R}}{1 - A_1 B_1}$	$C_{n_{\delta_R}}$, $C_{\ell_{\delta_R}}$
a(2,7)	$\frac{A_1 N_{\delta_A} + L_{\delta_A}}{1 - A_1 B_1}$	$C_{n_{\delta_A}}$, $C_{\ell_{\delta_A}}$

$$A_1 = I_{XZ}/I_{XX} \qquad B_1 = I_{XZ}/I_{ZZ}$$

such that the accurate determination of $C_{n_{\delta_R}}$, $C_{\ell_{\delta_R}}$, C_{n_β}, C_{ℓ_p}, C_{ℓ_β}, C_{n_p}, $C_{n_{\delta_A}}$, and $C_{\ell_{\delta_A}}$ has priority over the determination of other derivatives such as C_{Y_r} (element a(1,3)) and $C_{Y_{\delta_R}}$ (element a(1,5)).

In the following chapter, the results and conclusions reached so far are summarized. Also, some recommendations are given in the areas where additional research would improve the utility of the sensitivity analysis technique developed.

5. CONCLUSIONS AND RECOMMENDATIONS

In this section, a summary of the results obtained and the conclusions reached is presented. Also, some suggestions are given regarding the kind of research activities that should be continued to improve the utility of the sensitivity analysis technique presented so far.

5.1 SUMMARY AND CONCLUSIONS

The primary goal of this project was the development of a sensitivity analysis technique for multiloop flight control systems. The concept of singular values, as tools in the analysis of relative stability of multivariable-continuous flight control systems, was introduced. The development of a sensitivity analysis technique, based on singular-value concepts, has been completed for continuous-multivariable flight control systems; and its use has been demonstrated through several examples. The application of the singular-value concepts to sampled-data systems has also been explored; a possible extension of the sensitivity analysis technique to cover sampled-data systems has also been proposed in Appendix C.

A summary of general conclusions drawn from this research is presented below.

1) The combination of the singular-value plot and eigenvalue plot analyses is very useful in judging the relative stability of

multivariable control systems. Although the stability margins predicted are conservative, the singular value analysis provides information on the potential instabilities resulting from simultaneous phase and gain variations in all the loops, that cannot always be detected by a one-loop-at-a-time frequency response analysis of multiloop systems. The singular value analysis provides the designer with the concept of multiloop stability margins, similar to the stability margin concept for a single-input/single-output system.

2) The sensitivity analysis ($\underline{\sigma}$-gradients with respect to system and controller parameters) technique developed is very useful in the identification of the parameters that have the largest impact on the relative stability of multiloop control systems. The direct relationship to changes in the stability margins of the multiloop system is very convenient because the control system designer has already developed a "feel" for the concept of phase and gain margins for SISO systems.

5.2 SOME SUGGESTIONS FOR FURTHER RESEARCH

There are five main activities which could extend and thus improve the utility of the sensitivity analysis technique presented in this report:

1) Application of the singular-value analysis to sampled-data systems. The singular-value concepts and theoretical relations

presented are valid only for continuous systems, and they should be extended to handle sampled-data systems.

2) Development of singular-value gradients for sampled-data systems. A suggested Approach is presented in Appendix C.

3) Application of singular-value and singular-value gradient analyses to optimal feedback control systems, continuous and digital. The tools presented so far are applicable to optimal continuous feedback control systems. Lehtomaki, et al. [22], show that the stability margins for continuous-linear-quadratic (LQ) regulators are given by

Gain margin, GM = 1/2, ∞

Phase margin, PM = $\pm 60°$

and Maybeck [37] also gives the equivalent stability margins for digital LQ regulators. What remains to be done is to explore some examples of LQ regulators using the sensitivity analysis technique to learn how the sensitivity information could best be used. The concepts discussed by Cruz, et al. [16], and Safonov, et al. [17], on the relationship between stability and sensitivity of multiloop LQ regulators may prove very useful.

4) Study of possible ways to reduce the conservativeness of the stability margins predicted by the singular values. This could take the form of finding another norm to define closeness to singularity. Another possibility is presented by Doyle [39] in the analysis of feedback systems with structured uncertainties.

6. REFERENCES

1. Dorf, R. C., Modern Control Systems, 3rd Ed., Addison-Wesley Publishing Co., 1981.

2. Kuo, B. C., Automatic Control Systems, 4th Ed., Prentice-Hall, Inc., 1982.

3. Paraskevopoulos, P. N.; Tsonis, C. A., and Tzafestas, S. G., "Eigenvalue Sensitivity of Linear Time-Invariant Control Systems with Repeated Eigenvalues," IEEE Trans. Autom. Contr., October 1974.

4. Crossley, T. R., and Porter, B., "Eigenvalue and Eigenvector Sensitivities in Linear Systems Theory," Int. J. Control, 1969, vol. 10, No. 2, pp. 163-170.

5. Morgan, B. S., "Sensitivity Analysis and Synthesis of Multivariable Systems," IEEE Trans. Autom. Control, vol. AC-11, No. 3, July 1966.

6. Pareskevopoulos, P. N., Christodoulou, M. A., and Tsakiris, M. A., "Eigenvalue-Eigenvector Sensitivity Analysis of Linear Time-Invariant Singular Systems," Tech. Note, IEEE Trans. Autom. Contr., vol. AC-29, No. 4, April 1984.

7. Pagurek, B., "Sensitivity of the Performance of Optimal Control Systems to Plant Parameter Variations," IEEE Trans. Autom. Contr., 10, pp. 178, 1965.

8. Sobral, M., "Sensitivity in Optimal Control Systems" (survey), IEEE Trans. Autom. Contr., vol. 56, No. 10, October 1968.

9. Kreindler, E., "Comparative Sensitivity of Optimal Control Systems," Chapter 5 of Feedback Systems, by José B. Cruz, McGraw-Hill Book Co., 1972.

10. Kreindler, E., "On Performance Sensitivity of Optimal Control Systems," Int. J. Control, vol. 15, No. 3, pp. 481-486, 1972.

11. Becker, N., "A Note on Performance Index Sensitivity of Time Optimal Control Systems," IEEE Trans. Autom. Contr., vol. AC-25, No. 4, August 1980.

12. Schaechter, D. B., "Closed-Loop Control Performance Sensitivity to Parameter Variations," AIAA J. Guidance and Control, vol. 6, No. 5, Sept.-Oct. 1983.

13. Perkins, W., "Sensitivity Analysis," Chapter 2 of Feedback Systems, by José B. Cruz, McGraw-Hill Publishing Co., 1972.

14. Cruz, J. B., and Perkins, W., "A New Approach to the Sensitivity Problem in Multivariable Feedback System Design," IEEE Trans. Autom. Contr., July 1964.

15. Wells, W. R., and Pailoor, R., "Sensitivity of Digital Flight Control Design to Parameter Estimation Error," AIAA paper 83-2089, AIAA Atmospheric Flight Mechanics Conference, Gatlinburg, Tennessee, August 15-17, 1983.

16. Cruz, J. B., Freudenberg, J. S., and Looze, D. P., "A Relationship between Sensitivity and Stabilty of Multivariable Feedback Systems," IEEE Trans. Autom. Contr., vol. AC-26, No. 1, February 1981.

17. Safonov, M. G., Laub, A. J., and Hartmann, G. L., "Feedback Properties of Multivariable Systems: The Role and Use of the Return Difference Matrix," IEEE Trans. Autom. Contr., vol. AC-26, No. 1, Feb. 1981.

18. Lehtomaki, N. A., Castanon, N. A., Levy, D. A., Stein, B. C., Sandell, N. R. Jr., and Athans, M., "Robustness and Modeling Error Characterization," IEEE Trans. Autom. Contr., vol. AC-29, No. 3, March 1984.

19. Macfarlane, A. G. J., and Hung, Y. S., "Analytic Properties of the Singular Values of a Rational Matrix," Int. J. Control, vol. 37, No. 2, pp. 221-234, 1983.

20. Mukhopadhyay, V., and Newsom, J. R., "Application of Matrix Singular Value Properties for Evaluating Gain and Phase Margins of Multiloop Systems," AIAA Guidance and Control Conference, paper 83-1574, San Diego, Cal., August 9-11, 1982.

21. Laub, A. J., "Efficient Multivariable Frequency Response Computations," IEEE Trans. Autom. Contr., vol. AC-26, No. 2, April 1981.

22. Lehtomaki, N. A., Sandell, N. R. Jr., and Athans, M., "Robustness Results in Linear-Quadratic Gaussian Based Multivariable Control Designs," IEEE Trans. Autom. Contr., vol. AC-26, No. 1, Feb. 1981.

23. Doyle, J. C., and Stein, G., "Multivariable Feedback Design: Concepts for a Classical/Modern Synthesis," IEEE Trans. Autom. Contr., vol. AC-26, No. 1, Feb. 1981.

24. Newsom, J. R., and Mukhopadhyay, V., "The Use of Singular Value Gradients and Optimization Techniques to Design Robust Controllers for Multiloop Systems," AIAA Guidance and Control Conference, paper 83-2191, 1983.

25. Broussard, J. R., "Computation of Differential Equation Particular Solutions with Applications to Sigma Plots," IEEE Trans. Autom. Contr., vol. AC-29, No. 5, May 1984.

26. Anderson, L. R., "Direct Design of Multivariable Control Systems through Singular Value Decomposition," AIAA Guidance and Control Conference, paper 83-2276, 1983.

27. Yeh, H. H., Ridgely, Capt. B., and Banda, S. S., "Nonconservatiave Evaluation of Uniform Stability Margins of Multivariable Feedback Systems," AIAA Guidance and Control Conference, paper 84-1939, Seattle, WA, August 1984.

28. Hammond, T. A., Amin, S. P., and Paduano, J. D., "Design of a Digital Ride Quality Augmentation System for Commuter Aircraft," KU-FRL-6132-1, Flight Research Laboratory, University of Kansas Center for Research, Inc., Lawrence, KS 66045, July 1984.

29. Herrera, A., and Paduano, J., "Interim Report for NASA Cooperative Agreement NCC 2-293: Development of an Integrated Model Determination and Control System Design Procedure," KU-FRL-662-1, Flight Research Laboratory, University of Kansas Center for Research, Inc., Lawrence, KS 66045, October 1984.

30. Applied Optimal Estimation, written by the Technical Staff, Analytic Sciences Corporation, edited by Arthur Gelb, MIT Press, Cambridge, Massachusetts, 1974.

31. Roskam, J., Airplane Flight Dynamics and Automatic Flight Controls, vols. I and II, Roskam Aviation and Engineering Corporation, Ottawa, KS, 1979.

32. Armstrong, E. S., ORACLS: A Design System for Linear Multivariable Control, Marcel Dekker, Inc., New York, 1980.

33. Wilkinson, J. H., and Reinsch, C., Handbook for Automatic Computation: Vol. II, Linear Algebra, edited by F. L. Bauer, A. S. Householder, F. W. J. Olver, H. Rutishauser, K. Samelson, and E. Stiefel, Springer-Verlag, New York, 1971.

34. Broussard, J. R., and Halyo, N., "Investigation, Development, and Application of Optimal Output Feedback Theory: Vol. II, Development of an Optimal Limited State Feedback Outer-Loop Digital Flight Control System for 3-D Terminal Area Operation," NASA CR-3829, August 1974.

35. Klema, V. C., and Laub, A. J.; "The Singular Value Decomposition: Its Computation and Some Applications," IEEE Trans. on Autom. Contr., vol. AC-25, No. 2, April 1980.

36. Information and Control Systems, Inc., software package to calculate singular values for continuous and discrete control systems, 28 Research Drive, Hampton, VA 23666.

37. Maybeck, P., Stochastic Models, Estimation, and Control, vol. 3, Academic Press, 1982.

38. Franklin, G. F., and Powel, J. D., Digital Control of Dynamic Systems, Addison-Wesley Publishing Company, 1981.

39. Doyle, J., "Analysis of Feedback Systems with Structured Uncertainties," IEE Proc., vol. 129, Pt. D., No. 6, November 1982.

APPENDIX A

USER'S GUIDE TO SVANAL: THE SINGULAR VALUE GRADIENT PROGRAM

A.1 INTRODUCTION

The primary purpose of SVANAL is to calculate singular value plots (sigma-plots), eigenvalue plots, and singular-value gradient plots using the theoretical developments of Chapters Three and Four. The calculation of singular values is done by computing the singular-value decomposition (SVD) [33, 35] using the subroutine SNVDEC contained in ORACLS [32]. The computation of eigenvalues is done using the subroutine EIGEN, also contained in ORACLS [32]; and the computation of the singular-value gradients is done using Equations 4.25, 4.27, and 4.29. As an option, the user may select to compute the singular-value gradients with respect to elements of the control-law matrices using the method developed by Newsom and Mukhopadhyay [24].

The software described here consists of three main subroutines and several auxiliary subroutines. The flow chart in Figure A.1 shows the relationship between the different subroutines. The block named ORACLS refers to subroutines in the ORACLS package [32].

The user is required to write his (her) own driver program according to the specific needs of the task to be handled. The driver program must be used to read data, print or plot results, and set the different option flags required to calculate the sigma-plots, eigenvalue plots, and singular-value gradients.

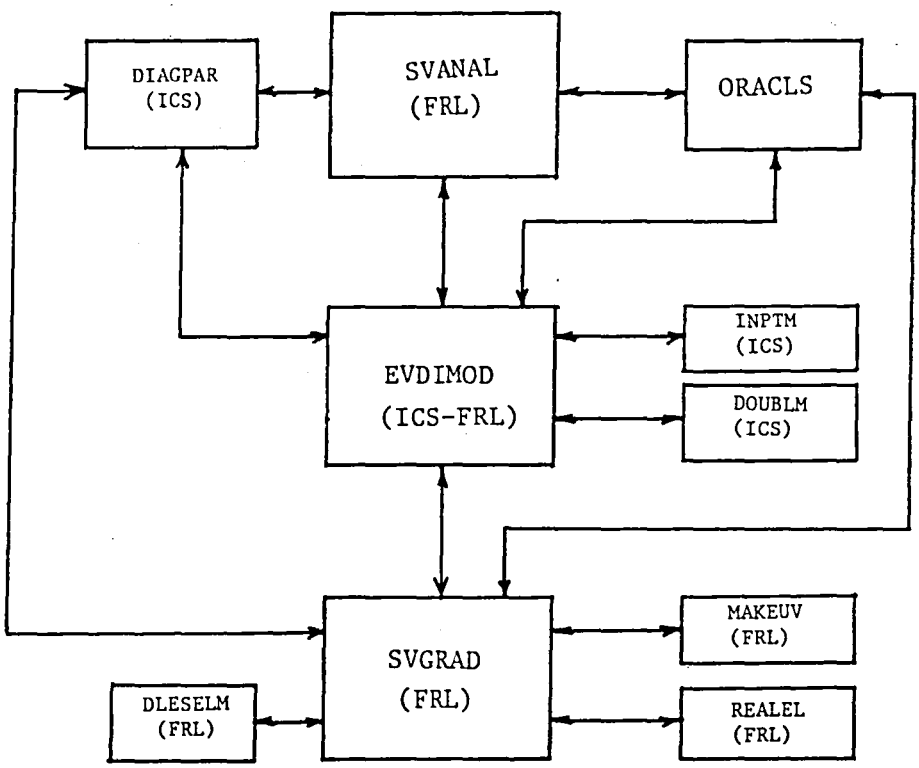

Figure A.1: Relationship between Subroutines SVANAL, EVDIMOD, SVGRAD, and the Auxiliary Subroutines

The three main subroutines are SVANAL, EVDIMOD, and SVGRAD. The function of SVANAL is to prepare the data according to the options selected by the user, calling subroutine EVDIMOD, and transferring input and output data from and to the user's driver program.

Subroutine EVDIMOD is a modified version of a subroutine provided by Information and Control Systems, Inc. [36]. The three most important functions of EVDIMOD are the handling and transformation of complex matrices into augmented real matrices (such that algorithms and software that utilize real-matrix operations can be used with complex matrices); the evaluation of the return difference matrix $(I + G_1)$, for continuous or single-rate digital feedback control systems for a range of frequencies; and serving as the platform for the evaluation of singular values, eigenvalues, and singular-value gradients, through calls to ORACLS (SNVDEC and EIGEN) and SVGRAD subroutines, respectively.

The main function of SVGRAD is the calculation of the singular-value gradients with respect to elements of the system and controller matrices, using the method described in Chapter Four, or with respect to the controller elements only, using the method described by Newsom and Mukhopadhyay [24].

In the following sections, the subroutines are described in more detail, the user is instructed in the use of the software, and an example of the kind of information that can be obtained is presented.

A.2 SUBROUTINE EVDIMOD

The subroutine EVDIMOD is a KU-FRL modification of the subroutine EIGVDI provided to us by Information and Control Systems, Inc. (ICS) [36]. EVDIMOD has three main functions (see also Figure A.2):

1. Handling and transformation of complex matrices into augmented real matrices. Since this software uses subroutines from ORACLS [32], and ORACLS handles only real matrices, the complex matrices of the form (X + jY), where X and Y are real matrices, are transformed into augmented real matrices of the form

$$\begin{bmatrix} X & Y \\ -Y & X \end{bmatrix} \tag{A.1}$$

allowing us to use real matrix subroutines.

2. Evaluation of the return difference matrix $(I + G_1)$, for continuous and single-rate digital feedback control systems for a range of frequencies. In the continuous case the plant is given by

$$\dot{\mathbf{X}} = \bar{A}\mathbf{X} + \bar{B}\mathbf{U} \tag{A.2}$$

the feedback control is

$$\mathbf{U} = -\bar{C}\mathbf{X} \tag{A.3}$$

and the return difference matrix is

$$\left(I + G_1(s)\right) = [I + \bar{C}(Is - \bar{A})^{-1}\bar{B}] \tag{A.4}$$

where $\mathbf{X}$ is the state-variable vector, $\bar{A}$ and $\bar{B}$ are the system matrices, $\bar{C}$ is the controller matrix, $\mathbf{U}$ is the control vector, and I is the identity matrix.

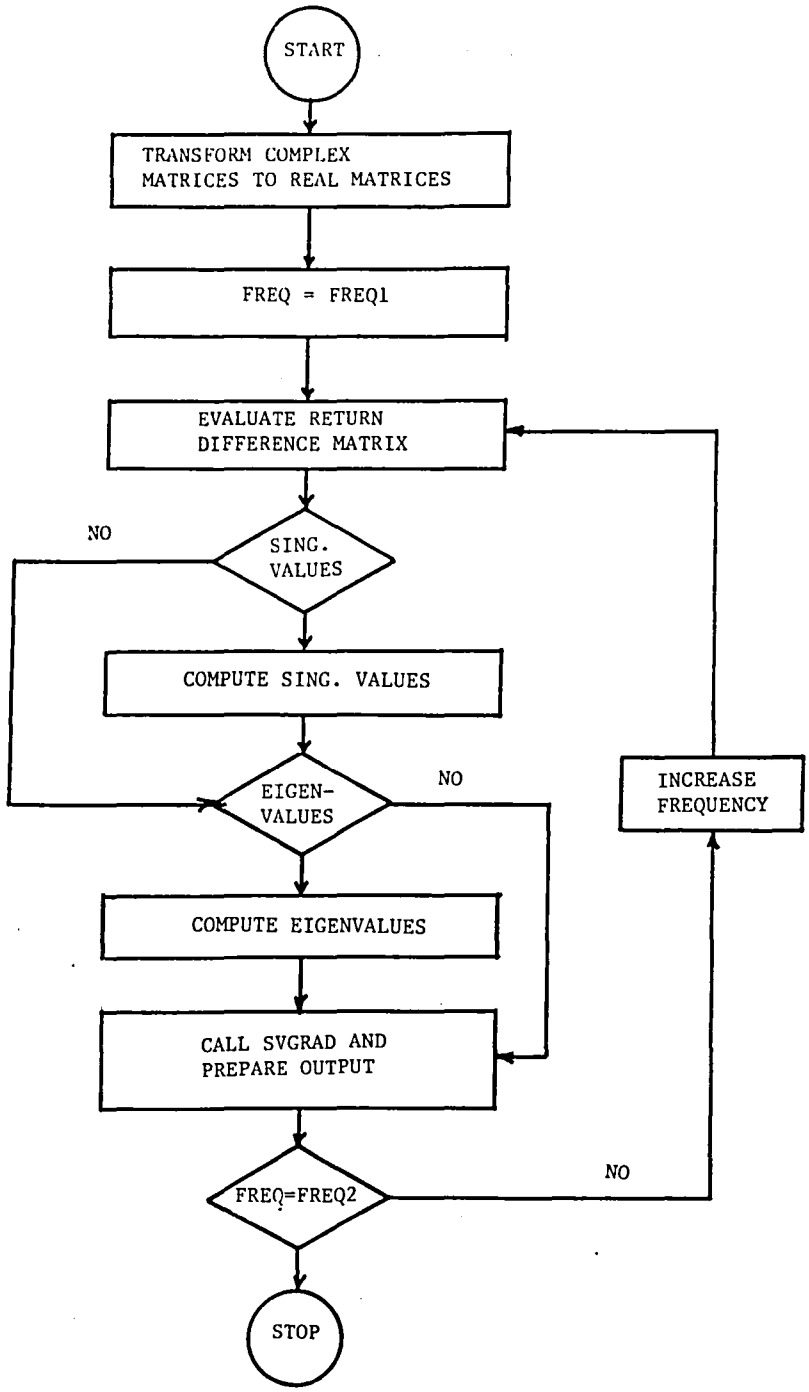

Figure A.2: General Flowchart of Subroutine EVDIMOD

In the digital system case, the plant is

$$\mathbf{X}_{k+1} = \Lambda \mathbf{X}_k + \Gamma \mathbf{U}_k \tag{A.5}$$

the feedback control is

$$\mathbf{U} = -\bar{C}\mathbf{X}_k \tag{A.6}$$

and the return difference matrix is

$$\left(I + G_1(z)\right) = [I + \bar{C}(Iz - \Lambda^{-1})\Gamma] \tag{A.7}$$

where $\mathbf{X}$ is the state-variable vector, $\mathbf{U}$ is the control vector, Λ and Γ are the discrete-system matrices, $\bar{C}$ is the controller matrix, and I is the identity matrix.

The method used to evaluate $\left(I + G_1(z)\right)$ is presented in Reference [25] and is an extension of the method used to evaluate $\left(I + G_1(s)\right)$ in the continuous case. $\left(I + G_1(z)\right)$ is evaluated at $z = e^{j\omega T}$ to obtain the complex matrix $\left(I + G_1(\cos\omega T + j \sin\omega T)\right)$, where $j = \sqrt{-1}$ and T is the sampling interval. EVDIMOD will evaluate the return difference matrix for the continuous or digital system, according to the option specified by the user at the time of data input.

3. EVDIMOD serves as the platform for the evaluation of singular values, eigenvalues (of the return difference matrix), and singular-value gradients, through calls to ORACLS (SNVDEC and EIGEN) and SVGRAD. The singular values of $\left(I + G_1(e^{j\omega T})\right)$, for the digital system, are determined using real matrix SVD, once the complex matrix is transformed into the augmented real matrix form discussed previously.

Subroutine EVDIMOD uses the following auxiliary subroutines:

INPTM: Used to input matrix A into a larger matrix, B, given a starting row and column number (I,J). The size of B will not change.

DIAGPAR: Used to combine two matrices such that they become the top left and bottom right matrices of a quad partition matrix. The top right and bottom left matrices are set to zero in the quad partition matrix.

DOUBLM: Used to create a real (2n x 2m) matrix from a real (n x 2m) by doubling the number of rows:

$$\begin{array}{lll} \text{Real Matrix} & & \\ \text{(n x 2m)} & n & \begin{bmatrix} A1 & B1 & A2 & B2 & A3 & B3 \ldots Am & Bm \end{bmatrix} \\ & & \\ \text{Double Matrix} & & \begin{bmatrix} A1 & A2 & A3 \ldots Am & B1 & B2 & B3 \ldots Bm \\ -B1 & -B2 \ldots\ldots -Bm & & A1 & A2 \ldots\ldots & Am \end{bmatrix} \\ \text{(2n x 2m)} & 2n & \end{array}$$

The purpose of this transformation is to do multiplication, addition, subtraction, and inversion of complex matrices using software for real matrices. Subroutines INPTM, DIAGPAR, and DOUBLM were provided to us by ICS.

A.3 SUBROUTINE SVGRAD

The flowchart for subroutine SVGRAD is shown in Figure A.3. The purpose of SVGRAD is to calculate the singular-value gradients with respect to elements of the system and controller matrices using the theoretical development of Chapter Four. As an option, the user can also use the method developed by Newsom and Mukhopadhyay [24] to

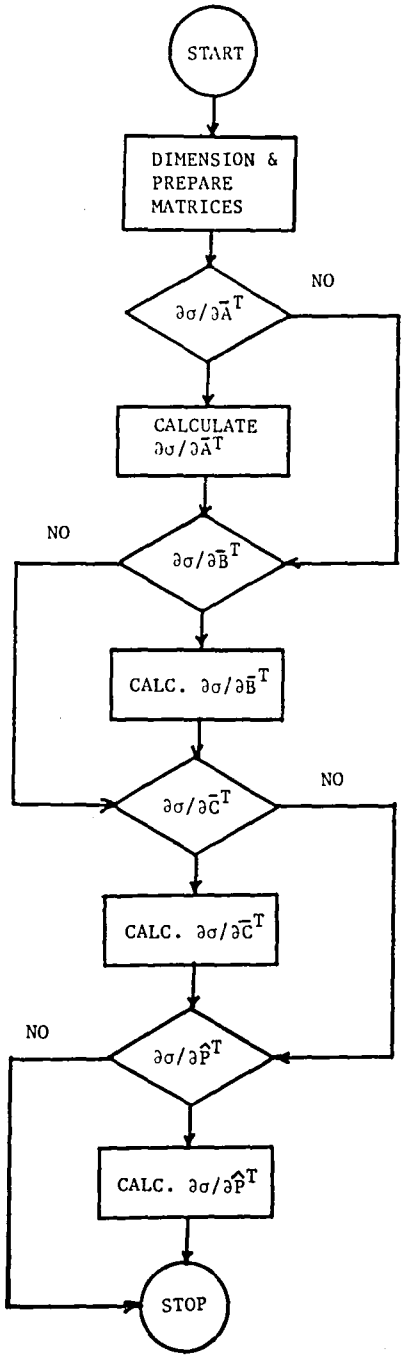

Figure A.3: General Flowchart of Subroutine SVGRAD

calculate the gradients with respect to the elements of the controller matrices.

For the system in Equations (A.2) and (A.3), SVGRAD uses the following expressions to evaluate the gradients with respect to elements in the $\bar{A}$, $\bar{B}$, and $\bar{C}$ matrices:

$$\frac{\partial \sigma_i}{\partial \bar{A}^T} = \mathrm{Re}[\Phi \bar{B} \mathbf{v}_i \mathbf{u}_i^* \bar{C} \Phi] \tag{A.8}$$

$$\frac{\partial \sigma_i}{\partial \bar{B}^T} = \mathrm{Re}[\mathbf{v}_i \mathbf{u}_i^* \bar{C} \Phi] \tag{A.9}$$

$$\frac{\partial \sigma_i}{\partial \bar{C}^T} = \mathrm{Re}[\Phi \bar{B} \mathbf{v}_i \mathbf{u}_i^*] \tag{A.10}$$

which correspond to Equations (4.25), (4.27), and (4.29) and therefore will not be discussed here again.

It is important to note that if a discrete system has been selected, the gradients obtained with Equations (A.8) and (A.9) will correspond to $\partial \sigma_i / \partial \Lambda^T$ and $\partial \sigma_i / \partial \Gamma^T$, which are the gradients with respect to the matrices of the discretized system (Equation A.5) and not of the original system in Equation (A.2). Since matrices $\Lambda(T)$ and $\Gamma(T)$ are a function of matrices $\bar{A}$ and $\bar{B}$, it is possible to find the gradients with respect to these latter matrices. One way in which this could be achieved is discussed in Appendix C; however, it has not been implemented at this point.

Another option available in SVGRAD is to obtain the gradients using the method developed in Reference [24]. However, in order to

use this option some words have to be said about the plant (airplane) and controller representation used.

Newsom and Mukhopadhyay [24] use the following representation of the plane and the feedback control law, which includes controller dynamics:

$$\dot{\mathbf{X}}_s = F\mathbf{X}_s + G_u\mathbf{U}$$

$$\mathbf{Z} = H\mathbf{X}_s \tag{A.11}$$

for the plant, where $\mathbf{X}_s$ is the state-variable vector, $\mathbf{U}$ is the control input vector, F and G_u are the system matrices, Z is the output-variable vector, and H is the output matrix; and

$$\mathbf{X}_c = A_c\mathbf{X}_c + B_c\mathbf{Z}$$

$$\mathbf{U} = C_c\mathbf{X}_c + D_c\mathbf{Z} \tag{A.12}$$

for the controller, where $\mathbf{X}_c$ is the controller-variable vector, and A_c, B_c, C_c, and D_c are the controller matrices.

The system in Equations (A.11) and (A.12) can also be represented by Equations (A.2) and (A.3), if we let

$$\mathbf{X} = \begin{bmatrix} \mathbf{X}_s \\ \mathbf{X}_c \end{bmatrix} \tag{A.13}$$

$$\bar{A} = \left[\begin{array}{c|c} F & 0 \\ \hline B_c H & A_c \end{array}\right] \tag{A.14}$$

$$\bar{B} = \begin{bmatrix} G_u \\ \hline 0 \end{bmatrix} \tag{A.15}$$

$$\bar{C} = \left[-D_c H \;\vdots\; -C_c\right] \tag{A.16}$$

The expression used by Reference [24] to calculate the gradients is

$$\frac{\partial \sigma_i}{\partial \hat{P}^T} = \mathrm{Re}\left[\hat{H}(Is - \bar{A})^{-1}\bar{B}(\mathbf{v}_i\mathbf{u}_i^*)[-I \,\vdots\, \bar{C}(Is - \bar{A})^{-1}\bar{I}]\right] \tag{A.17}$$

where $\hat{P}$, $\hat{H}$, and $\hat{I}$ are given by

$$\hat{P} = \left[\begin{array}{c:c} D_c & C_c \\ \hline B_c & A_c \end{array}\right] \tag{A.18}$$

$$\hat{H} = \left[\begin{array}{c:c} H & 0 \\ \hline 0 & I \end{array}\right] \tag{A.19}$$

$$\bar{I} = \left[\begin{array}{c} 0 \\ \hline I \end{array}\right] \tag{A.20}$$

and I is the identity matrix; and $\mathbf{u}_i$ and $\mathbf{v}_i$ are the left and right normalized eigenvectors.

The auxiliary subroutines used by SVGRAD are the following:

DIAGPAR: Discussed in Section A.2.

REALEL: This subroutine selects the real elements of a complex matrix which has been stored as an augmented-real matrix in column-packed form:

$$\left[\begin{array}{c:c} X & Y \\ \hline -Y & X \end{array}\right]$$

The returned values will correspond to matrix X in a column-packed form.

DLESELM: This subroutine selects the desired elements from an input matrix GRAD and stores them in a matrix GRAD2 which is the returned argument.

MAKEUV: This subroutine checks for the form in which the eigenvectors, **u** and **v**, are obtained from EVDIMOD and modifies them, if necessary, to the form required for the matrix operations in SVGRAD:

input: $\left[\begin{array}{c|c} x & y \\ \hline -y & x \end{array}\right]$ or $\left[\begin{array}{c|c} y & x \\ \hline x & -y \end{array}\right]$

output: $\left[\begin{array}{c|c} x & y \\ \hline -y & x \end{array}\right]$

where the eigenvector is $\mathbf{u} = \mathbf{x} + j\mathbf{y}$.

A.4 SUBROUTINE SVANAL

The subroutine SVANAL is the executive driver of the package of subroutines presented in this appendix (see Figure A.4). As such, it is the only subroutine which must actually be called by the user. SVANAL performs the following functions:

1. Optional echo check of all the input data
2. Matrix and matrix dimension initialization. This includes the creation of the $\hat{H}$ matrix, which is used by Newsom and Mukhopadhyay (see Equations A.11-A.19). The user inputs the H matrix from the equation

$$\mathbf{Z} = H\,\mathbf{X}_s \tag{A.11}$$

where $\mathbf{Z}$ is the output vector of dimension No, and $\mathbf{X}_s$ is the state vector of dimension Ns. SVNAL creates

$$\hat{H} = \left[\begin{array}{c|c} H & 0 \\ \hline 0 & I \end{array}\right] \qquad \left((No + M) \times (Ns + M)\right)$$

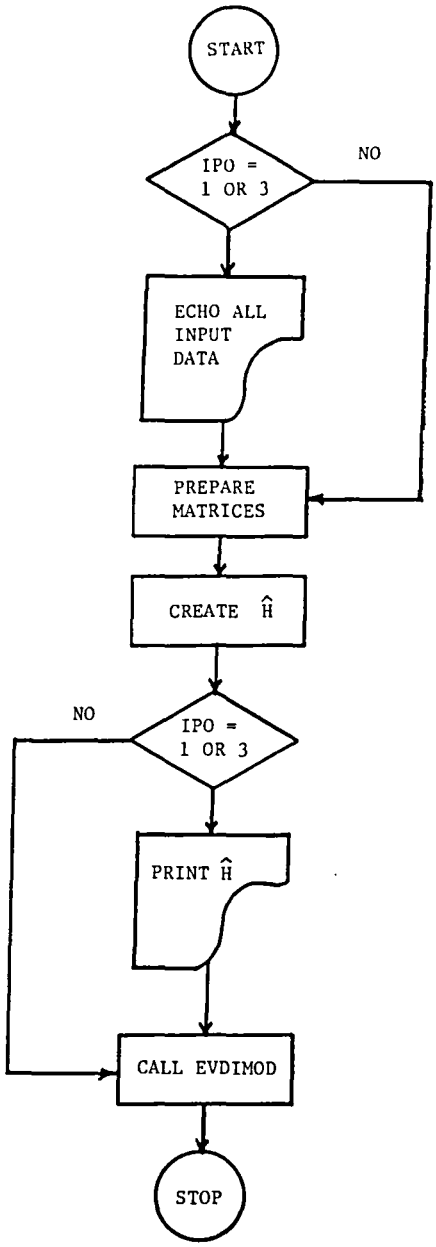

Figure A.4: General Flowchart of Subroutine SVANAL

where H is the observer matrix defined in Equation (A.11) and I is an M x M identity matrix. This matrix is only created if gradients with respect to controller parameters ($\hat{P}$ matrix) are desired. The user can also get a printout of $\hat{H}$ if desired.

3. Subroutine call to EVDIMOD, which handles the calculation of the singular values and their gradients.

4. Output of the desired information in matrix form. The following information is generated by EVDIMOD (and the subroutines to which it is linked):

   a) Minimum singular value and minimum eigenvalue at each frequency

   b) Singular value gradients with respect to selected elements of the system and controller matrices, at each frequency.

The format for the input and output matrices to specify and retrieve the desired singular-value gradients is described in Section A.5.

A.5 SVANAL USAGE

A.5.1 Calling Sequence

```
CALL SVANAL (ABAR, MA, BBAR, MB, CBAR, MC, H, MH, NSM, NC,
     NO,NS,M, FREQ1, FREQ2, NP, DELT, MI, LES, IPO, LUN1, LUN2,
     NWKDIM, WK, IWK, SVMAT, MSV)
```

A.5.2 Input Arguments

ABAR - Variable dimensioned two-dimensional real array containing the augmented system matrix, $\bar{A}$. $\bar{A}$ has dimensions (NSM x NSM). For discrete systems, ABAR must contain the state transition matrix, Λ.

MA - Maximum first dimension of the array ABAR as given in the DIMENSION statement of the calling program.

BBAR - Variable dimensioned two-dimensional real array containing the augmented control effectiveness matrix, $\bar{B}$. $\bar{B}$ has dimensions (NSM x NC). For discrete systems, BBAR must contain the discretized control power matrix, Γ.

MB - Maximum first dimension of the array BBAR as given in the DIMENSION statement of the calling program.

CBAR - Variable dimensioned two-dimensional real array containing the augmented feedback law matrix, $\bar{C}$. $\bar{C}$ has dimensions (NC x NSM).

MC - Maximum first dimension of the array CBAR as given in the DIMENSION statement of the calling program.

H - Variable dimensioned two-dimensional real array containing the augmented observer matrix, H. This matrix is not required unless gradients with respect to parametrs in $\hat{P}$ (Newsom and Mukhopadhyay method) are desired, but the variable name must appear in the call statement.

MH - Maximum first dimension of the array H as given in the DIMENSION statement of the calling program

NSM - Dimension of the augmented state-variable vector.

NC - Dimension of the control vector.

NO - Dimension of the output vector.

NS - State-vector dimension before augmentation.

M - Order of the controller-dynamics equation. See Equation (A.12).

NOTE: The variables MH, NO, NS, and M must appear in the call statement to SVANAL; but they do not have to be initialized if gradients with respect to parametrs in $\hat{P}$ are not desired. NO, NS, M, and NC are consistent with the definitions given in Reference [23] and Section A.3.

FREQ1 - Lowest frequency for the singular value analysis.

FREQ2 - Highest frequency for the singular value analysis.

NP - Number of frequencies between FREQ1 and FREQ2 where singular values, eigenvalues, and gradients are to be calculated.

DELT - Sampling interval for discrete system. This variable must be set to zero for continuous systems.

MI - Integer vector whose dimension is 4. Each entry indicates the number of gradients desired from the

$\bar{A}$, $\bar{B}$, $\bar{C}$, and $\hat{P}$ matrix, respectively. This input argument is described in more detail in Section A.5.8.

LES - Integer array whose first dimension must be 4. Second dimension must be $\max_k(MI(k))$. Entry (k,i) indicates the location (counting across the rows) in the k-th matrix ($\bar{A}$, $\bar{B}$, $\bar{C}$, or $\hat{P}$) of the parameter with respect to which gradient plot is desired. This input argument is described in more detail in Section A.5.8.

IPO - Integer variable indicating the type of output desired.

IPO = 0: All printout suppressed.

IPO = 1: Input matrix data echo; includes $\hat{H}$ matrix printout if $\hat{P}$ gradients are requested. This printout is directed to logical unit number LUN1.

IPO = 2: Data file printout. This printout is directed to logical unit number LUN2 and is described in Section A.5.8.

IPO = 3: Both matrix data echo and data file information are printed out to their respective logical unit numbers.

LUN1 - Logical unit number for the matrix data echo and error output. This variable should be set to the LUN for the terminal.

LUN2 - Logical unit number for the data file printout (see also Section A.5.8). The calling program must open and initialize the data file referenced by LUN2.

NOTE: LUN1 must be initialized to allow error statements. LUN2 need not be initialized if IPO < 2.

NWKDIM - Dimension of the work vector, WK, as given by the DIMENSION statement of the calling program. NWKDIM must be at least

$$\begin{aligned} NWKDIM = {} & 37NSM^2 + 36NSM + 6(NSM \cdot NC) + 28NC^2 + 42NC + 93 + \\ & + 5MAX\left(4NSM^2,\ 4(NO + M)(NC + M)\right) + MAX\left(MI(k),\ k = 1,4\right) + \\ & + 4(NO + M)(NSM + NC) + 4(NSM \cdot M) \end{aligned} \qquad (A.21)$$

WK - Real work vector dimensioned at least NWKDIM in the calling routine.

IWK - Integer work vector dimensioned at least 2NC + 2M in the calling routine.

MSV - Maximum first dimension of the array SVMAT as given in the DIMENSION statement of the calling program. MSV must be greater than NP.

A.5.3 Output Arguments

SVMAT - Two-dimensional array containing all output information. SVMAT must be dimensioned at least [NP x (MI(1) + MI(2) + MI(3) + MI(4) + 3)] in the calling routine. Data is organized as follows:

SVMAT (I, 1): frequency, in rad/sec, I = 1 to NP

SVMAT (I, 2): minimum singular value, I = 1 to NP

SVMAT (I, 3): minimum eigenvalue, I = 1 to NP

SVMAT (I, J + 3): gradients with respect to parameters in the $\bar{A}$ matrix, J = 1 to MI(1)

I = 1 to NP

SVMAT (I, J + MI(1) + MI(2) + 3): gradients with respect to parameters in the $\bar{C}$ matrix, J = 1 to MI(3)

I = 1 to NP

SVMAT (I, J + MI(1) + MI(2) + MI(3) + 3): gradients with respect to parameters in the $\hat{P}$ matrix,

J = 1 to MI(4)

I = 1 to NP

A.5.4 COMMON Blocks

The COMMON blocks employed by SVANAL are

GRADSTF and SAVE.

A.5.5 Error Messages

(1) If the work array is not large enough, the following message will be printed: "THE WORK ARRAY IS NOT LARGE ENOUGH IN SNGVDI."

(2) If errors occur within SNVDEC, the following message will be printed: "PASS # _____ THERE IS AN ERROR IN THE SECOND CALL TO SNVDEC, IERR = _____ IN SNGVDI."

A.5.6 Subroutines Employed by SVANAL

The following subroutines from ORACLS, ICS, and FRL are employed:

ORACLS - ADD, NULL, MULT, JUXTR, JUXTC, UNITY, EQUATE, PRNT, MAXEL, AXPXB, SCALE, SNVDEC, HSHLDR, BCKMLT, SCHUR, SHRSLV, SYSSLV, NORMS, LNCNT, EIGEN, INVIT, BALBAK, ELMBAK, HQR, ELMHES, BALANC

ICS - DOUBLM, DIAGPAR, INPTM

FRL - EVDIMOD, SVGRAD, DLESELM, MAKEUV, REALEL

A.5.7 Subroutines Employing SVANAL

None.

A.5.8 Concluding Remarks

A singular value gradient exists with respect to each element of the $\bar{A}$, $\bar{B}$, $\bar{C}$, and $\hat{P}$ matrix (these matrices are described in Section A.3). SVANAL outputs only those gradients which are specified by the user. To identify the gradients of interest, the following information must be given to SVANAL:

1) MI(k), k = 1, 2, 3, and 4.

   MI is a vector containing four integers. Each integer represents a particular matrix:

   MI(1) ====> $\bar{A}$ matrix

   MI(2) ====> $\bar{B}$ matrix

   MI(3) ====> $\bar{C}$ matrix

   MI(4) ====> $\hat{P}$ matrix

   The value of MI(k) indicates the number of gradients desired from the corresponding matrix. For instance, MI(3) = 7 indicates that 7 gradients with respect to variables in the $\bar{C}$ matrix are desired.

2) LES(k,j), k = 1, 2, 3, and 4

   j = 1, 2, 3,..., MI(k)

LES is an integer matrix containing four rows and enough columns to accommodate the largest value of MI(k). Each row corresponds to one of the four matrices, $\bar{A}$, $\bar{B}$, $\bar{C}$, and $\hat{P}$, respectively (in the same order as the elements of MI(k)). Each row contains exactly MI(k) nonzero elements, one for each of the desired gradients. The value of each element indentifies the matrix location (in the corresponding $\bar{A}$, $\bar{B}$, $\bar{C}$, or $\hat{P}$ matrix) of the parameter for which a gradient plot is desired. Matrix locations are numbered from left to right across the rows, continuing on the next row after each row is numbered. For instance, a 4 x 4 matrix is numbered as follows:

1	2	3	4
5	6	7	8
9	10	11	12
13	14	15	16

As an example, suppose the $\bar{A}$ matrix is 4 x 4. Note that the dimension of the array ABAR, in which $\bar{A}$ is stored, is of no consequence. If the user wants gradients with respect to elements 2, 7, 9, and 12 (as numbered above), he would set MI(1) = 4 (indicating that four gradients are desired from the A matrix) and

LES(1, 1) = 2

LES(1, 2) = 7

LES(1, 3) = 9

LES(1, 4) = 12.

Refer to Section A.6 for a complete example of how MI and LES are created.

Data-file output is provided to allow part of the information generated by SVANAL to be saved in the instance of a program abort. Numerical problems in the ORACLS subroutine SNVDEC sometimes cause errors, at the time of execution, which cannot be avoided. If the minimum singular value, minimum eigenvalue, and gradient are printed out at each frequency as they are calculated (IPO = 2 or 3), then this information will not be lost if an error occurs. The plots can then be continued at or near the frequency for which the error occurred. The user then proceeds, segment by segment, across the frequency range until the entire plot has been obtained.

The format of the output file is best described by the WRITE and FORMAT statements which create it. At each frequency, FREQ, SVMIN, and EVMIN are the minimum singular value and minimum eigenvalue, respectively. LGRAD(I, K) contains the gradients, where I = 1 to 4 represent each of the matrices $\bar{A}$, $\bar{B}$, $\bar{C}$, and $\hat{P}$ in that order. K goes from 1 to MI(I), the number of gradients desired from the respective matrix.

```
      WRITE (LUN2,4000) FREQ, SVMIN, EVMIN
      DO 1 I =1,4
    1 WRITE (LUN 2,4000) ( LGRAD(I,K) K = 1, MI(I) )
 4000 FORMAT (8F10.5)
```

A.6 EXAMPLE

In Section 4.3.1, a singular value analysis was done on the following single-input/single-output system. Two cases were examined, one in which the singular-value gradient with respect to a parameter in the $\bar{C}$ matrix was calculated, and one in which gradients with respect to parameters in the $\bar{A}$ matrix were calculated. In both of these cases, however, the nominal system is the same:

$$\begin{bmatrix} \dot{x}1 \\ \dot{x}2 \\ \dot{x}3 \end{bmatrix} = \underbrace{\begin{bmatrix} 0 & 1 & 0 \\ 0 & 0 & 1 \\ -40 & -28 & -6 \end{bmatrix}}_{\bar{A}} \begin{bmatrix} x1 \\ x2 \\ x3 \end{bmatrix} + \begin{bmatrix} 0 \\ 0 \\ 1 \end{bmatrix} \delta$$

$$\delta = - \underbrace{\begin{bmatrix} 0 & 200 & 0 \end{bmatrix}}_{\bar{C}} \begin{vmatrix} x1 \\ x2 \\ x3 \end{vmatrix}$$

In case I, the gradient with respect to element 1 in $\bar{C}$ was obtained. In case II, gradients with respect to elements 7, 8, and 9 in $\bar{A}$ were calculated. The frequency range for all the plots in Section 4.3.1 was .01 to 100. rad/sec. All four of these gradients, as well as the minimum singular value and minimum eigenvalue plots, can be found using one single call to SVANAL, with the following input information:

$$ABAR = \begin{bmatrix} 0 & 1 & 0 \\ 0 & 0 & 1 \\ -40 & -28 & -6 \end{bmatrix}$$

$$BBAR = \begin{bmatrix} 0 \\ 0 \\ 1 \end{bmatrix}$$

$$CBAR = \begin{bmatrix} 0 & 200 & 0 \end{bmatrix}$$

MA, MB, MC: Depend on dimension statement of calling program.

H, MH: Not needed; $\hat{P}$ gradients not being calculated.

NSM = 3

NC = 1

NO, NS, M: Not needed.

FREQ1 = .01

FREQ2 = 100.

NP = 150

DELT = 0.0 (Continuous System)

MI(1) = 3
MI(2) = 0
MI(3) = 1
MI(4) = 0

LES(1, 1) = 7
LES(1, 2) = 8
LES(1, 3) = 9
LES(3, 1) = 1

IPO = 3
LUN1 = 3 (LUN for the CRT)
LUN2 = 18 (LUN for the data file)

NWKDIM = 700 minimum required according to Equation (A.21)
MSV: Depends on dimension statement of calling program.

The output information all appears in the matrix SVMAT. Table A.1 is an image of this matrix, with the contents of each colunn labeled to indicate how output information is arranged in SVMAT.

Table A.1: An Example of Output-Matrix SVMAT Containing Information on Frequency, Minimum Singular- and Eigenvalues, and Singular-Value Gradients

SVMAT(I,J):

J=	1	2	3	4	5	6	7
I	Omega	MinSig	MinEig	dSig/dF1	dSig/dF2	dSig/dF3	dSig/dAlph
1	.	.	.	.	.	.	.
2							
3	.	.	.	.	.	.	.
4							
.	.	.	.	.	.	.	.
.							
.	.	.	.	.	.	.	.
	0.10000	1.14864	1.14864	0.00693	-0.00104	-0.00007	0.02169
	0.10965	1.17636	1.17636	0.00812	-0.00121	-0.00010	0.02117
	0.12023	1.20881	1.20881	0.00949	-0.00139	-0.00014	0.02058
	0.13183	1.24667	1.24667	0.01105	-0.00160	-0.00019	0.01994
	0.14454	1.29067	1.29067	0.01281	-0.00183	-0.00027	0.01923
	0.15849	1.34158	1.34158	0.01478	-0.00207	-0.00037	0.01848
	0.17378	1.40023	1.40023	0.01698	-0.00232	-0.00051	0.01767
	0.19055	1.46751	1.46751	0.01941	-0.00258	-0.00070	0.01683
	0.20893	1.54432	1.54432	0.02209	-0.00283	-0.00096	0.01595
	0.22909	1.63162	1.63162	0.02502	-0.00306	-0.00131	0.01505
	0.25119	1.73039	1.73039	0.02820	-0.00325	-0.00178	0.01414
	0.27542	1.84166	1.84166	0.03164	-0.00338	-0.00240	0.01323
	0.30200	1.96646	1.96646	0.03534	-0.00342	-0.00322	0.01233
	0.33113	2.10587	2.10587	0.03929	-0.00332	-0.00431	0.01144
	0.36308	2.26097	2.26097	0.04349	-0.00304	-0.00573	0.01058
	0.39811	2.43286	2.43286	0.04792	-0.00249	-0.00759	0.00974
	0.43652	2.62264	2.62264	0.05255	-0.00160	-0.01001	0.00894
	0.47863	2.83139	2.83139	0.05737	-0.00025	-0.01314	0.00818
	0.52481	3.06017	3.06017	0.06231	0.00171	-0.01716	0.00745
	0.57544	3.30996	3.30996	0.06732	0.00444	-0.02229	0.00676
	0.63096	3.58163	3.58163	0.07230	0.00818	-0.02878	0.00611
	0.69183	3.87593	3.87593	0.07715	0.01319	-0.03693	0.00550
	0.75858	4.19341	4.19341	0.08173	0.01977	-0.04703	0.00493
	0.83176	4.53439	4.53439	0.08586	0.02831	-0.05940	0.00439
	0.91201	4.89892	4.89892	0.08935	0.03921	-0.07432	0.00388
	1.00000	5.28674	5.28674	0.09195	0.05295	-0.09195	0.00341
	.	.	.	.	.	.	.
.	.	.	.	.	.	.	.
.							
.							
NP	.	.	.	.	.	.	.

APPENDIX B

AERODYNAMIC AND GEOMETRIC DATA FOR A TYPICAL BUSINESS JET

This appendix contains the geometric and lateral-directional aerodynamic data used in the example analyses of the yaw-damper and yaw-roll-damper SAS of a typical business jet. The data were obtained from Reference [31].

The lateral-directional, small-perturbation equations of motion of the airplane are shown in Table B.1. The formulas for the lateral-directional dimensional stability derivatives were also obtained from Reference [31] and are contained in Table B.2. The dimensionless derivatives and the initial characteristics of the airplane for approach flight condition and full-flaps down at sea level are shown in Table B.3.

Table B.1: Lateral-Directional, Small-Perturbation Equations of Motion for a Business Jet Airplane

$$
\begin{bmatrix} \dot{\beta} \\ \dot{p} \\ \dot{r} \\ \dot{\phi} \end{bmatrix} =
\begin{bmatrix}
\left(\frac{Y_\beta}{U_1}\right) & \left(\frac{Y_p}{U_1}\right) & \left(\frac{Y_R}{U_1} - 1\right) & g \cos\theta_1 \\
\left(\frac{A_1 N_\beta + L_\beta}{1 - A_1 B_1}\right) & \left(\frac{A_1 N_p + L_p}{1 - A_1 B_1}\right) & \left(\frac{A_1 N_r + L_r}{1 - A_1 B_1}\right) & 0 \\
\left(\frac{B_1 L_\beta + N_\beta}{1 - A_1 B_1}\right) & \left(\frac{B_1 L_p + N_p}{1 - A_1 B_1}\right) & \left(\frac{B_1 L_r + N_r}{1 - A_1 B_1}\right) & 0 \\
0 & 1 & \tan\theta_1 & 0
\end{bmatrix}
\begin{bmatrix} \beta \\ p \\ r \\ \phi \end{bmatrix} +
$$

$$
+
\begin{bmatrix}
\left(Y_{\delta_A}/U_1\right) & \left(Y_{\delta_R}/U_1\right) \\
\left(\frac{A_1 N_{\delta_A} + L_{\delta_A}}{1 - A_1 B_1}\right) & \left(\frac{A_1 N_{\delta_R} + L_{\delta_R}}{1 - A_1 B_1}\right) \\
\left(\frac{B_1 L_{\delta_A} + N_{\delta_A}}{1 - A_1 B_1}\right) & \left(\frac{B_1 L_{\delta_R} + N_{\delta_R}}{1 - A_1 B_1}\right) \\
0 & 0
\end{bmatrix}
\begin{bmatrix} \delta_A \\ \delta_R \end{bmatrix}
$$

$$A_1 = I_{XZ}/I_{XX}$$

$$B_1 = I_{XZ}/I_{ZZ}$$

Table B.2: Lateral-Directional Dimensional Stability Derivatives (from Reference [31])

$$Y_\beta = \frac{\bar{q}_1 S C_{y_\beta}}{m} \quad (\text{ft sec}^{-2})$$

$$Y_p = \frac{\bar{q}_1 S b C_{y_p}}{2mU_1} \quad (\text{ft sec}^{-1})$$

$$Y_r = \frac{\bar{q}_1 S b C_{y_r}}{2mU_1} \quad (\text{ft sec}^{-1})$$

$$Y_{\delta_A} = \frac{\bar{q}_1 S C_{y_{\delta_A}}}{m} \quad (\text{ft sec}^{-2} \text{ or } \text{ft sec}^{-2}\ \text{deg}^{-1})$$

$$Y_{\delta_R} = \frac{\bar{q}_1 S C_{y_{\delta_R}}}{m} \quad (\text{ft sec}^{-2} \text{ or } \text{ft sec}^{-2}\ \text{deg}^{-1})$$

$$L_\beta = \frac{\bar{q}_1 S b C_{\ell_\beta}}{I_{xx}} \quad (\text{sec}^{-2})$$

$$L_p = \frac{\bar{q}_1 S b^2 C_{\ell_p}}{2I_{xx}U_1} \quad (\text{sec}^{-1})$$

$$L_r = \frac{\bar{q}_1 S b^2 C_{\ell_r}}{2I_{xx}U_1} \quad (\text{sec}^{-1})$$

$$L_{\delta_A} = \frac{\bar{q}_1 S b C_{\ell_{\delta_A}}}{I_{xx}} \quad (\text{sec}^{-2} \text{ or } \text{sec}^{-2}\ \text{deg}^{-1})$$

$$L_{\delta_R} = \frac{\bar{q}_1 S b C_{\ell_{\delta_R}}}{I_{xx}} \quad (\text{sec}^{-2} \text{ or } \text{sec}^{-2}\ \text{deg}^{-1})$$

$$N_\beta = \frac{\bar{q}_1 S b C_{n_\beta}}{I_{zz}} \quad (\text{sec}^{-2})$$

$$N_{T_\beta} = \frac{\bar{q}_1 S b C_{n_{T_\beta}}}{I_{zz}} \quad (\text{sec}^{-2})$$

$$N_p = \frac{\bar{q}_1 S b^2 C_{n_p}}{2I_{zz}U_1} \quad (\text{sec}^{-1})$$

$$N_r = \frac{\bar{q}_1 S b^2 C_{n_r}}{2I_{zz}U_1} \quad (\text{sec}^{-1})$$

$$N_{\delta_A} = \frac{\bar{q}_1 S b C_{n_{\delta_A}}}{I_{zz}} \quad (\text{sec}^{-2} \text{ or } \text{sec}^{-2}\ \text{deg}^{-1})$$

$$N_{\delta_R} = \frac{\bar{q}_1 S b C_{n_{\delta_R}}}{I_{zz}} \quad (\text{sec}^{-2} \text{ or } \text{sec}^{-2}\ \text{deg}^{-1})$$

Table B.3: Aerodynamic and Inertial Characteristics Needed for the Yaw- and Yaw/Roll-Damper Analyses for a Typical Business Jet (from Reference [31])

The following data are for a business jet airplane in an approach flight condition.

Full Flaps - Sea level

V_E = 120 kts	U_1 = 202 fps	I_{xx_s} = 23,500 slug-ft^2
W = 11,800 lbs		
S = 232. ft^2		I_{xz_s} = -100 slug-ft^2
b = 34.2 ft		I_{zz_s} = 40,700 slug-ft^2
C_L = 1.05	M = .18	

C_{y_β} = - 0.73 rad^{-1}	C_{y_r} = + 0.4 rad^{-1}	C_{y_p} = 0
C_{ℓ_β} = - 0.13 rad^{-1}	C_{ℓ_r} = 0.30 rad^{-1}	C_{ℓ_p} = -.386 rad^{-1}
C_{n_β} = 0.107 rad^{-1}	C_{n_r} = -0.233 rad^{-1}	C_{n_p} = - 0.066 rad^{-1}
$C_{y_{\delta_R}}$ = .1375 rad^{-1}	$C_{y_{\delta_A}}$ = 0	
$C_{\ell_{\delta_R}}$ = .0194 rad^{-1}	$C_{\ell_{\delta_A}}$ = 0.149 rad^{-1}	
$C_{n_{\delta_R}}$ = -.0745 rad^{-1}	$C_{n_{\delta_A}}$ = -.0355 rad^{-1}	

Yaw-Rate-To-Rudder Transfer Function:

$$\frac{r}{\delta_R}(s) = -0.708 \frac{(s + 0.912)[(s - .136)^2 + (.521)^2]}{(s + 0.832)(s - .004)[(s + .0031)^2 + (1.10)^2]}$$

Roll-Rate-To-Aileron Transfer Function:

$$s\frac{\phi}{\delta_A}(s) = 2.44 \frac{s[(s + .120)^2 + (0.846)^2]}{(s + 0.832)(s - .004)[(s + .0031)^2 + (1.10)^2]}$$

APPENDIX C

A SUGGESTED APPROACH TO THE DEVELOPMENT OF SINGULAR-VALUE GRADIENTS FOR SAMPLED-DATA SYSTEMS

This appendix presents a suggested approach to the development of the singular-value gradients for sampled-data systems. The use of these expressions should extend the applicability of the sensitivity analysis technique to sampled-data systems.

Sampled-data systems are composed of a continuous dynamical subsystem and a discrete subsystem. The continuous subsystem is called the plant, and the discrete subsystem is called the digital controller. To analyze a sampled-data system, the continuous plant must be discretized so that the two subsystems have a common representation. If the continuous model of the plant is given by Equation (4.6), the following equation represents the discretized model:

$$\mathbf{X}_{k+1} = \Lambda(T)\mathbf{X}_k + \Gamma(T)\mathbf{U}_k \tag{C.1}$$

where $\mathbf{X}$ is the state-variable vector, $\mathbf{U}$ is the control vector, and $\Lambda(T)$ is called the transition matrix, given by

$$\Lambda(T) = I + \bar{A}T + \bar{A}^2\frac{T^2}{2} + \ldots \tag{C.2}$$

and $\Gamma(T)$ is given by

$$\Gamma(T) = \left[\int_0^T \Lambda(\tau)d\tau\right]\bar{B} \tag{C.3}$$

where $\bar{A}$ and $\bar{B}$ are the continuous system matrices, I is the identity matrix, and T is the sampling period. The digital feedback control

law is given by

$$\mathbf{U} = -\bar{C}\mathbf{X}_k \tag{C.4}$$

Therefore, if the expressions for singular-value gradients of Section 4.1 are applied, the gradients obtained will be with respect to elements of the discretized matrices, $\Lambda(T)$ and $\Gamma(T)$. In order to evaluate the gradients with respect to the original matrices $\bar{A}$ and $\bar{B}$, a different set of expressions must be developed. These expressions can be developed following the same technique used in Section 4.1; but since $\Lambda(T)$ and $\Gamma(T)$ are expressed in terms of series, some complications arise and a decision must be made as to how many terms of the series must be carried. The following is a description of the suggested approach, where only first- and second-order terms have been considered in Equations (C.2) and (C.3). In this case, Equation (C.3) can be expressed as

$$\Gamma(T) = [IT + \bar{A}\frac{T^2}{2} + \bar{A}^2\frac{T^3}{6}]\bar{B} \tag{C.5}$$

The general equation of the singular-value gradients (Equation 4.17) can now be written as

$$\frac{\partial \sigma_i}{\partial p} = \mathrm{Re} \cdot \mathrm{tr}[\frac{\partial(I + \bar{C}\Phi\Gamma)}{\partial p}\mathbf{v}_i\mathbf{u}_i^*] \tag{C.6}$$

where Φ is now given by

$$\Phi = (Iz - \Lambda)^{-1}\Big|_{z=e^{j\omega_i T}} \tag{C.7}$$

Expanding Equation (C.6), we obtain

$$\frac{\partial \sigma_i}{\partial p} = \mathrm{Re} \cdot \mathrm{tr}[(\frac{\partial \bar{C}}{\partial p} \Phi\Gamma + \bar{C}\Phi \frac{\partial \Gamma}{\partial p} + \bar{C}\Phi \frac{\partial \Lambda}{\partial p} \Phi\Gamma)\mathbf{v}_i \mathbf{u}_i^*] \qquad (C.8)$$

and it is possible to obtain three expressions for $\partial\sigma_i/\partial p$, one each for the following cases:

a) Let p be an element of $\hat{P}$ and $\hat{P} = \bar{B}$; then we obtain

$$\frac{\partial \sigma_i}{\partial p} = \mathrm{Re} \cdot \mathrm{tr}[(\bar{C}\Phi \frac{\partial \Gamma}{\partial p})\mathbf{v}_i \mathbf{u}_i^*] \qquad (C.9)$$

with

$$\Gamma = [IT + \bar{A}\frac{T^2}{2} + \bar{A}^2 \frac{T^3}{6}]\hat{P} = A'\hat{P} \qquad (C.10)$$

Equation (C.9) is then written as

$$\frac{\partial \sigma_i}{\partial p} = \mathrm{Re} \cdot \mathrm{tr}[(\bar{C}\Phi A') \frac{\partial \hat{P}}{\partial p} (\mathbf{v}_i \mathbf{u}_i^*)] \qquad (C.11)$$

and, by using Equations (4.22) and (4.23), we obtain

$$\frac{\partial \sigma_i}{\partial \hat{P}} = \mathrm{Re}[(\bar{C}\Phi A')^* (\mathbf{v}_i \mathbf{u}_i^*)^*] \qquad (C.12)$$

or, using the transpose,

$$\frac{\partial \sigma_i}{\partial \hat{P}^T} = \frac{\partial \sigma_i}{\partial \bar{B}^T} = \mathrm{Re}[(\mathbf{v}_i \mathbf{u}_i^*)(\bar{C}\Phi A')] \qquad (C.13)$$

b) Let p be an element of $\hat{P}$ and $\hat{P} = \bar{A}$, then we obtain from Equation (C.8)

$$\frac{\partial \sigma_i}{\partial p} = \mathrm{Re} \cdot \mathrm{tr}[(\bar{C}\Phi \frac{\partial \Gamma}{\partial p} + \bar{C}\Phi \frac{\partial \Lambda}{\partial p} \Phi\Gamma)\mathbf{v}_i \mathbf{u}_i^*] \qquad (C.14)$$

with

$$\Gamma = [IT + \frac{T^2}{2}\hat{P} + \frac{T^3}{6}\hat{P}\hat{P}]\bar{B}$$

$$\Lambda = I + T\hat{P} + \frac{T^2}{2}\hat{P}\hat{P} \tag{C.15}$$

Substituting (C.15) in (C.14), and rearranging, we obtain

$$\frac{\partial \sigma_i}{\partial \hat{P}} = \frac{\partial}{\partial \hat{P}} \text{Re} \cdot \text{tr}[\{(\bar{C}\Phi \frac{T^2}{2})\hat{P}(\bar{B}) + (\bar{C}\Phi \frac{T^3}{6})\hat{P}\hat{P}(\bar{B}) + \tag{C.16}$$

$$+ (\bar{C}\Phi T)\hat{P}(\Phi\Gamma) + (\bar{C}\Phi \frac{T^2}{2})\hat{P}\hat{P}(\Phi\Gamma)\}(\mathbf{v}_i \mathbf{u}_i^*)]$$

Using Equation (4.23) and

$$\frac{\partial}{\partial A} \text{trace}[BAAC] = B^T C^T A^T + A^T B^T C^T \tag{C.17}$$

we obtain, using the transpose

$$\frac{\partial \sigma_i}{\partial \hat{P}^T} = \frac{\partial \sigma_i}{\partial \bar{A}^T} = \text{Re}[(\bar{B}\mathbf{v}_i \mathbf{u}_i^* \bar{C}\Phi \frac{T^2}{2}) + (\bar{A}\bar{B}\mathbf{v}_i \mathbf{u}_i^* \bar{C}\Phi \frac{T^3}{6}) +$$

$$+ (\bar{B}\mathbf{v}_i \mathbf{u}_i^* \bar{C}\Phi \frac{T^3}{6} \bar{A}) + (\Phi\Gamma \mathbf{v}_i \mathbf{u}_i^* \bar{C}\Phi T) +$$

$$+ (\bar{A}\Phi\Gamma \mathbf{v}_i \mathbf{u}_i^* \bar{C}\Phi \frac{T^2}{2}) + (\Phi\Gamma \mathbf{v}_i \mathbf{u}_i^* \bar{C}\Phi \frac{T^2}{2} \bar{A})] \tag{C.18}$$

c) Let p be an element of $\hat{P}$ and $\hat{P} = \bar{C}$; then, from Equation (C.8)

$$\frac{\partial \sigma_i}{\partial p} = \text{Re} \cdot \text{tr}[\frac{\partial \bar{C}}{\partial p} \Phi\Gamma \mathbf{v}_i \mathbf{u}_i^*] \tag{C.19}$$

and

$$\frac{\partial \sigma_i}{\partial \hat{P}^T} = \frac{\partial \sigma_i}{\partial \bar{C}^T} = \text{Re}[\Phi\Gamma \mathbf{v}_i \mathbf{u}_i^*] \tag{C.20}$$

which is similar to Equation (4.29) with Γ instead of $\bar{B}$, and the discrete version of Φ.

1. Report No.	2. Government Accession No.	3. Recipient's Catalog No.
NASA CR-166619		

4. Title and Subtitle	5. Report Date
DEVELOPMENT OF A SENSITIVITY ANALYSIS TECHNIQUE FOR MULTILOOP FLIGHT CONTROL SYSTEMS	October 1985
	6. Performing Organization Code

7. Author(s)	8. Performing Organization Report No.
Alfredo Herrera Vaillard, James Paduano, and David R. Downing	
	10. Work Unit No. RTOP 505-34-01
9. Performing Organization Name and Address	11. Contract or Grant No.
Flight Research Laboratory University of Kansas Center for Research, Inc. Lawrence, Kansas 66045	NCC2-293
	13. Type of Report and Period Covered
12. Sponsoring Agency Name and Address	Contractor Report – Final
National Aeronautics and Space Administration Washington, D.C. 20546	14. Sponsoring Agency Code

15. Supplementary Notes

NASA Technical Monitor: Robert W. Kempel, Ames Research Center, Dryden Flight Research Facility, Edwards, California 93523-5000

16. Abstract

This report presents the development and application of a sensitivity analysis technique for multiloop flight control systems. This analysis yields very useful information on the sensitivity of the relative-stability criteria of the control system, with variations or uncertainties in the system and controller elements.

The sensitivity analysis technique developed is based on the computation of the singular values and singular-value gradients of a feedback-control system. The method is applicable to single-input/single-output as well as multiloop continuous-control systems. Application to sampled-data systems is also explored.

The sensitivity analysis technique was applied to a continuous yaw/roll damper stability augmentation system of a typical business jet, and the results show that the analysis is very useful in determining the system elements which have the largest effect on the relative stability of the closed-loop system.

As a secondary product of the research reported here, the relative stability criteria based on the concept of singular values were explored. This application to a single-loop yaw damper system and a multiloop yaw/roll damper system of a business jet was demonstrated. The results showed that the stability margins obtained through the singular-value analysis are conservative when compared to the margins obtained from a Bode analysis.

17. Key Words (Suggested by Author(s))	18. Distribution Statement
Sensitivity analysis Singular values Robustness criteria Multiloop control systems Frequency domain technique	Unclassified – Unlimited STAR category 08

19. Security Classif. (of this report)	20. Security Classif. (of this page)	21. No. of Pages	22. Price*
Unclassified	Unclassified	160	A08

For sale by the National Technical Information Service, Springfield, Virginia 22161.

End of Document